

AD-A042 245

STANFORD UNIV CALIF STANFORD ELECTRONICS LABS

F/G 20/12

SUPPRESSION EFFECTS ASSOCIATED WITH VLF TRANSMITTER SIGNALS INJ--ETC(U)

MAR 77 R.RAGHURAM

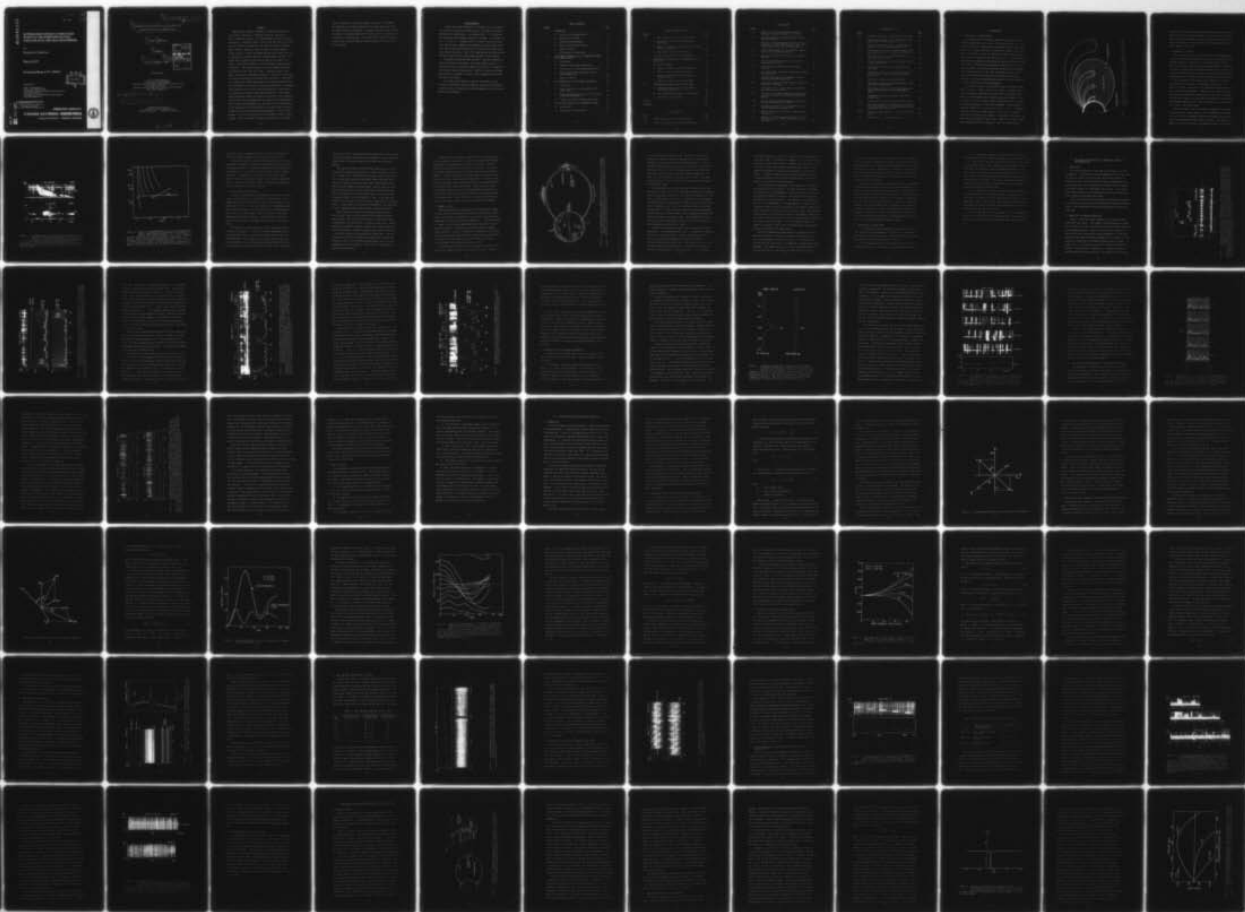
N00014-76-C-0689

UNCLASSIFIED

SU-SEL-77-007

NL

1 of 2
ADA042245



AD A 042245

SEL-77-007

5
B-3

SUPPRESSION EFFECTS ASSOCIATED WITH VLF TRANSMITTER SIGNALS INJECTED INTO THE MAGNETOSPHERE

by

Rajagopalan Raghuram

March 1977

Technical Report No. 3456-3



Prepared under

Office of Naval Research c
Contract Nonr N00014-76-0689
National Science Foundation Atmospheric Sciences Section
Grant ATM75-07707 A1,2
National Science Foundation Division of Polar Programs
Grant DPP-74-04093 A1,2

DISTRIBUTION STATEMENT A

Approved for public release;
Distribution Unlimited

RADIO SCIENCE LABORATORY

STANFORD ELECTRONICS LABORATORIES

STANFORD UNIVERSITY • STANFORD, CALIFORNIA



AD W
DDC FILE COPY

14 SU-SEL-77-007 MR-3456-3

6
SUPPRESSION EFFECTS ASSOCIATED WITH VLF TRANSMITTER
SIGNALS INJECTED INTO THE MAGNETOSPHERE

10 by
Rajagopalan/Raghuram

11
March 1977

9
115p.
Technical Report, No. 3456-3

ACCESSION for	
NTIS	White Section <input checked="" type="checkbox"/>
DDC	Bull Section <input type="checkbox"/>
UNANNOUNCED	<input type="checkbox"/>
JUSTIFICATION	
Per DDC Form 50	
BY on file	
DISTRIBUTION/AVAILABILITY CODES	
Dist.	MAIL or SPECIAL
A	

Prepared under

Office of Naval Research
Contract Nonr N00014-76-0689
National Science Foundation Atmospheric Sciences Section
Grant ATM75-07707 A1,2
National Science Foundation Division of Polar Programs
Grant DPP-74-0493 A1,2

15 Nddp 14-76-C-0689,
NSF-ATM-75-07707

Radioscience Laboratory
Stanford Electronics Laboratories
Stanford University Stanford, California

332,400

JB

ABSTRACT

Magnetospheric growth of coherent VLF signals transmitted from Siple Station, Antarctica is inhibited by whistler mode echoes of earlier transmitter signals. This new phenomenon, called echo-induced suppression, is observed at least a third of the time that transmissions from Siple Station are detected at the receiving station in Roberval, Quebec, Canada. Suppression levels as high as 20 dB are observed. Though the echo is usually much weaker than the direct signal the level of suppression is directly related to the amplitude of the echo. The echoes reduce triggering of emissions as well as the growth of the signal. Echo-induced suppression is not explained by linear wave-wave interference. The echoes are thought to restrict growth by reducing the coherence of the total input signal. According to quasi-linear theory, wave growth is regulated by changes in the particle pitch angle distribution that results from wave-particle interaction. These new results suggest that coherent waves tend to limit their own growth, even when modification of the particle pitch angle distribution is unimportant. Other phenomena such as whistler-induced suppression of signal growth are thought to be related to echo-induced suppression. Wave-induced growth suppression provides an indirect verification of the existence of discrete ducts for the propagation of VLF signals in the magnetosphere. Another suppression phenomenon, also discovered from VLF transmissions, is the suppression of mid-latitude hiss by as much as 6 dB in a band up to 200 Hz wide just below the transmitter frequency. This quiet band develops in 5 to 25 s and lasts up to a minute after the end of transmissions. There is evidence that power-line radiation in the magneto-

sphere at harmonics of 60 Hz also produces quiet bands. Quiet bands are explained by pitch angle scattering of electrons before they reach the growth region near the equator. A change in the distribution function of electrons in the appropriate parallel velocity range is thought to be responsible for the quiet band. Quiet bands lead to indirect estimates of duct widths, scattering regions and perturbations in electron distribution functions.

ACKNOWLEDGEMENTS

I would like to thank Professor R. A. Helliwell for his guidance of this research. He was an unlimited source of new ideas which made the tackling of any problem easy. I am indebted to Mr. J. P. Katsufakis for pointing out many important features in the data. I am grateful to Drs. T. F. Bell, D. L. Carpenter and C. G. Park for revising the manuscript and for their suggestions and comments at various stages of the work. Most of the data presented here is related to the transmitter at Siple Station, Antarctica. None of this data would be available but for the heroic efforts of the various people who went to Siple Station.

The computer program developed by Umran S. Inan was invaluable in doing the scattering calculations. My sincere thanks go to Mr. J. W. Yarbrough not only for making the spectra, but also for his suggestions on the various modes of data analysis. Finally, I would like to thank Doug Collins, my roommate for 5 years, for his cooperation and friendship during this period.

This research was supported in part by the Division of Polar Programs of the National Science Foundation, in part by the Atmospheric Sciences Section of the National Science Foundation, and in part by the Office of Naval Research.

TABLE OF CONTENTS

<u>Chapter</u>		<u>Page</u>
I.	INTRODUCTION	1
	A. Structure of the Magnetosphere	1
	B. Importance of VLF Range	3
	C. Ducted and Nonducted Waves	4
	D. Need for Controlled VLF Signals	8
	E. Summary of Thesis	10
	F. Contributions of Present Work	14
II.	ECHO-INDUCED SUPPRESSION OF VLF TRANSMITTER SIGNALS IN THE MAGNETOSPHERE	16
	A. Introduction	16
	B. Examples of Echo-Induced Suppression	16
	C. Characteristics of Echo-Induced Suppression	25
	D. Some Extensions and Implications of Echo- Induced Suppression	30
	E. Summary of Results	37
III.	AN INTERPRETATION OF ECHO-INDUCED SUPPRESSION	39
	A. Introduction	39
	B. Linear Theory Seen as an Extension of Cold Plasma Theory	40
	C. Reduced Phase Bunched Currents in the Presence of Whistler Mode Echoes	44
	D. Propagation at Non-Zero Wave Normal Angles.	55
IV.	A QUIET BAND PRODUCED BY VLF TRANSMITTER SIGNALS	61
	A. Introduction	61
	B. Description of the Quiet Band	62

TABLE OF CONTENTS (Cont.)

<u>Chapter</u>		<u>Page</u>
IV.	C. Onset and Decay Times for the Quiet Band.	65
	D. Enhancements in Noise Below and Above the Quiet Band	67
	E. Paths of Propagation, Interaction with Whistlers and Other Characteristics	69
	F. Quiet Bands Produced by Other Sources	74
	G. Applications and Uses of the Quiet Band	78
V.	SCATTERING CALCULATIONS AND THE PRODUCTION OF THE QUIET BAND	79
	A. Outline of Method	79
	B. Numerical Solution of the Electron Motion	82
	C. Results of the Scattering Calculations	88
	D. Consistency of Data Observations with the Scattering Theory	94
	E. Implications and Uses of the Quiet Band	95
VI.	CONCLUSIONS AND SUGGESTIONS FOR FUTURE WORK	98
	A. Differences Between the Quiet Band and The Echo-Induced Suppression	98
	B. Some Long Range Implications of the Phenomena	99
	C. Suggestions for Future Work	99
APPENDIX	102
REFERENCES	108

LIST OF TABLES

<u>Table</u>		<u>Page</u>
4.1	Onset and Decay Times for the Quiet Band	65
4.2	Trends in K_p Index Associated With Quiet Bands.	71

ILLUSTRATIONS

<u>Figure</u>		<u>Page</u>
1.1	Sketch of the inner magnetosphere showing the plasmopause and several ducts A, B, C and D.	2
1.2	Spectrogram showing multipath whistlers recorded at Eights Station	6
1.3	Sketch of a subprotonospheric whistler (with several components), a proton whistler, and a riser, all originating from the same lightning stroke at $t = 0$. . .	7
1.4	Sketch showing propagation of transmitter signals between Siple Station and Roberval	11
2.1	Variation in amplitude of 30 s pulses received at Roberval	17
2.2	Echo-induced suppression seen in a 31 s pulse transmitted at 5.9 kHz	20
2.3	Two second pulses separated by varying time intervals	22
2.4	Two second pulses, spaced two seconds apart, showing echo-suppression	24
2.5	Integrated amplitude versus frequency (A-scans) showing echo-induced suppression	27
2.6	Echo-induced suppression when successive pulses are stepped up in frequency	29
2.7	The results of Fig. 2.6 are shown in the form of amplitude versus time plots	31
2.8	A sine wave in frequency showing echo-induced sup- pression in the form of alternate strong and weak portions	32
2.9	Whistler induced suppression and echo-induced sup- pression are seen to occur together	33
2.10	Spectrograms showing a case of asymmetrical trig- gering along with echo suppression	35
3.1	Relation between various vectors in wave particle interaction	43
3.2	Helical loci of the perpendicular velocities of 12 electrons initially equally distributed in cyclo- tron phase:	46

ILLUSTRATIONS (Cont.)

<u>Figure</u>		<u>Page</u>
3.3	Resultant vectors due to the presence of two waves . .	48
3.4	Phase bunched currents for the two frequency case compared with the monochromatic case	50
3.5	Variation in the phase angle θ between the per- pendicular velocity and wave magnetic field	52
3.6	Plot showing the change in resonant frequency with wave normal angle for a constant parallel velocity . .	56
4.1	The middle panel in (a) shows quiet bands in a frequency time spectrogram	63
4.2	The spectrogram shows the onset and decay times of several quiet bands	66
4.3	Spectrograms illustrating the conjugacy of the quiet band	68
4.4	Spectrogram showing noise triggered by the trans- mitter signals in the absence of a quiet band and hiss	70
4.5	Spectrograms showing mixed path whistlers	73
4.6	Spectrogram showing quiet bands produced by sources other than the transmitter	75
4.7	Spectrograms showing the similarity between quiet bands and power system related magnetospheric lines	77
5.1	Propagation of transmitter signals along field- aligned ducts	80
5.2	Division of the distribution function into strips. . .	85
5.3	Phase angle between the perpendicular velocity and the wave magnetic field as an electron moves toward the equator from right to left	87
5.4	Scattering calculations at $L = 4$ for 1 m γ and 10 m γ waves	90
5.5	Scattering at $L = 3$ for a 10 m γ wave	93

I. INTRODUCTION

A. STRUCTURE OF THE MAGNETOSPHERE

The magnetosphere is the region extending from about 1000 km to 100,000 km above the earth's surface. As its name implies, it is the region of the earth's atmosphere controlled mainly by the earth's magnetic field. A good approximation to the earth's magnetic field, up to about 4 earth radii, is that of a dipole offset 436 km from the center and inclined with respect to the rotation axis by 11° . The study of the magnetosphere was made both complicated and intriguing by the fact that this region is influenced by interplanetary effects as well as by terrestrial effects. A big break-through was the discovery of geomagnetically trapped radiation in 1958. The simultaneous discovery of the solar wind by Parker [1958] provided many answers but raised more questions. The rapidly expanding space program in the next decade led to a fairly good model for the magnetosphere.

The region of interest in the present study is the inner magnetosphere. Figure 1.1 shows a sketch of this region. A prominent feature is the plasmopause, discovered in the early 1960's [Carpenter, 1963; 1966]. At the plasmopause the electron density drops suddenly, often by a factor of 100 or so within a tenth of an earth radius. The region inside the plasmopause is called the plasmasphere. The plasmopause is typically located at $L = 4$, but can vary from $L = 3$ to $L = 8$, depending on magnetic activity and other factors. (The L value of a magnetic field line for the simple dipole model is its geocentric distance in the equatorial plane measured in earth radii.) Most of the signals studied here propagated within the plasmopause. While the ionosphere has

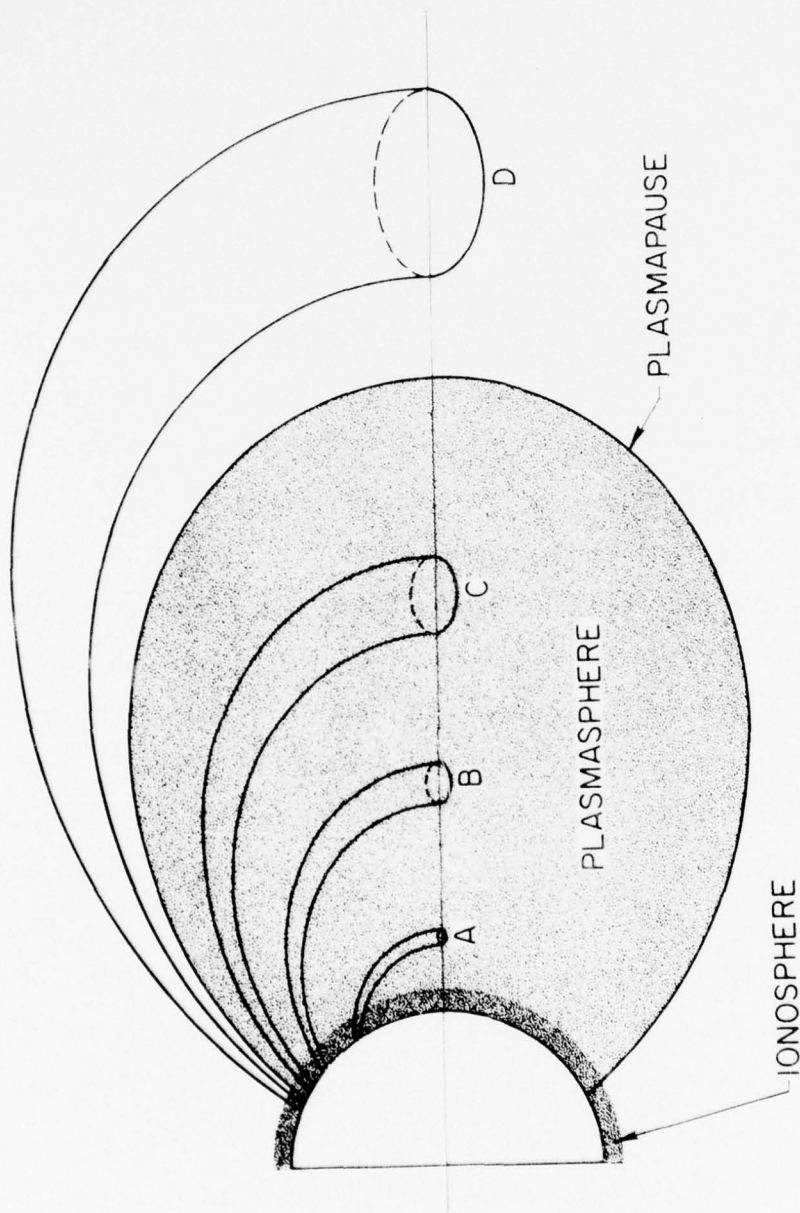


FIGURE 1.1 SKETCH OF THE INNER MAGNETOSPHERE SHOWING THE PLASMAPAUSE AND SEVERAL DUCTS A, B, C AND D. The plasmapause and the ducts are aligned with the earth's magnetic field lines (after Carpenter and Park [1973]).

various ionic constituents and neutral gases the magnetosphere consists almost entirely of electrons and protons. For this reason it is sometimes called the protonosphere. Figure 1.1 also shows enhancements in density called ducts which are aligned (like the plasmopause) with the earth's magnetic field lines.

B. IMPORTANCE OF VLF RANGE

The most obvious way to study the structure of the magnetosphere is to send up a spacecraft and measure electron densities, magnetic fields and other quantities. However, it is almost impossible to send up satellites to cover so vast a region as the magnetosphere. Furthermore, it is hard to separate spatial and temporal effects from satellite data. A study on the ground of electromagnetic waves which have propagated in the magnetosphere is a cheaper and better alternative for many purposes.

Very low frequency (VLF) waves are well suited for probing the magnetosphere from the ground. The frequency range 1-10 kHz is of particular interest, since waves in this range can probe the major portion of the inner magnetosphere. Frequencies above 30 MHz or so penetrate the earth's atmosphere and never return. Most modes of propagation below this frequency are reflected at or below the F-layer peak in the ionosphere, which typically occurs around 300 km. The major exception to this is the whistler mode.

The whistler mode is one of the modes of propagation in a plasma in the presence of a static magnetic field. Propagation in this mode is possible only for frequencies below the gyrofrequency and the electron plasma frequency [Helliwell, 1965; Stix, 1962]. The mode is in general elliptically polarized; for propagation parallel to the static

magnetic field it is circularly polarized. The sense of rotation is the same as that of the electrons. Waves which enter this mode at the base of the ionosphere are sometimes trapped in one of the field-aligned ducts shown in Fig. 1.1. They then travel along the duct until they reach the conjugate hemisphere where they are received on the ground. Trapping in an enhancement duct is possible only for frequencies less than half the gyrofrequency [Helliwell, 1965; Smith, 1960; 1961]. Since the gyrofrequency at altitudes of 3 or 4 earth radii is of the order of 20 kHz, only frequencies below 10 kHz remain trapped from the beginning to the end of a duct. (Ducts are thought to terminate above the F region.) Thus, only frequencies in the lower end of the VLF range can be used in studying the magnetosphere. The dispersion characteristics of whistler-mode waves are very dependent on magnetospheric parameters such as electron densities and static magnetic field intensities. This makes the probing of the magnetosphere using these waves more effective.

C. DUCTED AND NONDUCTED WAVES

VLF signals propagating in the magnetosphere can be broadly classified as ducted and nonducted. Ducted waves travel along field-aligned enhancements in the magnetosphere. This confines the wave normal to small angles from the static magnetic field. In the conjugate hemisphere, these waves are therefore able to penetrate the lower ionospheric boundary (for further details see Helliwell [1965]). All VLF signals received on the ground of magnetospheric origin are believed to be ducted.

The most widely studied ducted whistler-mode wave is the whistler. The whistler results from the dispersed propagation of a lightning im-

pulse. A lightning impulse or 'atmospheric' ideally contains all frequencies, each of which propagates with a different group velocity in the magnetosphere. The result is a long drawn-out signal which when detected sounds like a whistle. The upper panel of Fig. 1.2 shows a whistler in a frequency-time spectrogram. The time origin is the location of the causative spheric (short for atmospheric). The spherics are seen as vertical lines while the several traces of the whistler are seen as parabolas. All the traces originate from the same spheric. The different traces have propagated on different paths. The frequency of minimum time delay, called the nose frequency, gives the L value of the path (see Park [1972]), while the minimum time delay itself is a measure of the equatorial electron density. The plasmopause was discovered by studying a special kind of whistler called a 'knee whistler', which contains components that propagate outside the plasmopause. These components have lower nose frequencies and much lower time delays compared to those propagating inside (see Carpenter [1963]).

Nonducted waves are not generally received on the ground. They have been seen on various satellites and their study has helped formulate propagation theories in plasmas. Frequencies below 3 kHz are greatly affected by the presence of the various ions in the ionosphere and magnetosphere. Very complicated refractive index diagrams result, with two modes of propagation in many frequency ranges. The study of nonducted VLF and ELF waves on satellites has verified the many cutoffs, resonances and crossovers predicted by multiple-ion plasma propagation theory. Figure 1.3 shows a sketch of a spectrogram received on OGO-4 satellite. All the components in the figure originated from one spheric. The figure shows a proton whistler, a sub-protonospheric whistler and a

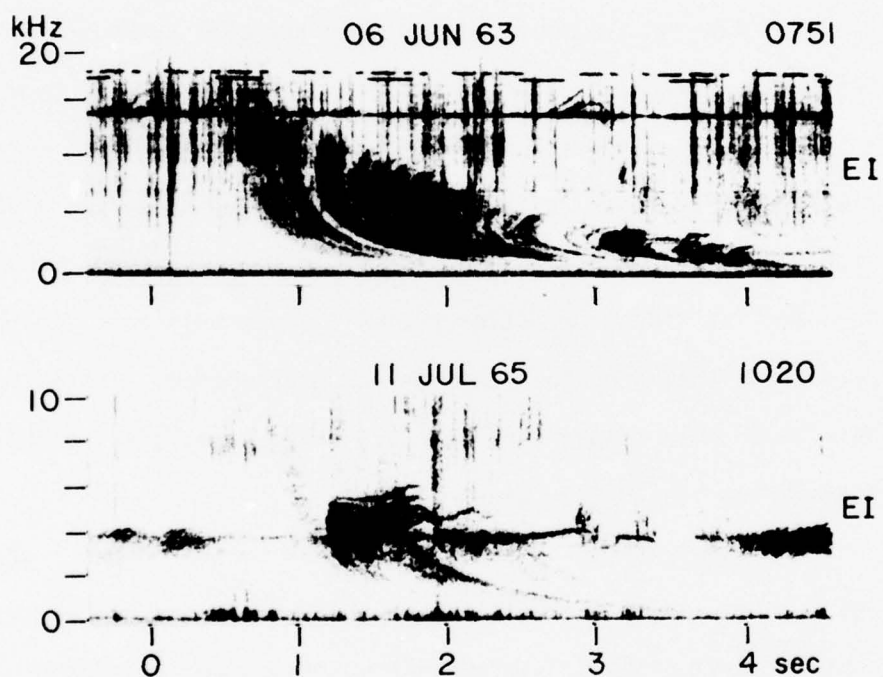


FIGURE 1.2 SPECTROGRAM SHOWING MULTIPATH WHISTLERS RECORDED AT EIGHTS STATION. The upper spectrogram shows several traces or components all of which originated from an atmospheric at 0 s. The lower spectrogram shows emissions triggered at the tops of nose whistlers. While the dispersion of the whistlers is due to the cold plasma, the emissions are produced by energetic particles (after Helliwell [1970]).

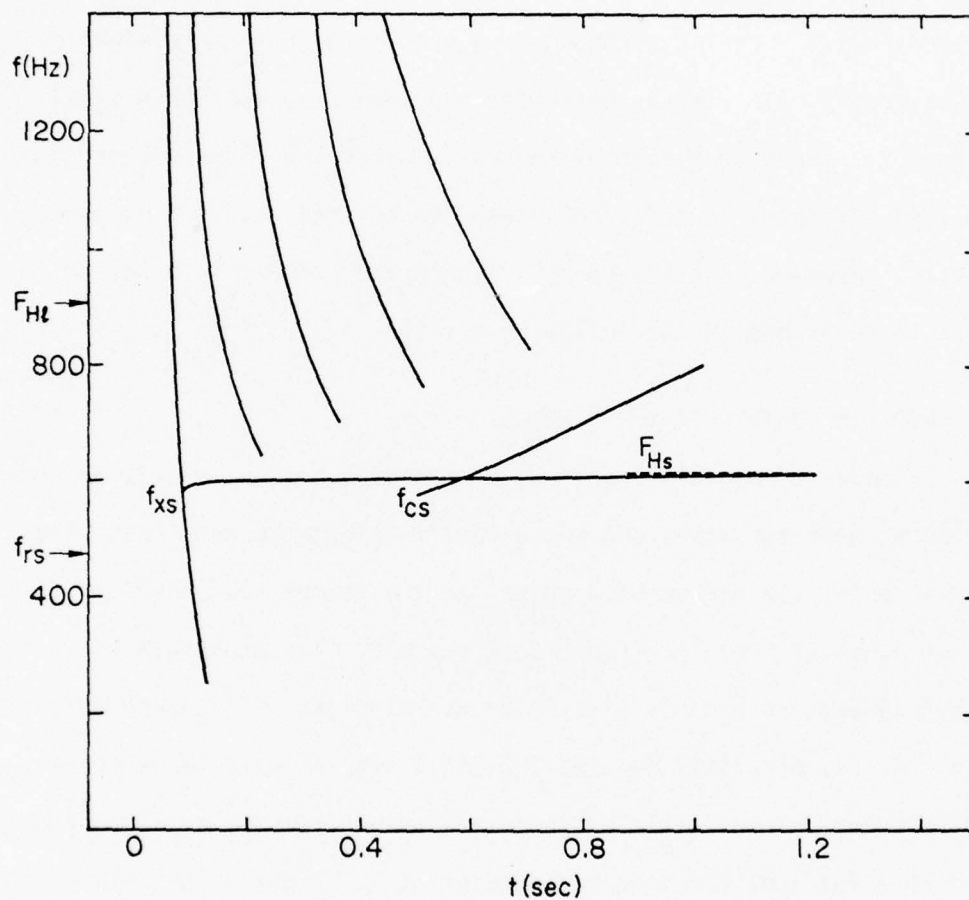


FIGURE 1.3 SKETCH OF A SUBPROTONOSPHERIC WHISTLER (WITH SEVERAL COMPONENTS), A PROTON WHISTLER, AND A RISER, ALL ORIGINATING FROM THE SAME LIGHTNING STROKE AT $t = 0$. These nonducted whistlers are typical for satellite altitudes around 1000 km. Here F_{H1} and F_{Hs} stand for the proton gyrofrequencies at the bottom of the ionosphere and at the satellite location respectively. f_{rs} , f_{cs} , and f_{xs} are the two-ion resonant, the ion cutoff, and the crossover frequencies, respectively at the satellite location (after Raghuram [1975]).

new type of riser (see Raghuram [1975]). The figure illustrates the complexity of wave propagation in the presence of multiple ions.

In short, the study of nonducted and ducted VLF signals in the past has helped to determine the structure of the magnetosphere and to verify propagation theories. Propagation phenomena can be explained by cold plasma theory, i.e., by assuming the electrons and ions have little or no energy. The propagation of naturally occurring signals such as spherics has been, by and large, adequate for the study of propagation effects. However, controlled VLF signals are essential for other purposes as described in the following section.

D. NEED FOR CONTROLLED VLF SIGNALS

A number of magnetospheric wave phenomena are the result of interaction between the waves and the energetic electrons and ions. The triggering of the narrow-band noises at the top of the whistlers in the bottom panel of Fig. 1.2 is one such example. Noises generated in the magnetosphere are broadly classified as emissions. Triggered emissions, hiss, chorus, etc. (see Helliwell [1965]) are examples of emissions generated by the energetic particles. These particles are also responsible for amplification and damping of VLF signals in the magnetosphere.

The explanation of these phenomena is rather complicated and has not been fully worked out. It was felt that these phenomena could be studied more effectively if controlled VLF signals were injected into the magnetosphere. As the input signal is then completely known, the hot plasma effects can be separated from cold plasma dispersion effects. A VLF transmitting station was established at Siple Station, Antarctica

(84°W, 76°S) for this purpose [Helliwell and Katsufrakis, 1974]. Signals from this transmitter are received at the conjugate station in Roberval, Canada. Most of the data analyzed in this report were recorded at Roberval.

VLF signals from other transmitters have been used in the past to study various propagation characteristics such as attenuation, fading, etc. Helliwell et al. [1962] describe the results from a study of signals from Navy VLF transmitters NAA (Cutler, Maine, USA), NBA (Summit Canal Zone), NPG (Jim Creek, Washington, USA), NPM (Lualaulei, Oahu, Hawaii) and NSS (Annapolis, Maryland, USA). Later on, emissions triggered by these transmitters called artificially stimulated emissions (ASE's) were observed. Helliwell [1965] contains an account of ASE's triggered by NPG at 18.6 kHz and NAA at 14.7 kHz. It was found that dashes (150 ms long) were far more likely to trigger emissions than dots (50 ms). Kimura [1967] gives statistical information on the occurrence of ASE's triggered by NAA and Omega Station, Forrestport, New York.

These transmitters operate in the frequency range 10-20 kHz. Ducted signals usually do not exceed half the minimum gyrofrequency along the path. When this restriction applies, the maximum L values corresponding to 10 and 20 kHz are 3.5 and 2.8, respectively. Many VLF emissions are generated at greater L values and at lower frequencies. The Siple transmitter, designed to operate mainly between 3 and 8 kHz, is thus better suited to study wave-particle interactions. Some preliminary results from the transmitter were reported by Helliwell and Katsufrakis [1974]. Stiles [1974] presented digital spectra of ASE's triggered by the Siple transmitter as well as ASE's triggered by the NAA and Omega transmitters.

The wave-particle interactions studied using VLF transmitters have so far had mainly to do with ASE's. Here two new suppression phenomena produced by VLF transmitters are described. In the past suppression effects associated with VLF emissions have been studied. For example, Brice [1964] showed that one set of periodic emissions often suppresses another. Ho [1973] reported that whistlers modify the period of quasi-periodic emissions and sometimes even terminate them. In general, when two VLF wave packets travel along the same path in the magnetosphere one of the packets often suppresses the other. These and similar effects are considered important not only for understanding the generation of VLF emissions, but also for providing a means of regulating wave growth in the magnetosphere. Their further study is greatly facilitated by a controlled VLF signal source as can be seen from the later chapters.

E. SUMMARY OF THESIS

Controlled experiments on wave-particle interactions were started in 1973, using the Siple transmitter [Helliwell and Katsufakis, 1974]. Figure 1.4 illustrates the propagation of VLF signals injected into the magnetosphere by the Siple transmitter denoted by T. Some of the energy is trapped in a field aligned magnetospheric duct and travels to the opposite hemisphere. The signals are recorded at Roberval, Quebec, Canada, denoted by R, which is magnetically conjugate to Siple Station. The waves pass through the wave-particle interaction region believed to be located close to the equator where amplification and triggering occur [Helliwell, 1967; Helliwell and Crystal, 1973].

The figure shows three 500 ms pulses separated in time by 1 s and traveling at roughly one twentieth the velocity of light. The three

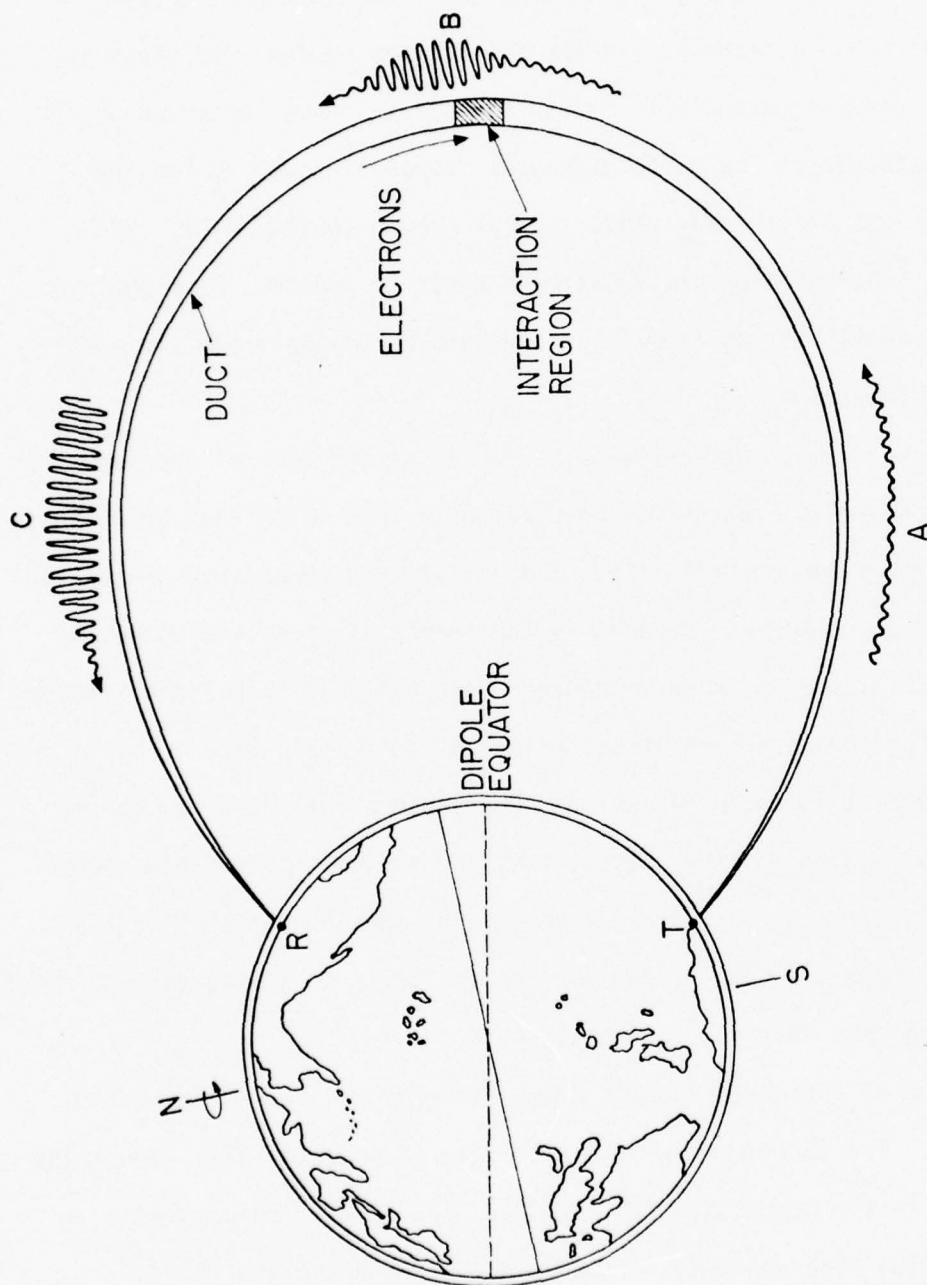


FIGURE 1.4 SKETCH SHOWING PROPAGATION OF TRANSMITTER SIGNALS BETWEEN SIPLER STATION AND ROBERVAL. Signals transmitted from Siple Station travel along a field aligned duct of enhanced ionization. Amplification takes place in a wave particle interaction region near the equator. Three 500 ms pulses at an instant in time are shown.

pulses are shown at an instant in time. The pulse at A has not yet entered the interaction region and therefore shows no amplification. The pulse at C has already passed the interaction region. It grows in amplitude roughly exponentially during the first 200 ms, after which the amplitude saturates. The pulse undergoes temporal growth during the first 200 ms but only steady state spatial growth subsequently. The pulse at B, near the equator, shows both types of growth. From power change experiments it was found that the saturation amplitude increases with transmitter power.

The ducted waves are partially reflected at the base of the ionosphere near R and can return to the hemisphere from which they originated where they may again be reflected. These reflected components are called echoes; the hop number of the echo is the number of times the component has traveled through the magnetosphere. When a signal from Siple Station travels to Roberval, part of it is reflected and travels back to Siple Station, where it is again reflected. When such a reflected component or echo travels with a direct signal from the transmitter the echo often inhibits the growth of the direct signal. This phenomenon will be referred to as echo-induced suppression and is the first of the two suppression phenomena described in this thesis.

A number of inferences can be drawn from the data on echo-induced suppression. The phenomenon provides a means of automatically regulating wave growth in the magnetosphere. The data are consistent with the theory that the observed propagation is ducted as described in Helliwell [1965] and Smith [1960; 1961]. The suppression is not caused by simple wave-wave interference, but is attributed to the effect of the echo on the wave-particle interaction process. It is postulated

that growth suppression results from a reduction in the coherence of the total input signal. The reduction in coherence is in turn caused by the emissions associated with the echoes. Whatever the explanation, it seems clear that a study of echo-induced suppression should lead to a more complete understanding of wave-particle interactions in the magnetosphere. It could for example explain the whistler-induced suppression of Siple transmitter signals [Helliwell and Katsufakis, 1974], which appears to be governed by the same mechanism.

The second suppression phenomenon is the suppression of naturally occurring noise by the transmitter. The noise suppressed is broadband mid-latitude hiss and the phenomenon is seen in the form of a quiet band just below the transmitter frequency. The conditions under which this phenomenon occurs are reported here. The explanation for this phenomenon lies in the inhomogeneity in the magnetosphere. The waves from the transmitter scatter particles at locations off the equator, reducing the number of particles in a certain parallel velocity range. These particles are responsible for amplification of waves in the frequency range of the quiet band at the equator and this results in the quiet band. Scattering calculations confirm this theory. It is also shown that power line radiation at harmonics of 60 Hz from the Canadian power system could be producing quiet bands in the magnetosphere.

Both of the phenomena described above can be roughly described as wave-wave interactions. However, the growth or amplification of all waves concerned depends on the particles and it is the wave-particle interaction process that really is of importance in understanding these phenomena. Echo-induced suppression is due to the reduced coherence of the input wave which in turn reduces the effectiveness of the wave-

particle interaction process. The quiet band results from a modification of the particle distribution function in the relevant part of the velocity spectrum. These two wave-wave interactions are the only ones detailed in this thesis. Other wave-wave interactions such as entrainment of one emission by another, reversal of slope of an emission (as seen on a frequency-time display) by a monochromatic signal, etc. are beyond the scope of this work.

The two suppression phenomena described here are of great importance in understanding wave-particle interactions in the magnetosphere. A study of the data reported here could help modify and improve existing interaction models and even suggest new mechanisms. These results could also find application in VLF communication. Inhibition of growth produced by echoes could be used to selectively receive the ground wave component rather than the magnetospheric component. By transmitting in a quiet band produced by another VLF transmitter a significant improvement in signal to noise ratio can be achieved. In the long run, the study of amplification mechanisms in the magnetosphere could also lead to a better understanding of laboratory plasmas.

F. CONTRIBUTIONS OF PRESENT WORK

1) A transmitter program was designed to study how the level of echo-induced suppression depended on the difference in frequency between the direct signal and the echo. Analysis of the results leads to an estimate of the interaction bandwidth (≈ 100 Hz).

2) Echo-induced suppression is explained in terms of reduced phase-bunched currents in the presence of a non-monochromatic wave.

3) It is shown that propagation at non-zero wave normal angles can be responsible for the frequency broadening of the transmitter pulses.

4) From a study of data from over a period of 2 years it was found that quiet bands are relatively infrequent and are observed only on 5% of the days that transmitter signals are detected at Roberval. They occur at times of extremely good echoing and deep quieting in the magnetic activity. Echo-induced suppression on the other hand can be seen on more than 30% of the days. It occurs at times which are generally favorable for the reception of the transmitter signals at Roberval as reported by Carpenter and Miller [1976].

5) It is shown that pitch angle scattering leads to a modification of the electron velocity distribution function. In particular, the quiet band is explained in terms of a reduction in electron flux in the appropriate parallel velocity range. Quiet bands can alternatively be explained by the slopes in the pitch angle distribution which are also produced at the same time by scattering.

6) It is found that the quiet band takes 5 to 25 s to develop and lasts up to a minute after the end of transmissions. The recovery time for the noise indicates that longitudinal duct widths are greater than 0.1° .

II. ECHO-INDUCED SUPPRESSION OF VLF TRANSMITTER SIGNALS IN THE MAGNETOSPHERE

A. INTRODUCTION

Echo-induced suppression is described in this chapter using data from Roberval. Though the initial mixing between the direct signal and the echo takes place near Siple Station, they are both observed at Roberval only after traveling together through the magnetosphere once. Echo-induced suppression is manifested in different forms that depend on the pulse sequence, as illustrated in this section. In all cases, echo-induced suppression occurs during periods of overlap between the direct signals and the higher order echoes.

In the next section particular examples of echo-induced suppression are described, while the third section presents the important characteristics. Some related effects are then discussed, and the results are summarized.

B. EXAMPLES OF ECHO-INDUCED SUPPRESSION

Figure 2.1 shows echo-induced suppression in 30 s pulses transmitted from Siple Station. The frequency-time spectrogram of a sample pulse is shown in (c) while (d) shows the first few seconds of the pulse on an expanded time scale. Figure 2.1a gives the time sequence of a pulse and its echoes at both Siple Station and Roberval. On this day the travel time from Siple Station to Roberval at 5.15 kHz was 1.9 s as shown by the separation in time between successive hops or echoes. In Figure 2.1d, t_0 indicates the time of first arrival of the pulse at Roberval. The pulse grows in amplitude; t_1 indicates the time at which the amplitude reaches saturation. The spectrum of the pulse be-

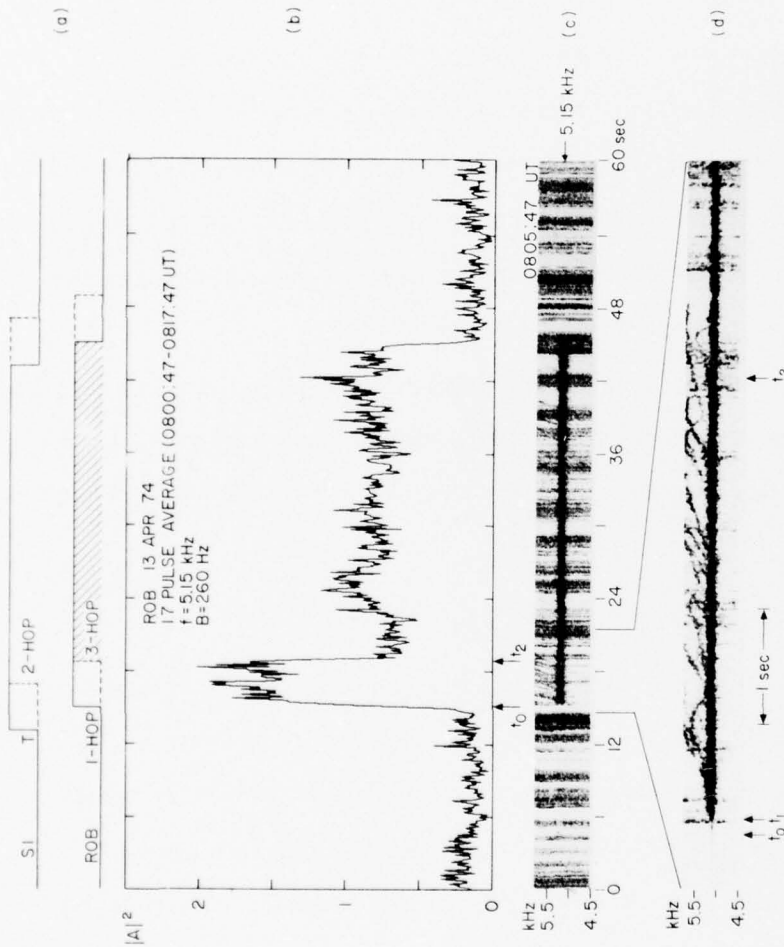


FIGURE 2.1 VARIATION IN AMPLITUDE OF 30 s PULSES RECEIVED AT ROBERVAL. The top panel shows the time sequence of the various hops. The middle panel (b) shows the square of the amplitude as a function of time. The plot is a 17 pulse average. Echo-induced suppression is seen in the form of a reduction in amplitude 4.0 s from the start of the pulse. The spectrogram in (c) shows the frequency time spectrogram of a typical pulse from this time interval while that in (d) shows the first few seconds on an expanded time scale. Echo-induced suppression is again clearly seen in the spectrograms. See text for an explanation of t_0 , t_1 and t_2 .

gins to broaden at t_1 . Such broadening is discussed in greater detail in the next section and is an important feature of the phenomenon. It takes 125 (± 50) ms for the amplitude to reach saturation, i.e., $t_1 - t_0 = 125$ ms. The initial growth rate on this day was 126 dB/s and the total growth from noise level to saturation was 20 dB.

Figure 2.1b is a plot of the square of the amplitude versus time, averaged over 17 pulses received at Roberval. (The averaging helps to smooth out the effect of background noise, such as atmospherics.) A narrow band (260 Hz) centered at the transmitter frequency was digitally sampled and the samples were averaged to produce the plot. There is a sharp drop in amplitude at t_2 which is 4.0 s after t_0 . The same effect can be seen in the spectrograms in (c) and (d). The period of overlap between the three-hop echo and the direct signal, when echo-induced suppression occurs, is shown cross-hatched in the time sequence. The times t_1 and t_0 are coincident in the time scale of Figure 2.1b.

If suppression were caused by the first arriving components of the echo, then the drop in amplitude should take place 3.8 s after the arrival of the one hop or direct signal, about 200 ms ahead of the observed drop. The delay in the onset of suppression can be accounted for by the time taken for the spectrum to broaden. The time when three-hop echoes can be expected to have a broadened spectrum is given by $t_2 = t_1 + 3.8$ s. Within measurement accuracy (± 50 ms), the onset of suppression is therefore coincident with the arrival of the spectrally broadened part of the three-hop echo. The spectrograms (Figures 2.1c and d) show that the arrival of the three-hop echo also inhibits the triggering of emissions.

Note that the three-hop echo itself is not discernible either on the spectrogram or on the averaged amplitude plot. Otherwise, there would be an extension in time of the signal beyond the termination of the direct signal. Three-hop echoes were either lost in the noise or were considerably weaker (< -20 dB) than the direct signal during periods of echo-induced suppression. Assuming the echoes are weaker in the magnetosphere as well as on the ground, they must affect the growth soon after entering the interaction region where the echoes and newly injected but unamplified signals probably are of comparable amplitude.

Suppression in Figure 2.1 is not uniform after t_2 . Instead there is a partial recovery in the amplitude 8.1 s from the start of the pulse. This is because the portion of the direct signal between 4.1 and 8.1 s is weaker and its subsequent echoes do not suppress as effectively. The level of suppression depends therefore on the amplitude of the echo. As a result, a variation in amplitude with roughly an 8 s period is seen over the entire length of the pulse. Though the suppression on this day was only 3.7 dB, it has been as high as 20 dB on other days. Using the whistler technique described in Park [1972], the path of propagation was located at $L = 4.2$.

An example of echo-induced suppression on two frequencies is shown in Fig. 2.2. In the top panel is the frequency-time spectrogram showing a 31 s pulse and some shorter pulses on lower frequencies, all received at Roberval. The transmitter pattern, corrected for the one-hop travel time, is shown below the actual spectrum. The lower two panels are amplitude-versus-time plots of the received signal on two of the transmitted frequencies, 5.90 and 5.65 kHz. As in Fig. 2.1, suppression of the 31 s pulse at 5.9 kHz occurs after an initial two-hop whistler-mode

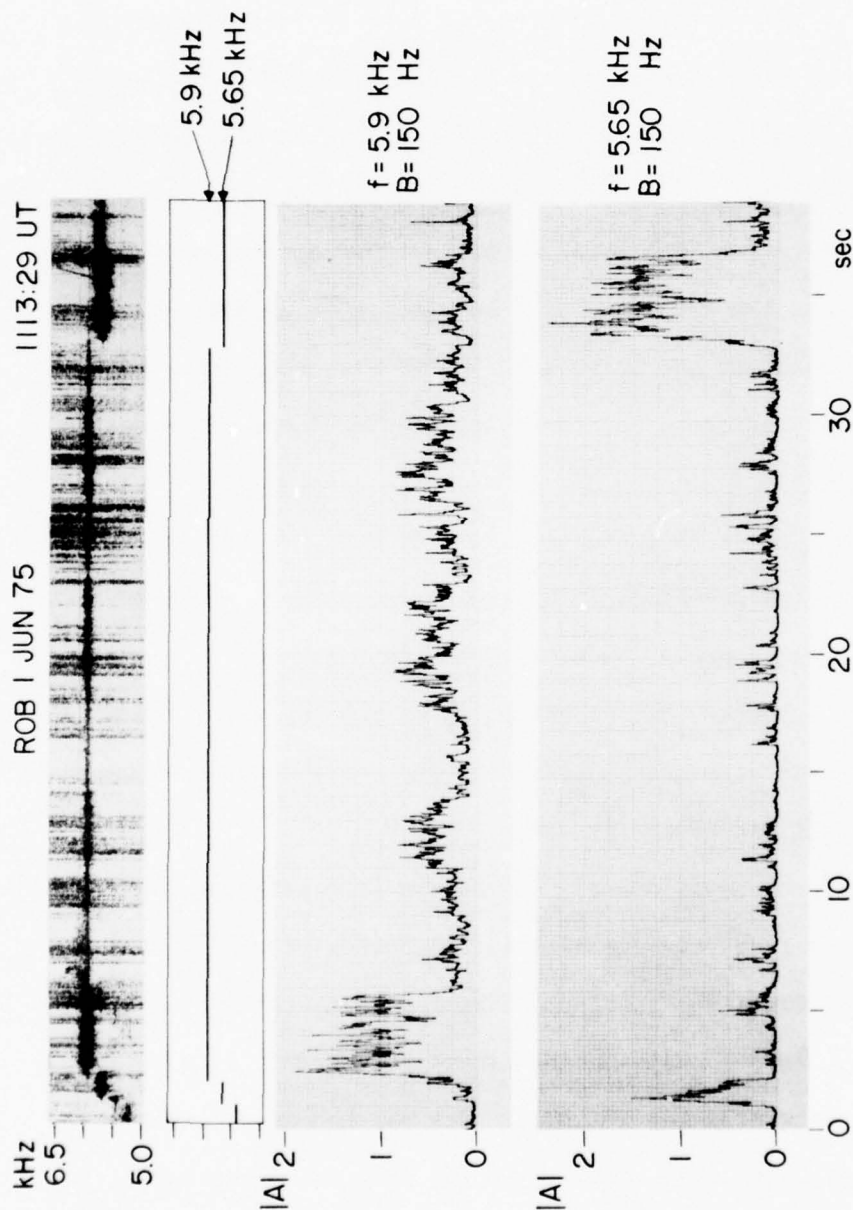


FIGURE 2.2 ECHO-INDUCED SUPPRESSION SEEN IN A 31 s PULSE TRANSMITTED AT 5.9 KHZ. The top panel shows the frequency time spectrogram with the transmitter format below it. The lower two panels show amplitude versus time. The amplitude data were obtained by passing the signal through 150 Hz filters centered at 5.9 kHz and 5.65 kHz respectively. The three-hop echoes of the 1 s pulses at the beginning as well as that of the 31 pulse are visible.

travel time. The signals on this day were multipath, i.e., they propagated along several paths with different travel times. There were two prominent paths with two-hop travel times of 3.7 s and 4.1 s, respectively. Here suppression begins at 3.9 s from the start of the pulse. This is about 200 ms after the first three-hop echo arrives at Roberval. This delay is equal to the time taken for the spectrum to broaden as explained in connection with Fig. 2.1. There is again a partial recovery in the amplitude at 11 s. The alternating weak and strong segments can be seen over the entire length of the pulse. The direct pulse terminates at 33.05 s and the frequency of transmission is changed to 5.65 kHz. The extension of the pulse seen in the spectrogram beyond 33.05 s at 5.9 kHz is caused by the three-hop echo, which is much weaker than the direct signal.

The bottom panel shows that transmissions at 5.65 kHz, beginning at 33.1 s, are not affected by echoes at 5.9 kHz. The pulse at 5.65 kHz also shows echo-induced suppression 4.2 s from the beginning of the pulse. The level of suppression for the pulse at 5.9 kHz was 15 dB and the unsuppressed growth rate was 133 dB/sec. The corresponding numbers at 5.65 kHz were 20 dB and 85 dB/sec.

A different form of echo-induced suppression is manifested in Fig. 2.3. At the top is a time sequence of 3.45 kHz pulses as received at Roberval. The solid lines represent the direct signal, the broken lines the three-hop echo, and the cross-hatched areas the periods of overlap when suppression can be expected to occur. The two-hop travel time is denoted by τ . Below the time sequence is the observed spectrogram. At the bottom is a plot of the amplitude in a 150 Hz wide passband centered on the carrier. Two-second pulses were transmitted with varying

ROB 11 OCT 74

1845:02 UT

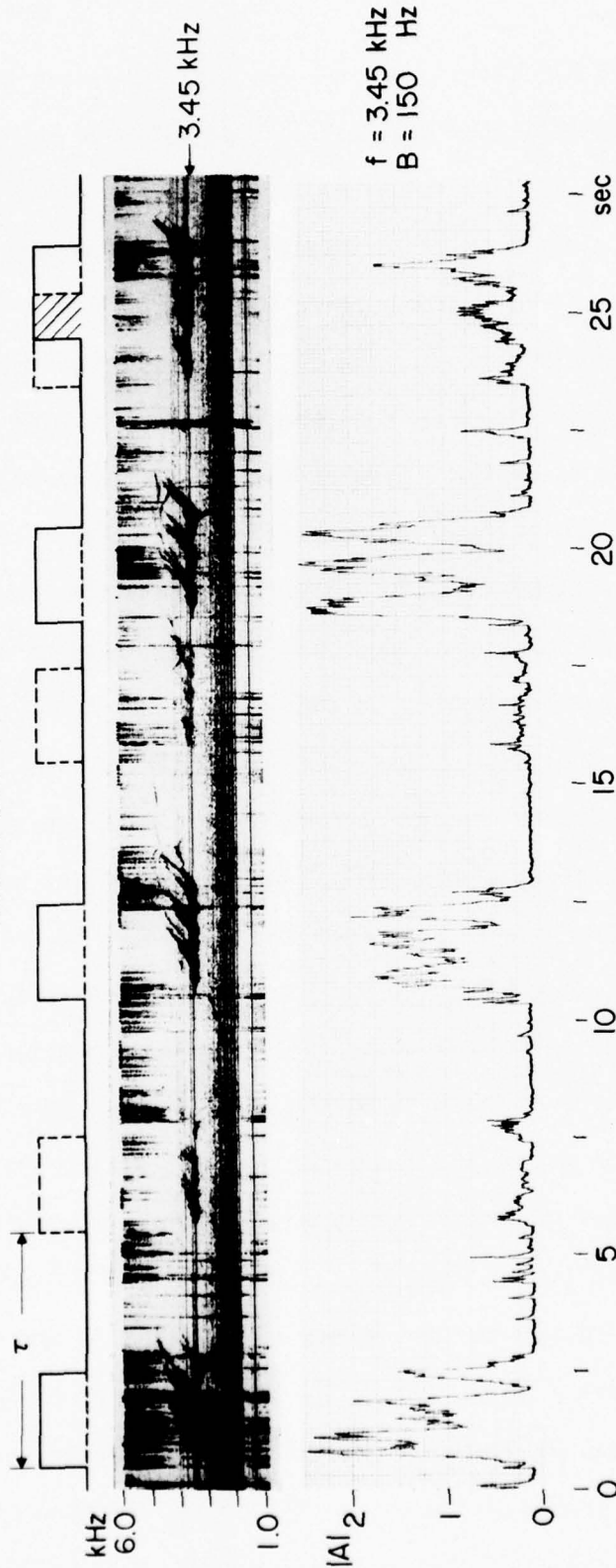


FIGURE 2.3 TWO SECOND PULSES SEPARATED BY VARYING TIME INTERVALS. The timing sequence at the top shows the direct signal by solid lines and the three-hop echoes by dashed lines. The cross-hatched region represents the period of overlap when echo-induced suppression can be expected to occur. The two hop whistler mode delay, τ , is 5 s. Echo-induced suppression is seen in the last pulse in both the spectrogram and the amplitude plot. The amplitude plot was obtained using a 150 Hz filter centered at the transmitter frequency as in Fig. 2.2. Note that the amplitude of the echoes is far weaker than that of the direct signals.

time intervals between them. (During these intervals there were transmissions at 2.45 and 2.65 kHz; they were barely detectable at Roberval and are not of interest here.) The three-hop echoes of the 2-s pulses are weak but are seen clearly both on the spectrogram and the amplitude plot. The first half of the last direct pulse starting at 2.45 s shows echo-induced suppression. In Figs. 2.1 and 2.2 the received pulses were initially stronger. Here in Fig. 2.3, the opposite effect is seen; the initial part of the pulse is weaker. Even at the end of the echo this pulse does not reach the amplitude of the earlier direct pulses. Here again the presence of the three-hop echo inhibits not only the growth but also the triggering of emissions. For this case the level of suppression was 9.5 dB and the growth rate 98 dB/sec.

Another example of echo-induced suppression, similar to Fig. 2.3, is shown in Fig. 2.4. The spectrum and narrowband amplitude are shown in the middle and lower panels, respectively. Two-second pulses were transmitted with two-second intervals between them, as shown by the sketch in the top panel. Here the first parts of four pulses received at Roberval are seen to be relatively weaker. The two-hop whistler mode travel time τ was 2.9 s so that the three-hop echo of the latter half of each pulse arrived with the direct signal of the next pulse. As in Fig. 2.3, the cross-hatched regions in the top panel represent times of overlap, when echo-induced suppression takes place. Each of the arrows along the time scale indicates the time at which the amplitude starts to recover after the termination of the echo. The termination of the corresponding direct pulse can be seen τ s before each arrow except the first. Note that the emissions at the end of the pulses increase the apparent length of the pulses. (The thin lines at 6060 Hz and 5340 Hz

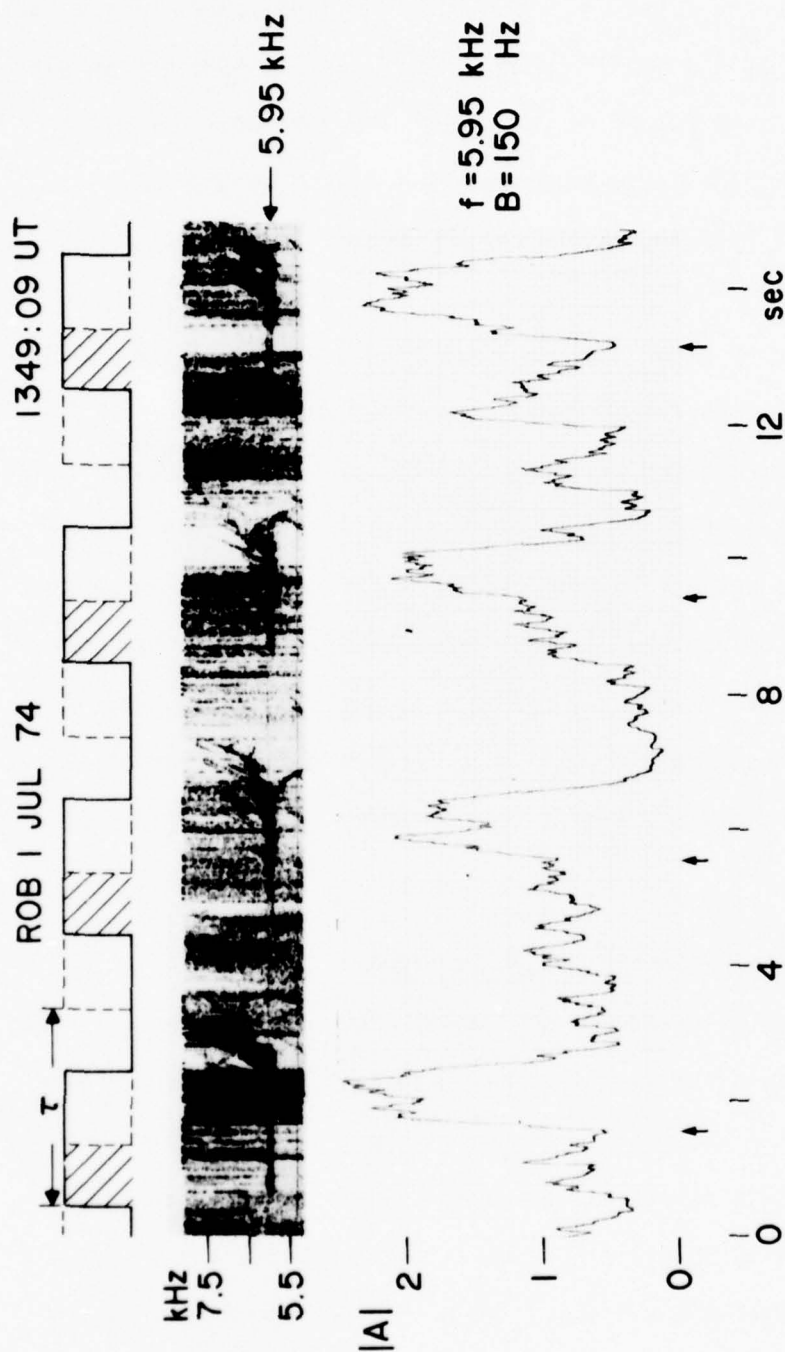


FIGURE 2.4 TWO SECOND PULSES, SPACED TWO SECONDS APART, SHOWING ECHO-SUPPRESSION. As in Fig. 2.3 the periods of overlap which correspond to periods of echo-induced suppression are shown cross-hatched. The arrows mark the start of the recovery in amplitude.

on the spectrogram are caused by induction fields at harmonics of 60 Hz from the Canadian power system.) As in Fig. 2.1, the echoes affect the triggering as well as the amplification. The level of suppression was more than 13 dB on some pulses on this day. The path of propagation calculated from whistler measurements was $L = 3.7$. The growth rate during the times of recovery at the end of suppression was about 110 dB/sec.

At first sight it might seem that echo-induced suppression could be explained by destructive linear interference between the echo and the one-hop signal. However the repetition of the phenomenon in every pulse, as in Fig. 2.4, makes this interpretation unlikely. Radial drifts of the ducts can cause changes in path length of the order of a wavelength per second [Carpenter and Seely, 1976; McNeil, 1967]. One would expect therefore to see constructive interference as well as destructive interference. Since constructive wave interference has not been observed, wave-wave interference as a cause of echo-induced suppression can be ruled out.

C. CHARACTERISTICS OF ECHO-INDUCED SUPPRESSION

The features of echo-induced suppression that are obvious from the data were described in the last section. Some other features are described here.

The phenomenon is relatively frequent and the features are repeatable. In 7 months (April 2-November 1) of transmissions in 1974, echo-induced suppression was observed on a third of the days on which transmitter signals were detected at Roberval. (This frequency of occurrence represents a lower bound, because the transmitted program is

quite often not suitable for the detection of this phenomenon.) Echo-induced suppression is always accompanied by temporal growth and quite often by triggering.

The path of propagation was estimated in 18 cases to determine if the phenomenon was restricted to any range of L values. The paths were calculated from the nose frequencies of whistlers which had the same travel times as the transmitter signals [Park, 1972; Carpenter and Miller, 1976]. The paths ranged from $L = 3.5$ to $L = 5$. The distribution was similar to the more complete histogram shown by Carpenter and Miller [1976] for transmitter signals observed at Roberval.

Echo-induced suppression tends to occur during periods of magnetospheric quieting following a moderate disturbance. Carpenter and Miller [1976] observed similar behavior in the occurrence of transmitter signals at Roberval. Thus the conditions under which echo-induced suppression occurs are similar to those for the observation of transmitter signals at Roberval, and no further special conditions are necessary.

A feature of echo-induced suppression, which was suggested by several of the spectrograms in the last section, is that the signals received at Roberval have bandwidths as large as 150 Hz. A monochromatic input generates these additional frequencies mainly on the higher side, as illustrated in Fig. 2.5. The case analyzed here is the 31-s pulse shown in Fig. 2.2. The data were sampled and transformed using a Fast Fourier Transform routine similar to that described in Stiles and Helliwell [1975]. The time segments were 0.64 s long with an overlap of 0.32 s between successive transforms. Thus, a separate transform was obtained every 0.32 s with alternate transforms being completely independent. Each A-scan is an average over 13 such transforms. The

ROB 1 JUN 75

1113:31 UT

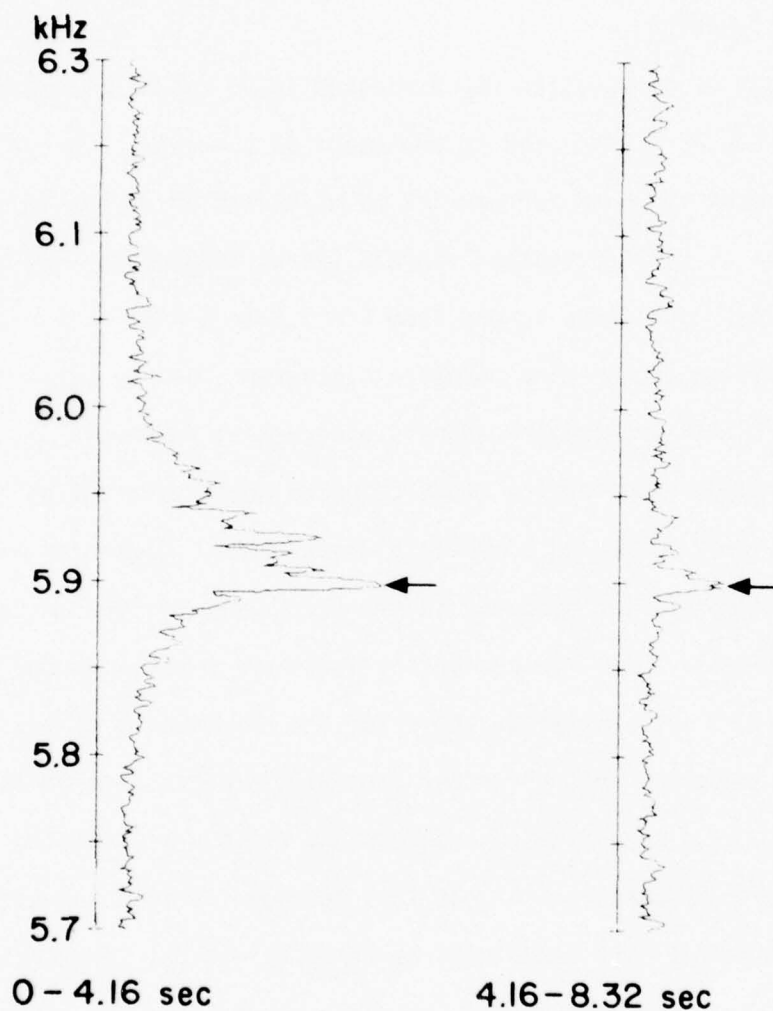


FIGURE 2.5 INTEGRATED AMPLITUDE VERSUS FREQUENCY (A-SCANS) SHOWING ECHO-INDUCED SUPPRESSION. Each A-scan is an average of 13 separate scans in frequency. The left A-scan shows the un-suppressed signal and the right shows the suppressed signal. The case analyzed here is the 31 s pulse shown in Fig. 2.2. During periods of echo-induced suppression both the transmitter frequency and the upper sideband are suppressed. Note that in the absence of echoes the received signal at Roberval has a bandwidth of more than 100 Hz.

A-scan on the left is an average over the first 4.16 s of the pulse when there was no suppression. The transmitter frequency is shown by the arrow. The bandwidth is almost 100 Hz, the amplitude decaying at higher frequencies. Also, the additional frequencies are predominantly above the transmitter frequency. Usually the three-hop echoes also contain these additional frequencies. Sometimes only the additional frequencies above the transmitter frequency are present in the three-hop echo, the transmitter frequency itself being below the noise level. The A-scan on the right is an average over the next 4.16 s when the signal was suppressed. Not only is the amplitude at the transmitter frequency reduced, but so is the bandwidth.

From evidence such as that of Fig. 2.5, it was hypothesized that an echo of finite bandwidth would be able to suppress a direct input signal anywhere within its band. To test this proposition successive transmitted pulses were stepped up in frequency by Δf . The results as received at Roberval are shown in Fig. 2.6. The transmitted format is shown in the bottom panel. The pulses are separated by varying intervals of time. The sequence begins with a 10 s pulse at 5.4 kHz. The Δf steps in the five data panels are 100, 0, 10, 25 and 50 Hz. Echo-induced suppression is evident in the 10 s pulse from 4 s. Note that the three-hop echoes of most of the pulses are seen clearly, for example at 13 s and 21 s. The variations in amplitude of the three-hop echoes of the 10 s pulses (near 12 s) reflect variations in the direct signal caused by echo-induced suppression. The two-hop time delay for the various propagation paths varied from 3 to 4.8 s. However, the delay for the most prominent path was 4.4 s so that the three-hop echo of the third pulse arrived near 26 s, at roughly the same time (0.4 s later) as the

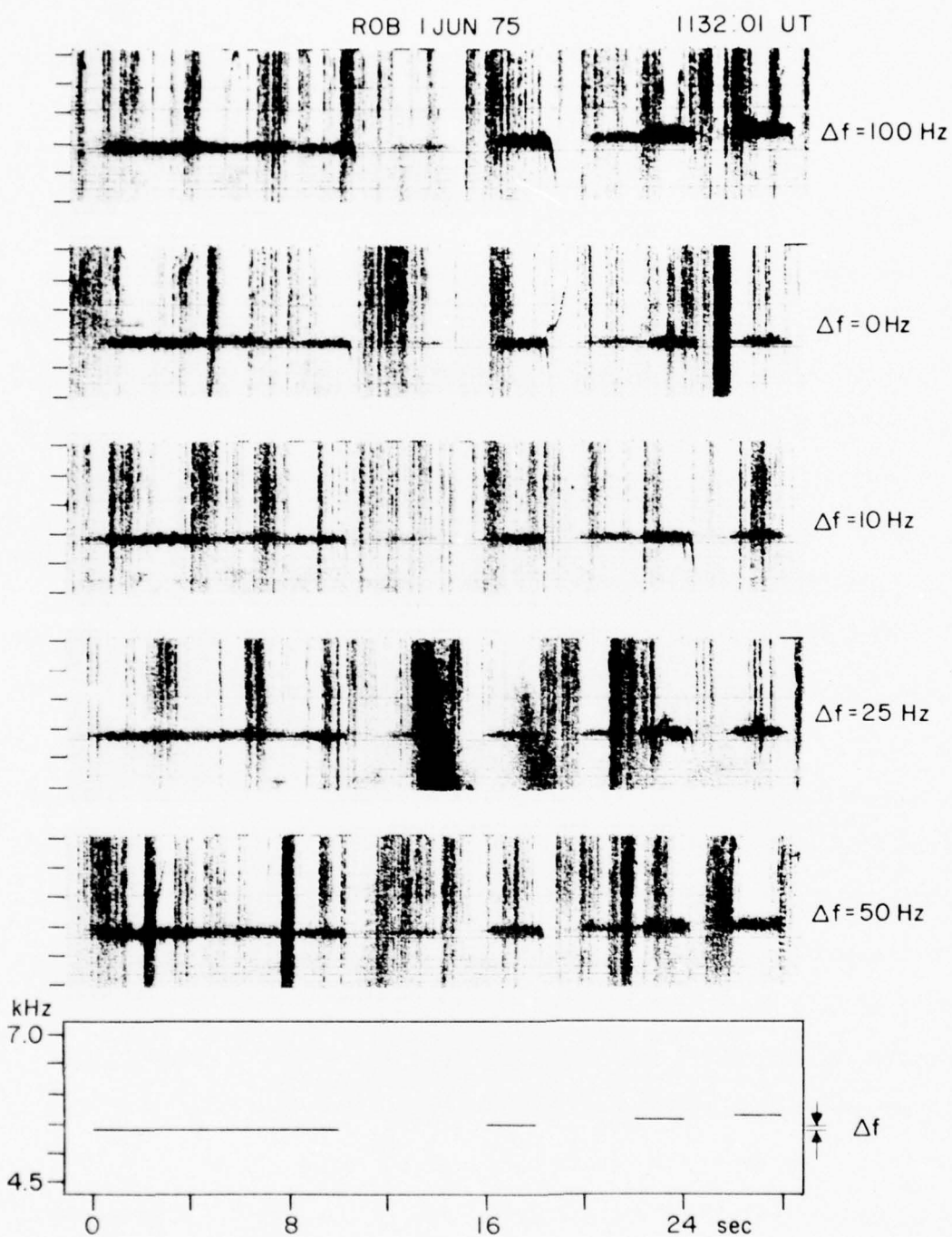


FIGURE 2.6 ECHO-INDUCED SUPPRESSION WHEN SUCCESSIVE PULSES ARE STEPPED UP IN FREQUENCY. The transmitter program is shown in the bottom panel, with the time scale corrected to allow for the one-hop travel time. The parameter, Δf , is varied as shown. The last pulse is weaker because of echo-induced suppression for all values of Δf . Three-hop echoes are clearly visible on these spectrograms.

fourth pulse, suppressing its growth. The bandwidth of these signals is typically more than 100 Hz, thus providing a sufficient spread in the echoing components to account for suppression at each value of Δf . The fourth pulse is suppressed for all values of Δf , although the spectrogram does not show this very convincingly. Figure 2.7 shows the same data in the form of amplitude versus time plots. Suppression in the fourth pulse is seen for all values of Δf , the magnitude being about 9 dB. Although there is growth, the triggering on this day (see also Fig. 2.2) is less than in Figs. 2.1, 2.3, and 2.4. This may be caused by the multi-hop echoes of earlier transmissions (below the threshold of detection here) suppressing the emissions rising in frequency.

Figure 2.8 gives another example of the broadband nature of the signals during echo-induced suppression. A sine wave in frequency (upper panel) was transmitted with a period of 4 s. The alternating light and dark portions seen on the Roberval spectrogram (lower panel) are caused by echo-induced suppression. The prominent two-hop travel time was 4.4 s which is greater than the period of the sine wave. The three-hop echoes therefore travel with direct signals at a slightly different frequency. The fact that echo-induced suppression still occurs is evidence that the spectrum of the echo was broadened.

D. SOME EXTENSIONS AND IMPLICATIONS OF ECHO-INDUCED SUPPRESSION

The suppression of transmitter signals by whistlers reported earlier by Helliwell and Katsufrakis [1974] bears a strong resemblance to echo-induced suppression. The two effects often occur together and the mechanism of growth inhibition appears to be the same. Figure 2.9 shows a long pulse at 3.75 kHz displaying both effects. The upper

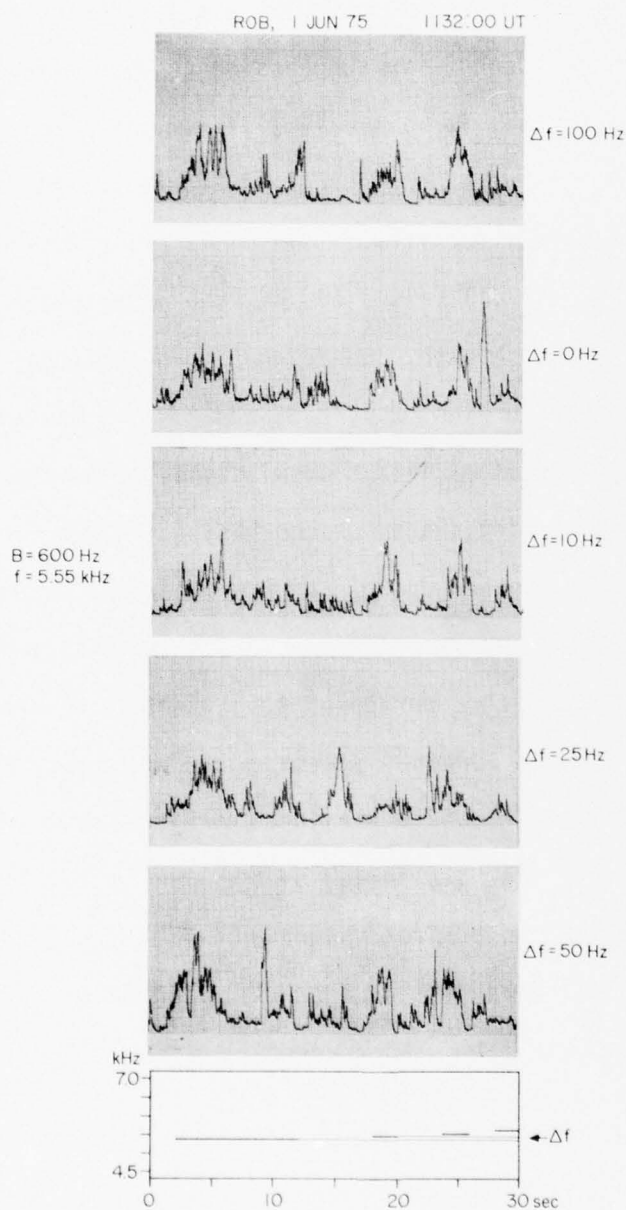


FIGURE 2.7 THE RESULTS OF FIG. 2.6 ARE SHOWN IN THE FORM OF AMPLITUDE VERSUS TIME PLOTS. The last pulse, the start of which is marked by the arrows, is again seen to be weaker for all values of Δf . From 6 s echo-induced suppression in the 10 s pulse is seen. The variations in amplitude of the pulses is far greater than variations in the filter response over its 600 Hz bandwidth.

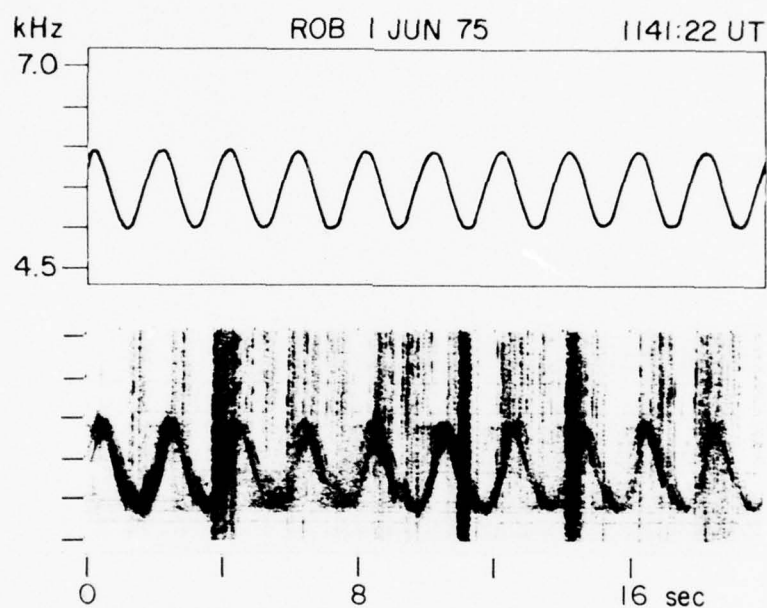


FIGURE 2.8 A SINE WAVE IN FREQUENCY SHOWING ECHO-INDUCED SUPPRESSION IN THE FORM OF ALTERNATE STRONG AND WEAK PORTIONS. The upper panel shows the transmitted signal with a one-hop travel time taken into account. The distortion of the sine wave in the spectrogram is partly due to multipath propagation and partly due to triggering of emissions.

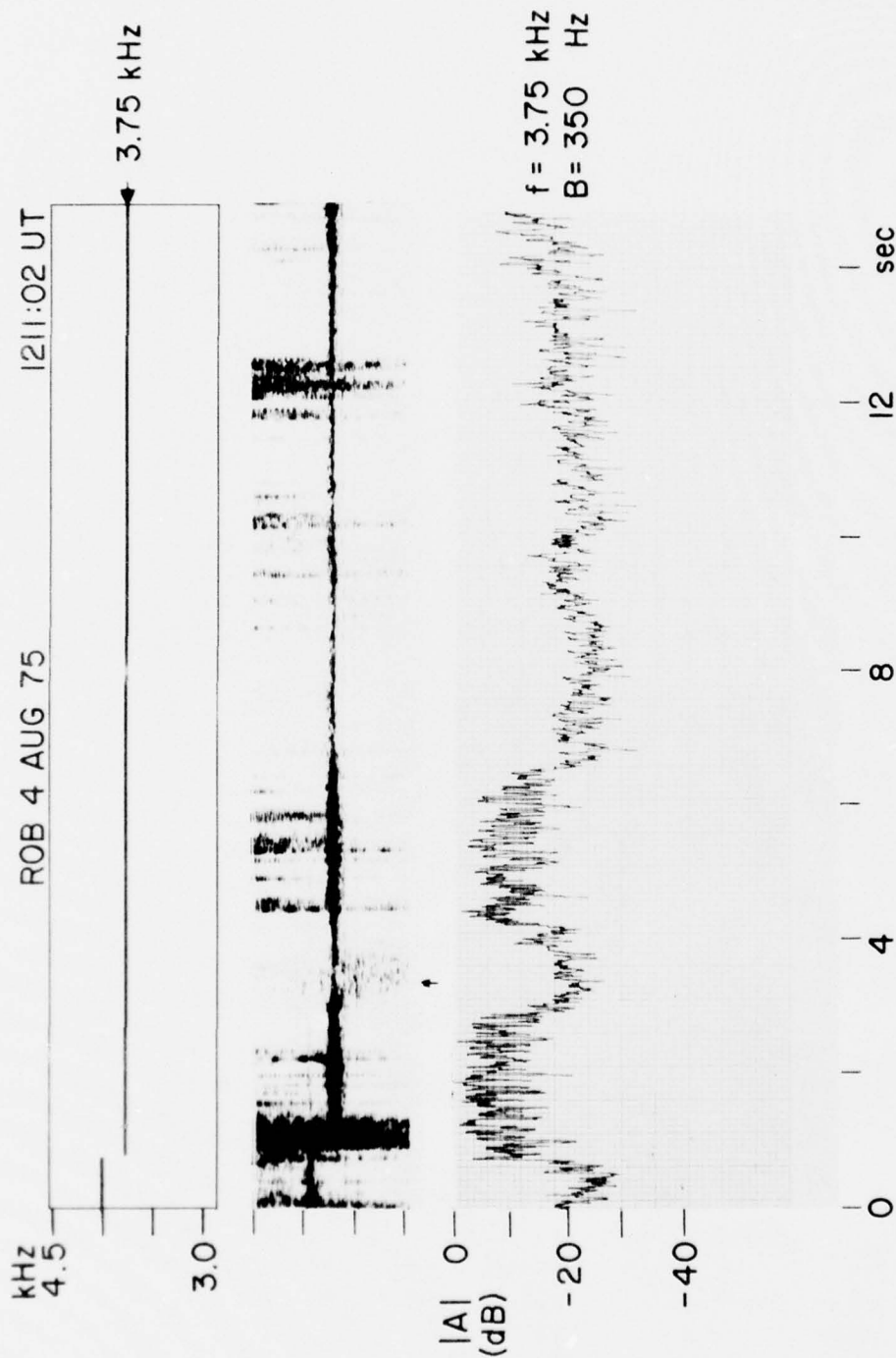


FIGURE 2.9 WHISTLER INDUCED SUPPRESSION AND ECHO-INDUCED SUPPRESSION ARE SEEN TO OCCUR TOGETHER. The top panel shows the transmitter program corrected for the one-hop travel time. Both the spectrogram and amplitude plot show suppression caused by a diffuse whistler between 3 and 4 s marked by an arrow. Echo-induced suppression occurs at 6.6 s. The partial recovery at 9 s is related to the whistler-induced suppression and the two events are separated by the two-hop travel time.

panel shows the transmitter format as it would be seen at Roberval. The middle panel is a Roberval spectrogram and the bottom panel an amplitude plot on a dB scale. The drop in amplitude at 6.6 s is due to echo-induced suppression, while that from 3 to 4.2 s is due to whistler-induced suppression. The whistler indicated by an arrow can be seen clearly though faintly on the spectrogram. Because of path mixing, the whistler appears as a diffuse noise burst, lasting about a second, instead of a discrete trace. (Path mixing is described in greater detail in Chapter 4.) The third-hop echo of the portion of signal between 2 and 4.2 s is weaker and does not suppress as effectively. This accounts for the partial recovery in amplitude at 9 s. The two suppression effects frequently are observed together, as in this case. They are probably governed by the same mechanism, with the diffuse whistlers playing the role of the transmitter signal echo.

Figure 2.10 shows another case of echo-induced suppression along with some anomalous triggering effects which appear related. The transmitting format is shown below the spectrograms with the one-hop travel time taken into account. In (a) each of the three 10 ms pulses shows a reduction in amplitude after 5.5 s because of echo-induced suppression. What is more interesting is a noise band, 500 Hz wide that appears at times when the transmitter signal is weak. In (b) the same noise is observed. It disappears in the period of partial recovery of the transmitter signal. At first sight it seems that the noise band somehow inhibits the transmitter signal or vice versa. Unfortunately, conjugate data from Siple Station are not available during periods of transmission. However the two hop echoes received later during breaks in the transmission (for example, at 0635 UT and 0655 UT) showed the noise as

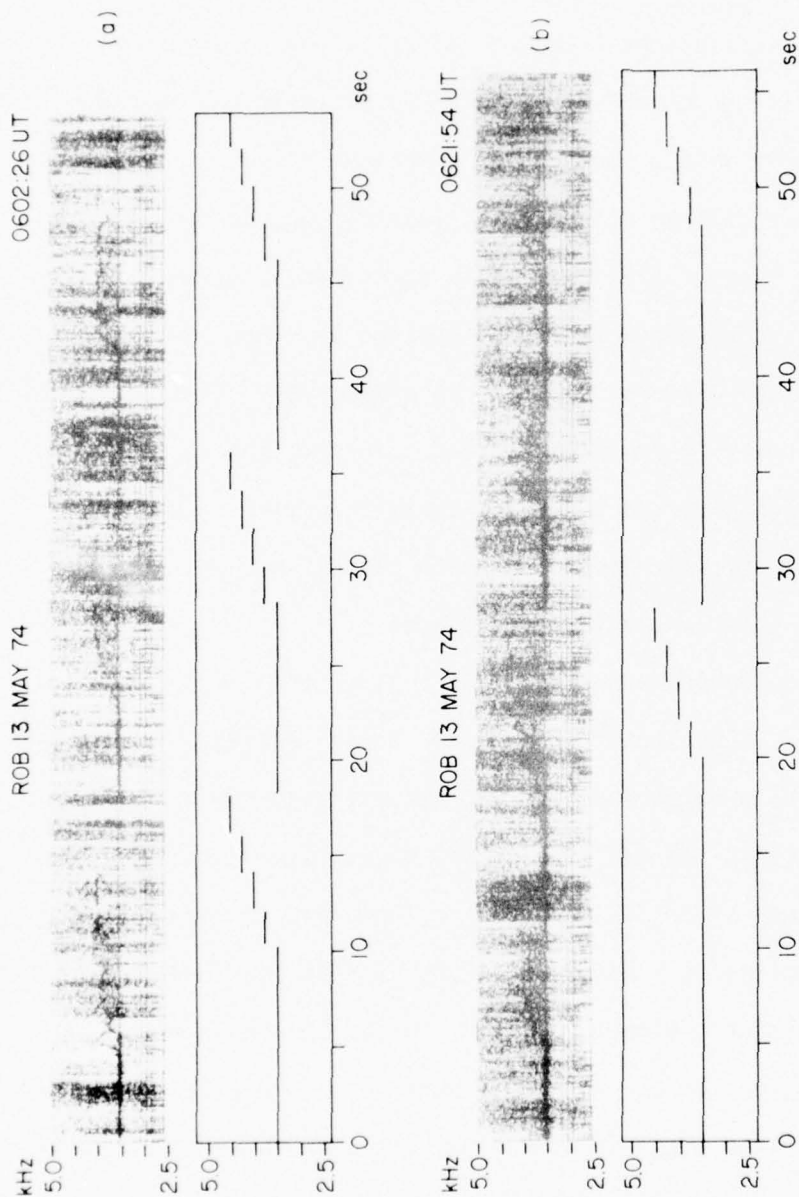


FIGURE 2.10 SPECTROGRAMS SHOWING A CASE OF ASYMMETRICAL TRIGGERING ALONG WITH ECHO SUPPRESSION. The transmitter format in both (a) and (b) is shown below the spectrograms. Echo suppression is seen in the form of a reduction in amplitude 5.5 s from the start of the long 10 s and 20 s pulses. Noise, 500 Hz wide, is triggered above the transmitter frequency only when the transmitter signal is suppressed. This is because triggering occurs when signals travel from Roberval to Siple Station and not in the other direction. In (b) the noise is absent during periods of partial recovery due to the inability of the preceding suppressed signals to trigger on the way back to Siple Station.

well as the uninhibited signal at the transmitter frequency at the same time. The inference to be drawn, then, is that waves traveling towards Roberval do not trigger emissions, while waves traveling in the opposite direction do. The noise band was therefore seen at Roberval only after an initial two-hop whistler mode delay. The absence of the noise band during the periods of partial recovery of the transmitter signal in (b) is related to echo-induced suppression. Suppressed portions of the pulse on the way back to Siple Station are too weak to trigger emissions.

Apart from the echo-induced suppression effects, this record is of special interest because transmitter signals triggered noise while traveling along a duct one way and not the other. A possible explanation is that a minimum wave amplitude was needed to trigger this noise and that the transmitter signals reached this level only after one pass through the magnetosphere. This would mean that there is no asymmetry in susceptibility to triggering, but only in the location of the transmitter.

Echo-induced suppression is a natural means of regulating the growth process in the magnetosphere. If the amplification increases, the echoes get stronger and thereby reduce the amplification. In addition, the amplitude of the echoes is regulated whatever the conditions for echoing are. At times of relatively good echoing the growth of the direct signal is suppressed and the amplitude of the echoes is thereby decreased. When echoing conditions are poor there is less suppression and hence increased amplification of the direct signal. Echo-induced suppression, therefore, provides a form of automatic gain control for narrowband VLF waves in the magnetosphere. It is interesting to compare these findings with the predictions of the quasi-linear theory described by Kennel and Petschek [1966] in connection with natural VLF

broadband hiss. In their model the output signal increases with increased reflection coefficient. They therefore require a consequent reduction in trapped particle flux to limit wave growth. Echo-induced suppression, on the other hand, suggests that waves can limit their own growth as a result of the echoing process and that modification of particle fluxes need not be invoked. This is definitely true for the relatively coherent narrowband waves described here and might even apply to the broadband hiss considered by Kennel and Petschek [1966].

Echo-induced suppression can take place only if the three-hop echo and the direct signal are traveling along the same or closely adjacent paths. This is consistent with the model for ducted propagation described by Smith [1960, 1961].

E. SUMMARY OF RESULTS

A new magnetospheric wave-particle interaction phenomenon called echo-induced suppression has been described. Whistler mode echoes of VLF transmitter signals are observed to suppress the growth of the direct signals. The important characteristics and some of the implications of this echo-induced suppression are summarized below.

(1) Echo-induced suppression is a relatively frequent phenomenon. It occurs on at least a third of the days on which transmitter signals are detected at Roberval.

(2) The suppression is not due to linear wave-wave interference. This is evident from the consistent suppression in every pulse as in Fig. 2.4. The explanation is related to the nonlinear wave-particle interaction process.

(3) Echo-induced suppression must occur at the input to the ampli-

fication region where the echo and the direct signal are expected to have comparable amplitudes.

(4) During periods of echo-induced suppression, any unsuppressed first hop signals and their echoes show spectral broadening at frequencies predominantly above the transmitter frequency. The broadband nature of the echo reduces the coherence of the direct signal, thereby reducing its growth. Linear plasma instability theories do not predict echo-induced suppression, as described in detail in the next chapter.

(5) Quasi-linear theories such as that of Kennel and Petschek [1966] require interaction between the waves and the trapped particle flux to limit wave growth. Echo-induced suppression indicates that waves can regulate their own growth through the echoing process.

(6) Echo-induced suppression is consistent with the ducting model described by Smith [1960; 1961].

In short, echo-induced suppression is fundamental to an understanding of wave particle interactions in the magnetosphere; other phenomena such as whistler-induced suppression appear related. It may even play a role in VLF communications. For example it could be used selectively to suppress the magnetospheric component by equating the time between pulses to the two-hop travel time. For magnetospheric studies suppression can be avoided by preventing overlaps of the direct signal and the echo. Echo-induced suppression also brings out the importance of controlled VLF signals for magnetospheric studies as it probably would not have been discovered by other means.

III. AN INTERPRETATION OF ECHO-INDUCED SUPPRESSION

A. INTRODUCTION

In the last chapter several characteristics of echo-induced suppression were described. An interpretation, based on these characteristics, is offered here. It must first be emphasized that there is still some doubt as to the nature of the amplifying mechanism for VLF waves in the magnetosphere. It is generally believed that the mechanism depends on doppler shifted cyclotron resonance between electrons and waves. However, beyond that there is no general agreement [Helliwell and Crystal, 1973; Kennel and Petschek, 1966; Nunn, 1974]. It is therefore not the intention here to give a complete theory for a more complicated phenomenon such as echo-induced suppression, even though the study of the data helps in the interpretation.

The key to an explanation seems to be the presence of additional frequencies just above the transmitter frequency. As shown earlier, the echoes also contain these additional frequency components, which appear to suppress the growth of the transmitter signal. The combination of echo and direct signal is less coherent than the direct signal alone. It has a coherence time roughly equal to the reciprocal of its bandwidth. If this time is less than the time required to organize the particles to produce amplification, then suppression is seen. More specifically, it is shown in this chapter that the phase bunched currents required for amplification in the model developed by Helliwell and Crystal [1973] are reduced when the coherence time is less than the bunching time.

Quite often linear plasma instability theory is used to predict

growth (e.g. Kennel and Petschek [1966]; Liemohn [1967]). An imaginary frequency or wave number is calculated from the dispersion relation. Such an approach was not considered suitable here for a variety of reasons. For example, in the linear theory the presence of additional frequency components would not in any way affect the growth of the transmitter signal. The different frequencies would grow independently and though there would be beating, there would be no reduction in amplitude. Therefore a nonlinear approach is followed here. Helliwell and Crystal [1973] (see also Nunn [1974]; Dysthe [1971]) showed that nonlinear phase bunched currents are produced by monochromatic whistler mode waves. These currents then produced wave growth through a feedback process. Calculations described here show that VLF waves of a finite bandwidth produce reduced phase bunched currents thereby inhibiting growth.

The development of linear theory from cold plasma dispersion relations is described in the next section. Then the monochromatic model of Helliwell and Crystal [1973] and its modification due to the presence of more than one frequency are discussed. Finally some possible explanations are offered for the generation of components at additional frequencies by a monochromatic whistler mode signal with a distribution of wave normal angles.

B. LINEAR THEORY SEEN AS AN EXTENSION OF COLD PLASMA THEORY

It is instructive to consider cold plasma small signal theory before going into how amplification (or damping) can be predicted from hot plasma linear theory. In cold plasma theory the electrons and ions are considered to be stationary in the absence of time-varying electric and magnetic fields. They are perturbed only very slightly by a wave.

Their excursions in space are directly proportional to the amplitude of the wave but 90° out of phase with the electric field. Consider the Maxwell's equation

$$\nabla \times \underline{H} = \underline{J} + \frac{\partial \underline{D}}{\partial t} = \underline{J} + \epsilon_0 \frac{\partial \underline{E}}{\partial t} \quad (3.1)$$

If only small perturbations are considered then the problem can be linearized, i.e., terms involving products of the perturbations can be neglected. This enables one to obtain solutions using Fourier or Laplace transforms more easily. Transforming Eq. (3.1) in space and time:

$$\underline{k} \times \underline{H} = i \underline{J} - \omega \epsilon_0 \underline{E} \quad (3.2)$$

where

$$\underline{J} = \rho_0 \underline{v}$$

The velocity \underline{v} is calculated from the usual equation of motion for a charged particle, excluding second-order quantities, which is

$$i\omega m \underline{v} = q (\underline{E} + \underline{v} \times \underline{B}_0) \quad (3.3)$$

where

\underline{B}_0 = static magnetic field

\underline{E} = electric field of the wave and

q = charge of the particle.

After putting \underline{v} from Eq. (3.3) into Eq. (3.2) and using the Maxwell's equation involving $(\underline{k} \times \underline{E})$ we arrive at the dispersion relation. The refractive index is calculated for the various modes from the dispersion relation. In the absence of collisions, it is found that the refractive index is either purely imaginary or real. The former corre-

sponds to evanescent waves and the latter to undamped plane wave propagation. In either case there is no energy transfer between the wave and the particles.

For a cold plasma, in the absence of collisions, every component of \underline{J} in Eq. (3.2) has a 90° phase shift with respect to the corresponding component of \underline{E} . Otherwise the refractive index $(= \frac{ck}{\omega})$ would be complex. The whistler mode is a right hand circularly polarized wave for propagation parallel to the static magnetic field. The electric and magnetic field vectors rotate in the same direction as the thermal electrons. Thus the polarization is right handed or clockwise only if one is looking in the direction of the static magnetic field. Figure 3.1 shows the relation between the various field vectors and the currents. The cold plasma current, J_c , is in the same direction as the displacement current and is therefore usually taken into account by defining an equivalent permittivity. The cold plasma, for the whistler mode, behaves like an anisotropic dielectric whose dielectric constant is a function of frequency.

Cold plasma theory has been extremely successful in describing wave propagation in the magnetosphere and ionosphere. The inclusion of ion motions gives many resonances, cutoffs and crossovers, most of which have been observed in waves received on satellites or on the ground. Proton whistlers, helium whistlers, ion cutoff whistlers, subprotonospheric whistlers, etc. have been explained by these effects (e.g., Gurnett et al. [1965]; Muzzio [1968]; Raghuram [1975]).

Linear plasma instability theory, in a way, is an extension of cold plasma theory to hot plasmas. The calculation of \underline{J} in Eq. (3.2) is more complicated because the particles are initially in motion. A dis-

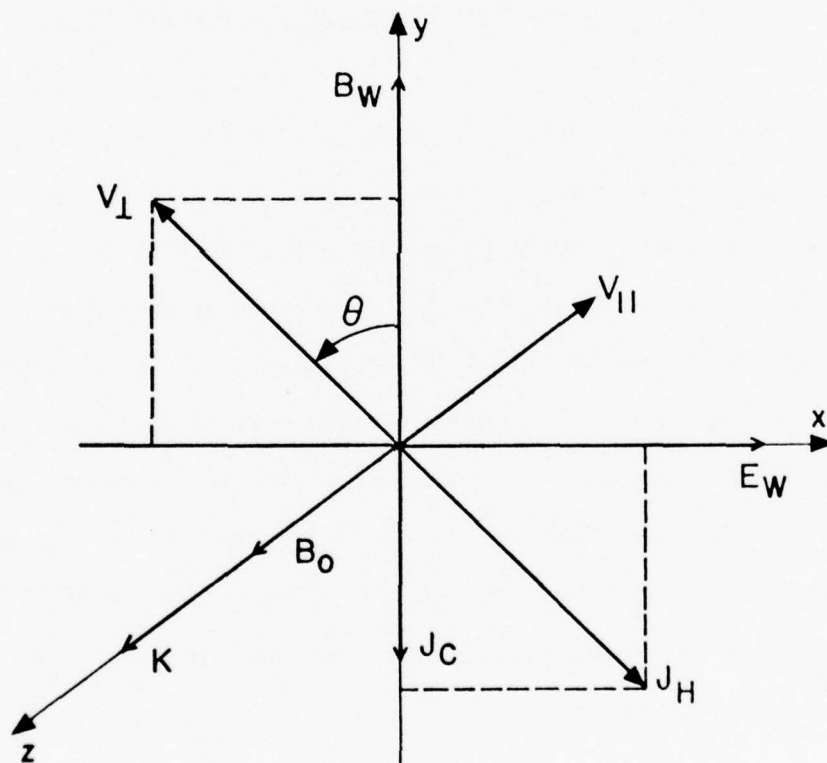


FIGURE 3.1 RELATION BETWEEN VARIOUS VECTORS IN WAVE PARTICLE INTERACTION.

tribution function is assumed and the currents are calculated from the perturbation of the distribution function, using the Boltzmann-Vlasov equation. The current could then have a component in phase or out of phase with the electric field, depending on the distribution function. An in-phase current would cause damping and an out of phase current growth. This damping is the classical collisionless cyclotron damping. If growth is predicted then the plasma is said to be unstable. The instability can be convective or absolute (for a more detailed discussion of these two instabilities see Stix [1962] or Clemmow and Dougherty [1969]).

The major virtue of linear theory is that it is an extension of the well tested cold plasma theory. However, there are at least two major problems in using linear theory to explain the data shown in the last chapter. The first is that in linear theory the growth rate at a particular frequency is unaffected by the presence of signals at other frequencies. This would make it hard to explain echo-induced suppression, which appears to be due to the presence of additional frequency components. Another problem is that it is hard to account for triggered noise and emissions using this theory. For these reasons echo suppression is explained on the basis of a nonlinear model developed by Helliwell and Crystal [1973].

C. REDUCED PHASE BUNCHED CURRENTS IN THE PRESENCE OF WHISTLER MODE ECHOES

The nonlinear model used here is only briefly described and the reader is referred to Helliwell and Crystal [1973] for more details. A homogeneous magnetosphere, with monochromatic whistler mode waves traveling parallel to the earth's magnetic field is assumed. Electrons which

satisfy the doppler shifted cyclotron resonance condition alone are considered. The phases of twelve electrons equally distributed initially in cyclotron phase are followed as shown in Fig. 3.2. (B_{\perp} is used instead of B_w in this figure reproduced from Helliwell and Crystal [1973]). These electrons are perturbed in the longitudinal direction by the $q(\mathbf{v}_{\perp} \times \mathbf{B}_w)$ force. This leads to a phase bunching of the electrons as described in Brice [1964] and shown in Fig. 3.2. The phase bunching produces a net current in the direction of \mathbf{B}_w .

There are some very fundamental differences between this current and the currents described in linear theory. This current is nonlinear, i.e., it is not directly proportional to the amplitude of the wave. Although it is in the same direction as the cold plasma current, it is much smaller in magnitude. In linear theory any currents due to the hot plasma in quadrature with \mathbf{E} are not considered because they do not cause growth or damping, but only insignificantly modify the refractive index. The nonlinear current generated in the Helliwell and Crystal [1973] model is treated as a source current which radiates a new wave coherent in the $+z$ direction. This combines with the old wave causing it to grow. A feedback calculation is shown in Helliwell and Crystal [1973] which takes into account the changes in wave amplitude and phase along the path of propagation.

The model, without feedback, is extended here to include non-monochromatic waves. As stated earlier, echo-induced suppression is believed to be due to the presence of additional frequencies in the echo. It will be shown that the nonlinear currents generated are smaller when additional frequencies are introduced. The case considered here is that of waves at two frequencies spaced 50 Hz apart and initially in phase.

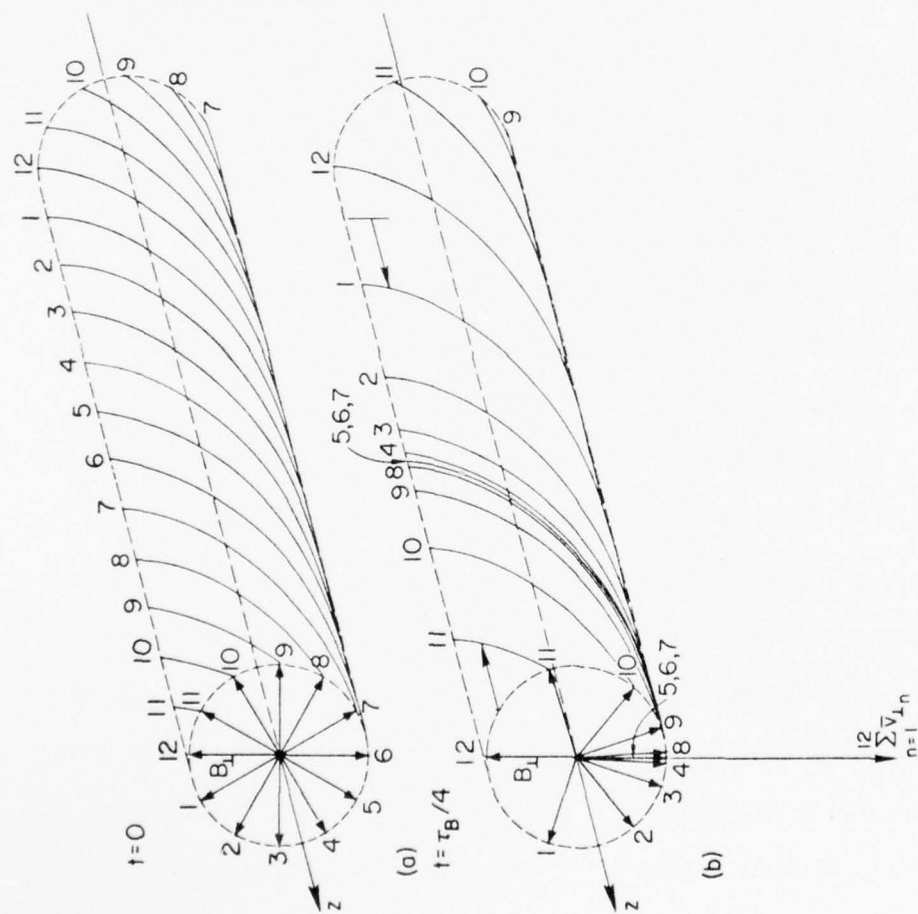


FIGURE 3.2 HELICAL LOCI OF THE PERPENDICULAR VELOCITIES OF 12 ELECTRONS INITIALLY EQUALLY DISTRIBUTED IN CYCLOTRON PHASE: (a) before bunching; (b) after some bunching (after Helliwell and Crystal [1973]).

The equations that govern the motion of an electron in the presence of two whistler mode waves traveling along the earth's magnetic field are derived in the Appendix. A homogeneous magnetosphere is assumed. Let $v_{||}$ and v_{\perp} denote the velocity of an electron parallel and perpendicular to the magnetic field respectively. Also let ω_1 , k_1 , B_{w1} , and E_{w1} be the angular frequency, propagation constant, magnetic field, and electric field, respectively, of the first wave. B_{wr} , E_{wr} are the instantaneous amplitudes of the sum of the waves at the two frequencies; θ = cyclotron phase angle between B_{w1} and v_{\perp} , measured anticlockwise from B_{w1} as shown in Fig. 3.3; $\dot{\theta}$ = angular velocity of the electrons; ψ = phase angle between B_{wr} and B_{w1} ; ψ' = phase angle between E_{wr} and E_{w1} ; B_{wr} and ψ are, in general, functions of time. The angle θ must be found to calculate the phase bunched current.

From Eq. (A.5)

$$\ddot{\theta} = k_1 \dot{v}_{||} = \frac{e}{m} k_1 B_{wr} v_{\perp} \sin(\psi + \theta) \quad (3.4)$$

Before considering the solution of this equation, a few observations can be made. The phase θ of the electron is measured with reference to the magnetic field of the wave with frequency ω_1 . This choice was made rather arbitrarily and sometimes it might be more useful to use some other reference. Also, two initial conditions need to be specified. One is the initial cyclotron phase θ of the electron. The second is the initial $\dot{\theta}$, which indicates how much off-resonance the electron initially is with respect to the wave with frequency ω_1 . The movement of any electron can be solved for by choosing the appropriate initial conditions. It is also instructive to consider some special cases.

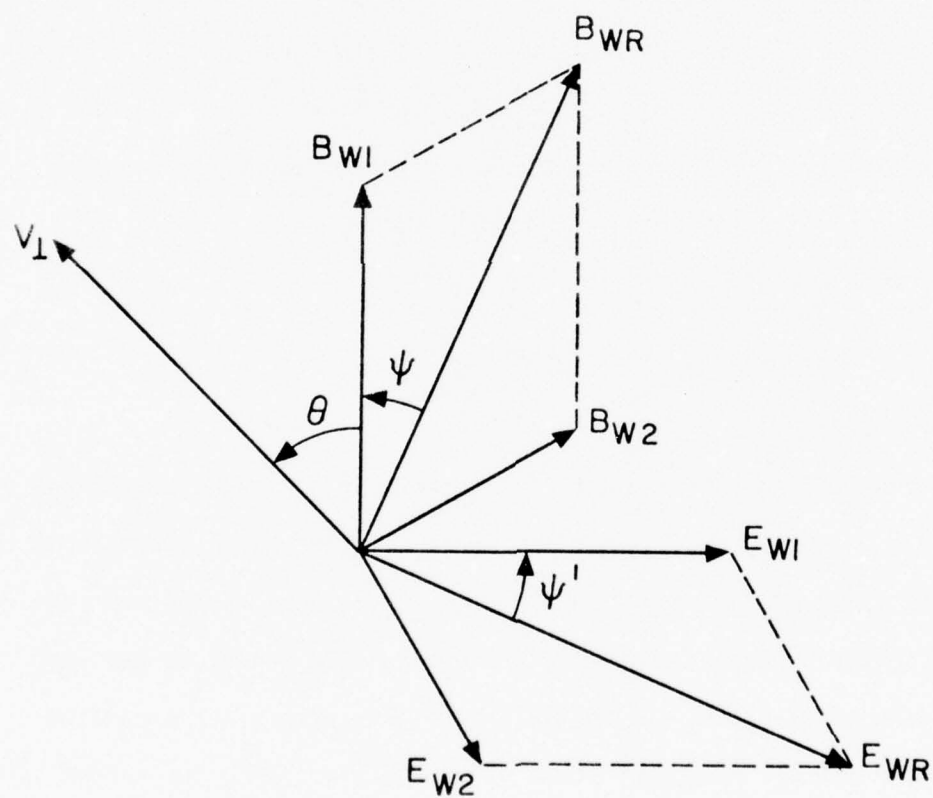


FIGURE 3.3 RESULTANT VECTORS DUE TO THE PRESENCE OF TWO WAVES.

For the monochromatic case $B_2 = 0$. Therefore $B_{wr} = B_1$ and $\psi = 0$.

Equation (3.4) then becomes

$$\ddot{\theta} = k_1 v_{\perp} \frac{e}{m} B_1 \sin \theta$$

which is the equation solved in Helliwell and Crystal [1973]. There $\dot{\theta}(0)$ was equal to zero corresponding to electrons initially in exact resonance and $\theta(0)$ was varied from 0 to 360° in steps of 30°.

It can be shown now that the bunching current is considerably less for the case of two frequencies separated by 50 Hz than for the monochromatic case. Figure 3.4 shows the results with the monochromatic phase bunched current reproduced from Helliwell and Crystal [1973]. The L value was 3 and the gyrofrequency and plasma frequency were 33 kHz and 180 kHz respectively. For the monochromatic case the frequency was 16.5 kHz which was also the upper frequency for the two frequency case. The wave amplitude for the monochromatic case was 1 mV. The waves at both the frequencies for the two frequency case each had the same amplitude of 1 mV. In both cases twelve electrons with initial phases varying from 0 to 360° in steps of 30° were considered. For the monochromatic case $\dot{\theta}(0)$ was simply chosen to be zero corresponding to exact resonance. For the two frequency case $\dot{\theta}(0)$ was chosen such that the initial parallel velocity satisfied the condition

$$\left(\frac{\omega_1 + \omega_2}{2}\right) - \left(\frac{k_1 + k_2}{2}\right) v_{\parallel}(0) = \Omega \quad (3.5)$$

This corresponds to an electron at resonance with a fictitious wave having $\omega = \frac{\omega_1 + \omega_2}{2}$ and $k = \frac{k_1 + k_2}{2}$. This value for $\dot{\theta}(0)$ has the advantage that variations in θ are symmetric about $\theta = 180^\circ$ if θ is

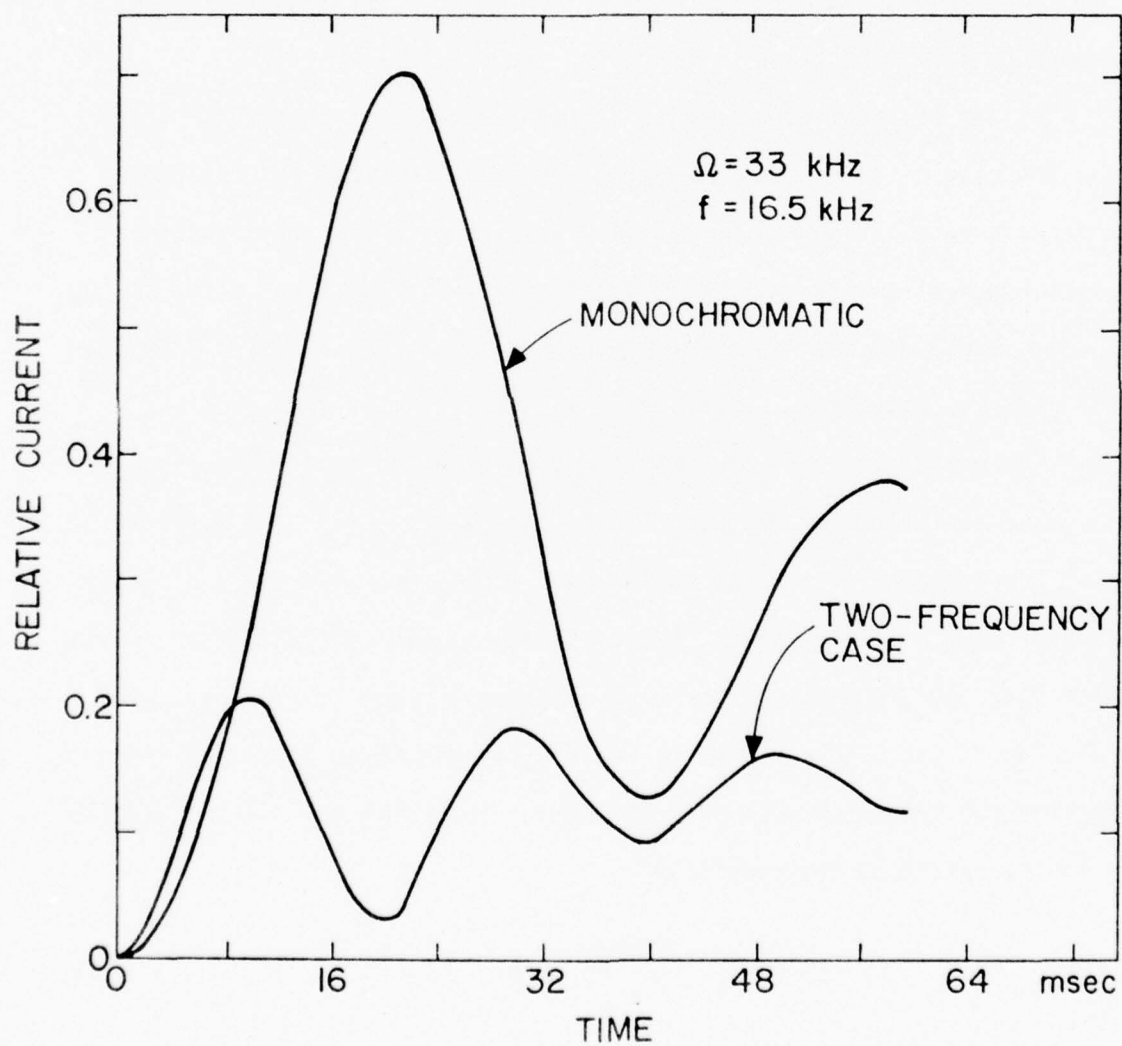


FIGURE 3.4 PHASE BUNCHED CURRENTS FOR THE TWO FREQUENCY CASE COMPARED WITH THE MONOCHROMATIC CASE.

measured with respect to this wave. Thus, Eq. (3.4) needs to be solved only for six values of $\theta(0)$ instead of twelve. Figure 3.4 shows that the phase bunched current for the monochromatic wave is 3.5 times greater considering only the peaks.

It is easy to see why this is so. The resultant wave magnetic field, which is due to the beating of the two waves changes phase by 180° when it passes through zero amplitude. The electrons are therefore phase bunched first one way and then the other with no net phase bunching. Figure 3.5 shows θ as a function of t for the monochromatic case (reproduced from Helliwell and Crystal [1973]) and the two frequency case. Curves starting in the top half, i.e., $180^\circ < \theta(0) \leq 360^\circ$, correspond to the monochromatic case, while curves starting in the bottom half correspond to the two frequency case. Only one half is shown for each case as both sets of curves are symmetric about $\theta = 180^\circ$. While the phases of all electrons for the monochromatic case converge to $\theta = 180^\circ$ around 18 ns, the phases for the two frequency case just oscillate near the initial value with very little phase bunching.

The calculations described above should be done for a continuous spectrum about 100 Hz wide to accurately represent the combined input consisting of the echo and the direct signal. The nature of the spectrum would then determine how much the phase bunched current is reduced. In general, this depends on the coherence time of the input signal which varies roughly as the reciprocal of its bandwidth. In Fig. 3.5 the time required for phase bunching for the monochromatic case is around 18 ns. Therefore, one would expect a significant reduction in the bunching current if the coherence time were less than this value. As Figs. 3.4 and 3.5 indicate, phase bunching takes place even after the initial bunching

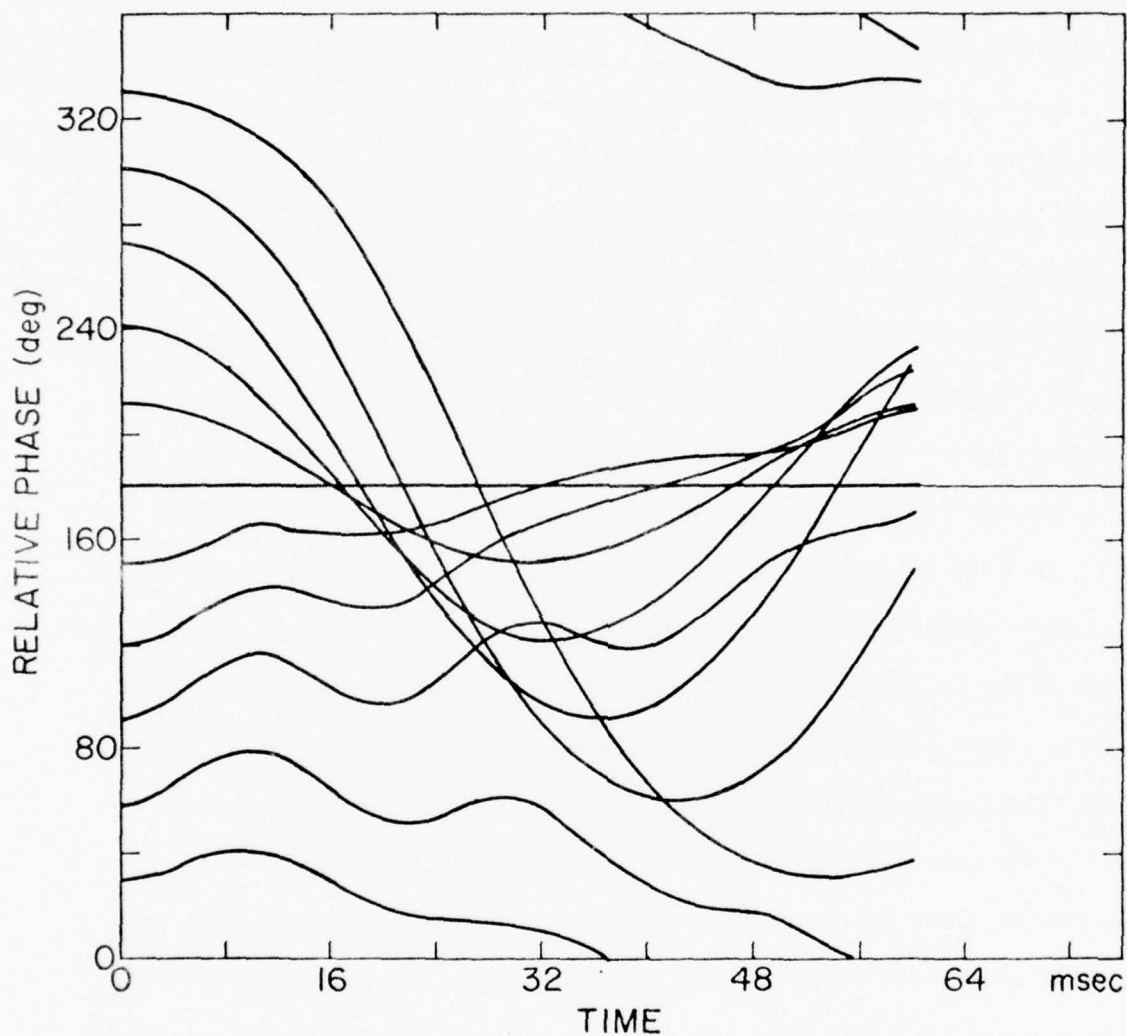


FIGURE 3.5 VARIATION IN THE PHASE ANGLE θ BETWEEN THE PERPENDICULAR VELOCITY AND WAVE MAGNETIC FIELD. Curves starting in the upper half ($180^\circ < \theta < 360^\circ$) correspond to the monochromatic case while curves starting in the lower half correspond to the two frequency case. Both sets of curves are symmetrical about the $\theta = 180^\circ$ line. The two waves for the two frequency case were separated by 50 Hz and each had an amplitude of 1 mV. Note that there is very little phase bunching for the two frequency case.

period. Even if the coherence time is larger than the bunching period but less than the total interaction time, some reduction will take place. The bunching period is roughly inversely proportional to the square root of the wave amplitude and the interaction time is dependent on the L value [Helliwell, 1967]. Thus, for a given magnetosphere, the factors that determine the level of echo-induced suppression are the wave amplitude, the nature of the spectrum and the L value along the path of propagation.

The total transverse current is obtained by summing over all initial parallel velocities and pitch angles. The summation over parallel velocities is more important as particles of all pitch angles with the same v_{\parallel} behave qualitatively in the same way. An anomaly in the calculation done above is then resolved. From what has been said, the greater the separation between the two frequencies, the smaller the current. This is not true for large separations as the two monochromatic waves would then interact with different electrons and be amplified independently. As the frequency spacing Δf increases, the current contribution from electrons initially resonant with the intermediate frequency wave decreases. However, beyond a certain critical spacing the increased current contribution from electrons near resonance at the two frequencies more than compensates for this decrease. There is therefore a frequency spacing for which the total transverse current is a minimum. Roughly speaking, two waves will not affect each other if their frequencies are separated by much more than this critical value. For example, in Fig.2.2 the echoes at 5.9 kHz do not suppress transmissions at 5.65 kHz near $t = 34$ s.

Echo-induced suppression takes place when an echo has components within a certain interaction bandwidth around the transmitter signal. An approximate calculation for the interaction bandwidth can be made considering the echo and the direct signal to be monochromatic waves spaced Δf apart. Let Δf_{Te} and Δf_{Td} represent the maximum possible off-resonance frequency for trapped electrons interacting with the echo and direct signal respectively. Then the maximum value for Δf for which echo-induced suppression occurs is given by

$$\Delta f_{\max} = \Delta f_{Te} + \Delta f_{Td}$$

This value of Δf is then the interaction bandwidth. The maximum possible off resonance frequency for trapped electrons is also equal to twice the small amplitude oscillation frequency, $\overline{\Delta f}$ [Crystal, 1975; Brinca, 1972b]. Therefore the interaction bandwidth is given by

$$\Delta f_{\max} = \Delta f_{Te} + \Delta f_{Td} = 2(\overline{\Delta f}_e + \overline{\Delta f}_d)$$

At $L = 3$, $\overline{\Delta f} = 16$ Hz for a 1 mV wave and 30° pitch angle electrons. If the echo and the direct signal each have an amplitude of 1 mV, $\Delta f_{\max} = 64$ Hz. In other words, a transmitter signal would be suppressed by echoes having components within 64 Hz of the transmitter frequency.

Helliwell and Crystal [1973] show how wave amplification takes place through a feedback process because of the phase bunched transverse currents. Nunn [1974] shows that this current is rotated in phase by the inhomogeneity in the magnetosphere and can develop a component opposite to the wave electric field. The electrons then lose energy to the wave even if feedback is not considered. It is not the object of this work to explain amplification through phase bunched currents but

merely to show that phase bunched currents are reduced in the presence of a less coherent wave as compared to a monochromatic wave. Consequently, any mechanism for amplification which depends on phase bunched currents would predict an inhibition of amplification or growth.

It has been assumed above that all waves are traveling parallel to the earth's magnetic field. The echoes which are reflected at the base of the ionosphere will, in general, have larger wave normal angles than the direct signals. This is because waves with larger wave normal angles fall outside the transmission cone and are more likely to be reflected [Helliwell, 1965]. Waves at different wave normal angles at a given frequency resonate with particles of different parallel velocities. The larger wave normal angles of the echoes at the transmitter frequency could therefore be responsible for the suppression. The effect of the two plane waves at the same frequency but with slightly different wave normal angles would be the same as that of two waves at slightly different frequencies but with the same wave normal angle.

D. PROPAGATION AT NON-ZERO WAVE NORMAL ANGLES

Most of the literature on wave-particle interaction deals with whistler mode waves traveling parallel to the earth's magnetic field. This leads to a considerable simplification of the algebra. Further, since whistler mode waves received on the ground are believed to be ducted, the wave normal angles are small anyway. Work by Brinca [1972a] and Kennel [1966] showed that nothing very new or drastic could result from non-zero wave normal angles. However, the literature on this subject has failed to exploit the variation in the wave number k with wave normal angle α at a given frequency. Stated differently, the

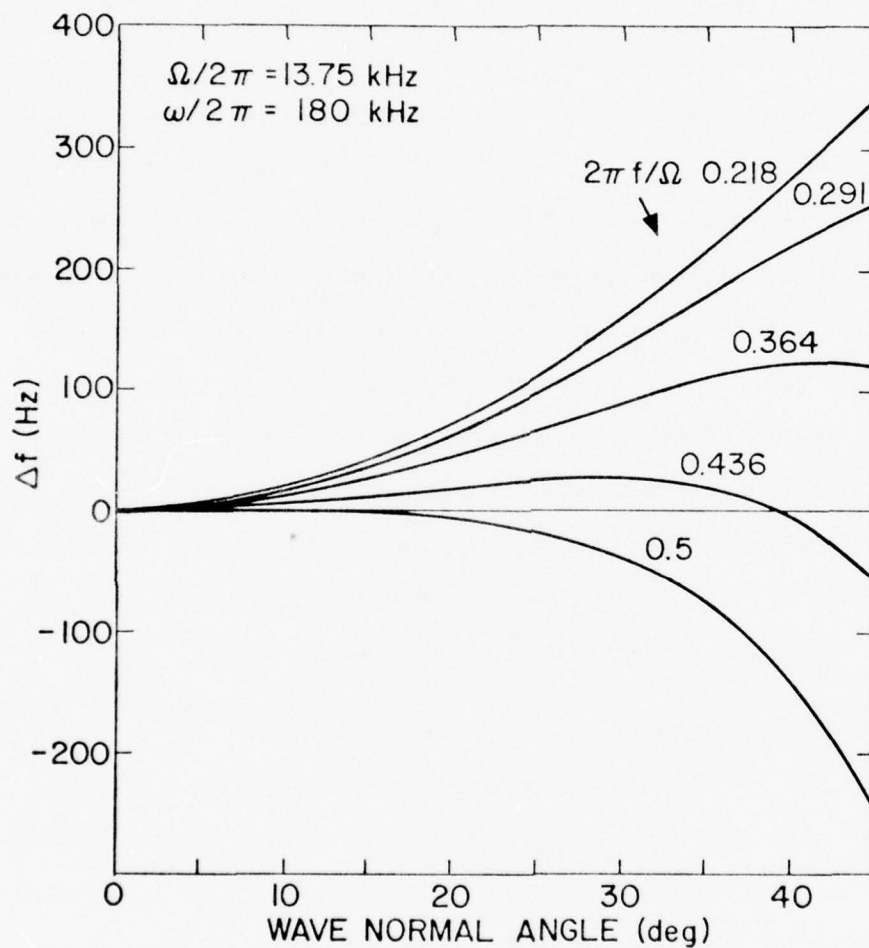


FIGURE 3.6 PLOT SHOWING THE CHANGE IN RESONANT FREQUENCY WITH WAVE NORMAL ANGLE FOR A CONSTANT PARALLEL VELOCITY. Δf is the change in resonant frequency from that for zero wave normal angle.

parallel velocity required for the fundamental doppler shifted gyroresonance at a given frequency is a function of wave normal angle. Even for ducted waves the wave normal angle can be as large as 30° , and this is enough to produce several very interesting effects.

The condition for the fundamental doppler shifted cyclotron resonance is

$$\omega - k_{\parallel} v_{\parallel} = \Omega \quad (3.6)$$

As $\Omega > \omega$ for the whistler mode v_{\parallel} must be negative, i.e., the wave and the electron travel in opposite directions. Equation (3.6) can be written as

$$\omega + k(\alpha) \cos \alpha |v_{\parallel}| = \Omega \quad (3.6a)$$

where α is the wave normal angle. For the conditions valid here the QL approximation is good even for large wave normal angles, so that

$$k^2(\alpha) = \frac{\omega \omega_0^2}{c^2 (\Omega \cos \alpha - \omega)} \quad (3.7)$$

where ω_0 is the plasma frequency. Substituting for $k(\alpha)$ in Eq. (3.6a) we get a cubic equation in ω

$$\omega^3 - \omega^2 [\Omega \cos \alpha + 2\Omega] + \omega [2\Omega^2 \cos \alpha + \Omega^2 + (\frac{v_{\parallel} \omega_0 \cos \alpha}{c})^2] - \Omega^3 \cos \alpha = 0 \quad (3.8)$$

This equation can be solved for ω and plotted as a function of α , keeping v_{\parallel} constant. This has been done in Fig. 3.6. Various values of frequency were chosen and v_{\parallel} calculated for parallel propagation. Then, holding v_{\parallel} fixed, α was varied in Eq. (3.8) and ω calculated. The difference between this frequency and that for parallel propagation Δf is plotted as a function of α in Fig. 3.6.

Figure 3.6 shows that as α is increased the frequency of interaction first increases, reaches a maximum and then drops. The angle at the maximum corresponds to the minimum for the longitudinal component of $k(\alpha)$ and the refractive index. This angle is also called the Gendrin angle. It is also the limiting angle for trapping in enhancement ducts [Smith, 1960, 1961; Helliwell, 1965]. The region of interest is therefore confined to wave normal angles less than this limiting value. As the frequency is reduced, Δf increases at a given α . Δf can be as high as 200 Hz for the parameters chosen here. This means that electrons with the same $v_{||}$ can resonate with a band of frequencies as much as 200 Hz wide.

Propagation at non-zero wave normal angles could conceivably explain the upper sideband of the transmitter frequency. Assume that the transmitter signal before amplification is propagating parallel to the magnetic field. It resonates with particles of a given $v_{||}$ producing phase bunched currents. The electrons so bunched can in turn generate waves at different frequencies propagating at different wave normal angles. This is similar to the radiation from an electron following a helical path [Clemmow and Dougherty, 1969]. These frequencies would all be at and above the transmitter frequency as indicated in Fig. 3.6. This would not be true if the wave before amplification had a range of wave normal angles, i.e., a spread in k . However, it can be argued as below that waves propagating with zero wave normal angles are likely to phase bunch electrons most effectively.

It is also interesting to note that at half the gyrofrequency there is no change in the resonant frequency for first order changes in α . Thus waves at a given frequency with slightly different wave normal

angles close to zero would resonate with the same electrons. This produces larger phase bunched currents and might explain the half-gyrofrequency triggering [Carpenter, 1968; Helliwell, 1969] by whistlers.

It must be pointed out that waves propagating parallel to the magnetic field are best suited for amplification whatever the proposed mechanism for amplification. Waves propagating at an angle have an electric field along the static magnetic field. This can cause Landau damping. For non-parallel propagation there are an infinite number of resonances at harmonics of the gyrofrequency. However most of these involve very high energy electrons and can be neglected. Kennel [1966] showed that the amplification according to linear theory was maximum for parallel propagation at frequencies small compared to the gyrofrequency. Brinca's [1972a] work extended the work to half the gyrofrequency. He showed that, by and large, for most cases growth again maximized for zero wave normal angles. The exceptional cases of low anisotropy and high energies are probably not applicable here.

The equations derived in the last section to calculate the bunching currents can be extended to include non-zero wave normal angles. To simplify matters the monochromatic case will be considered. The only assumption relaxed is that of parallel propagation. The others still hold. The coordinate system is chosen such that the static magnetic field is along the z direction and the \underline{k} vector is in the xz plane, i.e., $k_y = 0$. The electric and magnetic fields are elliptically polarized. The equations are given in the Appendix. It is also shown in the Appendix that Eq. (3.4) can now be written as

$$\ddot{\theta} = k_z \dot{v}_{||} + k_x \dot{v}_x \quad (3.9)$$

Substituting for $\dot{v}_{||}$ and \dot{v}_x it is shown that

$$\begin{aligned} \ddot{\theta} = & k_z \frac{e}{m} Br v_{||} \sin\theta - k_z \frac{e}{m} E_z \\ & - \frac{e}{m} k_x Br v_{||} \sin\theta \cos(\Omega t) \\ & + \frac{e}{m} k_x E_r \sin\theta \cos(\Omega t) \\ & - k_x \Omega v_{||} \sin(\Omega t) \end{aligned} \quad (3.10)$$

where

$$Br = [B_{wx}^2 + B_{wy}^2]^{1/2}, \quad Er = [E_{wx} + E_{wy}]^{1/2}$$

For wave amplitudes of the order of 1 mV and $k_x \approx k_z$ the last term is 3 to 4 orders of magnitude greater than the other terms on the right hand side. Even for very small wave normal angles ($\approx 0.01^\circ$) this term is dominant. In spite of this, this term is always neglected under the assumption of parallel propagation. Assuming that $v_{||}$ and v_{\perp} are approximately constant, it can be argued that this term just introduces a rapid oscillation in θ but does not affect the phase bunching. An attempt was made to verify this by a numerical solution of the equation. However a numerical solution is prohibitively expensive as the steps in time have to be far less than the cyclotron period. This stems from rapid variation of all terms at the gyrofrequency. Therefore the integration steps have to be an order of magnitude smaller than the gyroperiod.

In conclusion it can be stated that propagation at non-zero wave normal angles could be of importance in wave particle interaction studies. Of special relevance here is the fact that the same electrons can generate waves at different frequencies at different wave normal angles.

IV. A QUIET BAND PRODUCED BY VLF TRANSMITTER SIGNALS

A. INTRODUCTION

In the last two chapters the suppression of growth of the VLF transmitter signals was described. This chapter deals with another suppression phenomenon; but this is related to naturally occurring noise. One of the objectives of studying VLF emissions is to improve VLF communications by getting rid of these interfering emissions of magnetospheric origin. Though many types of emissions have been studied and catalogued in the past (see Brice [1964]; Ho [1973]; Helliwell [1965]; Burtis [1969, 1974]), no means of suppressing these emissions or noises artificially has ever been suggested. The phenomenon described here shows that using a relatively low power (100 kw) ground-based VLF transmitter, hiss occurring in a frequency range just below the transmitter frequency can be suppressed. Of course, hiss is only one type of magnetospheric noise and it is suppressed only in a narrow frequency range (up to 200 Hz), and that too only at certain times. Still, a study of this phenomenon is probably a first step towards controlling noise originating in the magnetosphere. In any case, the phenomenon is definitely useful in understanding wave particle interactions and is studied here mainly for this purpose.

The type of noise suppressed by the transmitter is broadband mid-latitude hiss. The suppression is seen in the form of a quiet band up to 200 Hz wide just below the transmitter frequency. The level of suppression is as much as 6 dB. The quiet band is seen only on days of extremely good whistler mode echoing. The quiet band takes 5 to 25 s to develop and lasts up to a minute at the end of transmissions. Unlike

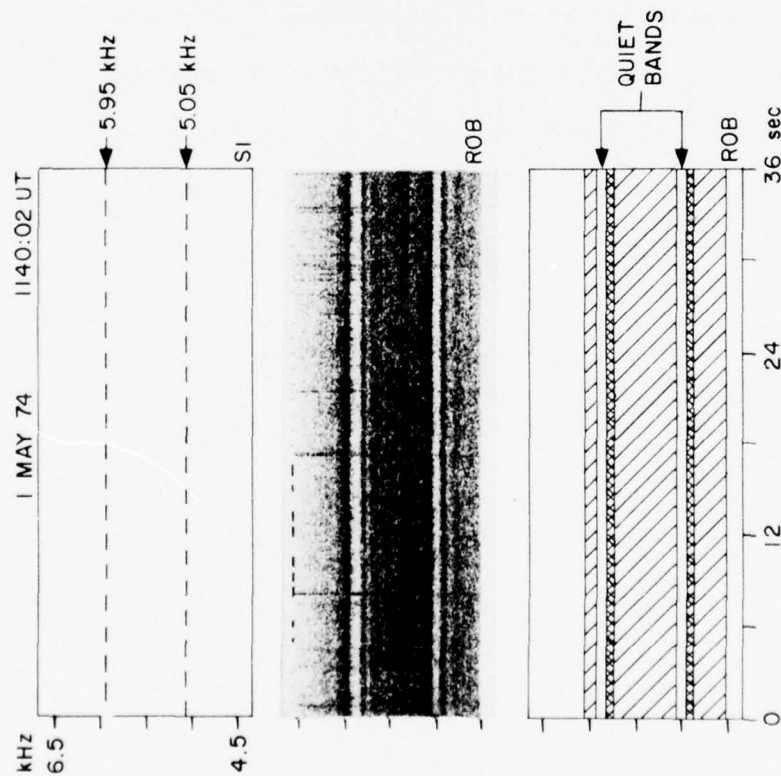
echo-induced suppression the quiet band is very rare. Only 4 or 5 examples have been seen. In spite of their rarity some unmistakable and repeated characteristics are observed.

As in the case of echo-induced suppression, the observed characteristics help greatly in the interpretation. The interpretation again has to do with wave particle interactions and is treated in the next chapter.

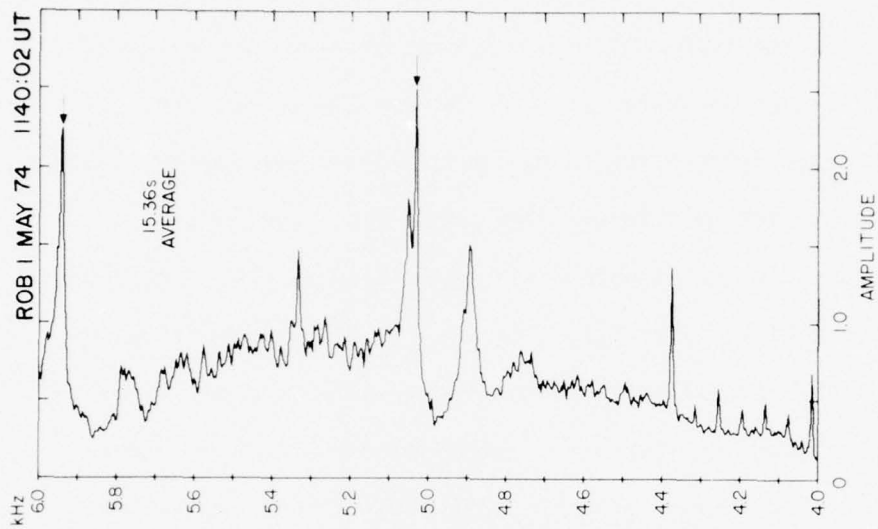
B. DESCRIPTION OF THE QUIET BAND

The middle panel in Fig. 4.1a shows a frequency-time spectrogram of a quiet band event. The top panel shows the format as transmitted from Siple Station. The bottom panel contains a sketch of the event. Though discrete 1 s pulses were transmitted at the two frequencies indicated, a continuous tone is seen at both frequencies as a result of good echoing. The transmissions occur in a band of hiss. The hiss seen here is mid-latitude hiss as opposed to plasmaspheric hiss or auroral hiss [Dowden, 1971; Gallet, 1959; Helliwell, 1965; Fig. 7-29c]. It is characterized by a periodicity in its structure equal to the two hop whistler mode travel time. It is usually accompanied by long echoing whistler trains. Plasmaspheric hiss, on the other hand, is not observed on the ground and occurs at lower frequencies. Auroral hiss, though observed on the ground, does not show the two hop periodicity and occurs at higher latitudes than midlatitude hiss.

A quiet band can be seen beneath both transmitter frequencies in the spectrogram in Fig. 4.1a. The upper band is about 140 Hz wide and the lower one about 80 Hz. The triggering of rising tones by the transmitter signals is responsible for the noise enhancement above the transmitter frequency. An interesting feature is the enhancement in noise,



(a)



(b)

FIGURE 4.1 THE MIDDLE PANEL IN (a) SHOWS QUIET BANDS IN A FREQUENCY TIME SPECTROGRAM. The format transmitted is shown at the top while a sketch of the received data is shown at the bottom. In (b) part of the same data is shown in an amplitude versus frequency plot.

seen as a line, just below the quiet bands. These lines in turn generate and sustain quiet bands of their own.

Figure 4.1b shows the same data in the form of an amplitude versus frequency plot with the transmitter frequencies shown by arrows. The quiet bands can be seen as depressions in the average noise level just below the transmitter frequencies. The ratio between the average noise amplitude at nearby frequencies and the lowest amplitude in the quiet band is about 6 dB. The noise within the quiet band is only partly due to the unsuppressed hiss. Therefore, the hiss is really suppressed by more than 6 dB. The remnant noise within the quiet band consists of other magnetospheric noises, non-magnetospheric noises such as atmospherics and induction fields from the local power lines, and system noise. Of these, noise due to atmospherics can be eliminated by considering portions of data which do not have atmospherics. An A-scan averaged over 0.96 s without any detectable atmospherics showed that the noise level in the quiet band was down by 9.5 dB. As the noise from the other sources cannot be isolated from the unsuppressed hiss, this figure represents a lower bound for the level of suppression at this time.

Several peaks are visible between 4 kHz and 4.6 kHz spaced 60 Hz apart in the A-scan in Fig. 4.1b. They are induction fields picked up from power lines in the vicinity of Roberval.

Figure 4.1b also shows the noise enhancements just above the two transmitter frequencies. The combined bandwidth of the transmitter signal and the noise is about 75 Hz at both frequencies. The enhancements in noise below the quiet bands are seen at 4900 Hz and 5775 Hz.

C. ONSET AND DECAY TIMES FOR THE QUIET BAND

The data shown in Fig. 4.2 provide a measurement of the onset and decay times of the quiet band. The upper panel shows the transmitted format adjusted for a one hop travel time. The 30 s pulses were transmitted starting at each minute with 30 s intervals between them. The frequency was stepped up by 100 Hz after each pulse starting from 5150 Hz at 1046 UT. From 1048 UT a quiet band is seen beneath the pulses at 5350, 5450, 5550 and 5650 Hz. Table 4.1 gives the time taken for the quiet band to develop and the recovery time for the hiss. The recovery

TABLE 4.1 ONSET AND DECAY TIMES FOR THE QUIET BAND

FREQ. (kHz)	TIME FOR QUIET BAND TO DEVELOP (sec)	RECOVERY TIME FOR THE NOISE (sec)	MAXIMUM WIDTH OF QUIET BAND (Hz)
5.35	22 \pm 2	30 \pm 2	53
5.45	16 \pm 2	36 \pm 4	73
5.55	11 \pm 2	42 \pm 4	80
5.65	8 \pm 2	44 \pm 5	80
5.95	-	90 \pm 10	200

time is the time during which the quiet band can be detected after the transmitter is turned off. The quiet band develops faster, lasts longer and also has a greater bandwidth at higher frequencies. The measurements were made on spectrograms with better time resolution than the one in Fig. 4.2. Amplitude versus time plots made with 38 Hz narrow-band filters centered on the quiet bands agreed with these measurements. Let A_1 be the amplitude before and after a quiet band event and A_2

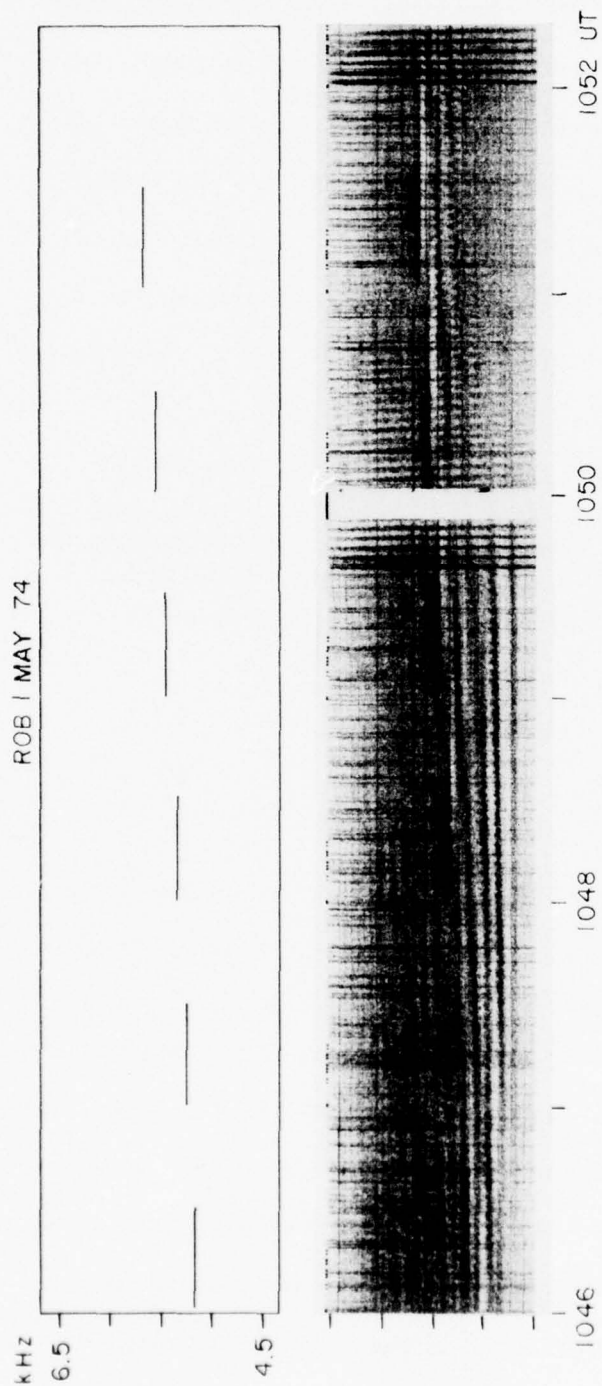


FIGURE 4.2 THE SPECTROGRAM SHOWS THE ONSET AND DECAY TIMES OF SEVERAL QUIET BANDS. The format transmitted is shown at the top. Successive 30 s pulses are stepped up in frequency by 100 Hz. Note that the induction fields from the power lines near Roberval drift in frequency near 1051:00 UT.

the amplitude during the event. The beginning and end of the quiet band was then determined by the times when the amplitude was $A_1 - 0.707 (A_1 - A_2)$. Measurements at 5.95 kHz are from transmissions made about an hour later which are not shown here.

At this time the echoes persist for more than a minute after the transmitter is turned off. At first it appears that the echoes are mainly responsible for the prolongation of the quiet band. However, the amplitude of the three-hop echoes is 6 dB less than the direct one-hop. Yet there is no change in the quiet band when the direct signal terminates. Figure 4.2 shows that the noise does not begin to recover until about 30 s later. The conclusion then is that the recovery time for the quiet band is mainly due to the recovery of the magnetosphere. Figure 4.3 shows conjugate data from Siple Station and Roberval on the prolongation of the quiet band. This, incidentally, is a means of obtaining conjugate quiet band spectrograms as one cannot receive and transmit simultaneously at Siple Station. The Siple record starts when the transmitter is turned off at 1050:30 UT. The quiet band is seen for more than 30 s afterwards.

D. ENHANCEMENTS IN NOISE BELOW AND ABOVE THE QUIET BAND

It was pointed out in Fig. 4.1 that an enhancement in noise could be seen just above and below the quiet band. The two enhancements are very different in their origin and form. The lower enhancement takes a long time to develop — in this case almost 20 minutes. It is definitely associated with the quiet band. Figure 4.1 shows this enhancement after it has developed. It seems to produce a quiet band of its own. Secondary enhancements are then produced and there were several enhancements and

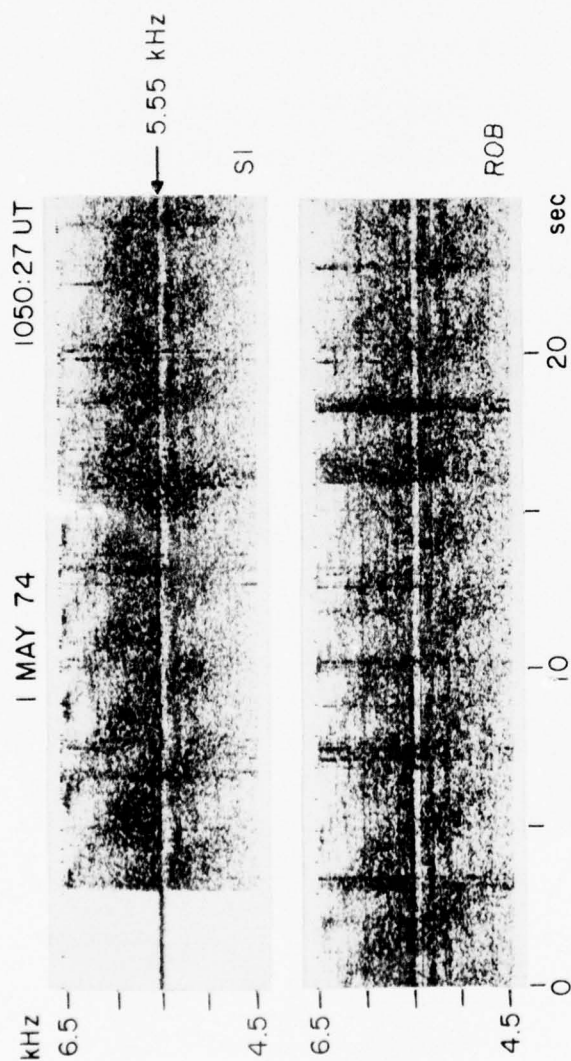


FIGURE 4.3 SPECTROGRAMS ILLUSTRATING THE CONJUGACY OF THE QUIET BAND. It is present at both Siple Station and Roberval below the transmitter frequency at 5.55 kHz. Though the transmitter was turned off at 3 s (when Siple started receiving) the quiet band persists till the end of the spectrogram.

quiet bands between 4.5 and 5 kHz around 1148 UT (not shown). The enhancements below the quiet band are produced in the same way as the hiss itself and are part of the hiss band. It will be shown in the next chapter that an explanation for the quiet band automatically leads to one for the noise enhancements below the quiet band.

The enhancement in noise just above the transmitter frequency is of a completely different nature. This is similar to the broadbanding effects described in connection with echo-induced suppression. The enhancements above the transmitter frequency are present at times even when there is no hiss or quiet band as seen in Fig. 4.4. As in Fig. 4.2 the 30 s pulses were transmitted with 30 s intervals in between. Here the frequency was stepped down by 100 Hz after each pulse instead of up. The frequency of the pulse starting at 1030 UT is 5550 Hz, the frequency of the next pulse 5450 Hz, and so on. The upper enhancement is different from the quiet band and the lower enhancements in that it does not have an onset or decay time. It essentially appears and disappears with the transmitter signals. It consists of many small risers and is quite distinct from the hiss.

E. PATHS OF PROPAGATION, INTERACTION WITH WHISTLERS AND OTHER CHARACTERISTICS

There are not yet enough examples of the quiet band to make any general comments on the path of propagation. On two days at Roberval the quiet band was clearly seen. It is remarkable that on both these days the path of propagation was $L = 3.5$, though signals from the Siple transmitter are more frequently seen near $L = 4$ as reported by Carpenter and Miller [1976]. The implication of this feature is discussed in the next chapter. On both these days the quiet band occurred at a time when

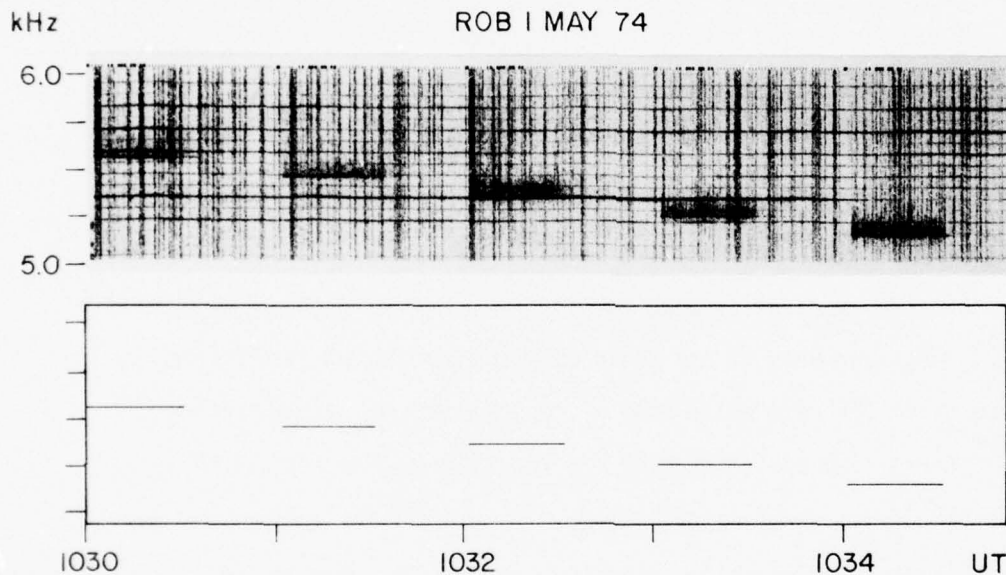


FIGURE 4.4 SPECTROGRAM SHOWING NOISE TRIGGERED BY THE TRANSMITTER SIGNALS IN THE ABSENCE OF A QUIET BAND AND HISS. The 30 s pulses start at the beginning of each minute. The frequency is stepped down by 100 Hz in each succeeding pulse starting with 5550 Hz at 1030 UT.

there was deep quieting in magnetic activity in a time interval of a few hours whereas echo-induced suppression is associated with general quieting which could occur even over a period of days. A similar trend in K_p index was associated with a quiet band produced by the Omega transmitter at 10.2 kHz. The K_p index for the preceding and succeeding 3 hour periods is given in Table 4.2 and shows this trend very well. The quiet band is seen only at times when there is extremely good whistler mode echoing such that whistlers have as many as 50 hops. It is likely that these special conditions are necessary for the production of the hiss rather than for the quiet band itself.

TABLE 4.2 TRENDS IN K_p INDEX ASSOCIATED WITH QUIET BANDS

DAY	TRANSMITTER AND TRANSMITTER FREQUENCY	K_p INDICES				
		-2	-1	0	1	2
1 May 1974	Siple transmitter between 5 and 6 kHz	2	0+	1-	1-	3-
30 Aug 1974	Omega transmitter at 10.2 kHz	3+	1+	2+	2+	2
21 Apr 1975	Siple transmitter at 5.9 kHz	6	2+	2	3	4

One of the most puzzling features of the quiet band is its association with multi-hop whistlers received during the same time period. There is some evidence that the whistlers are multipath and some that they are not. The several discrete components with different nose frequencies are definite evidence that the one-hop whistlers are multipath. Yet, the later hops do not have discrete traces and also have

only one echoing period. Further they merge into the hiss band (see Fig. 4.3) suggesting that the hiss itself is partly or entirely made up of echoing whistler trains. Ho [1974] encountered the same problem in connection with quasi-periodic emissions. The hiss band is probably not multipath because it is unlikely that the transmitter signals travel along as many paths as a one-hop whistler and produce a quiet band on all these paths! The only plausible explanation, then, is that there is a mixing of paths. Though the one-hop whistlers are multipath the mixing of paths results in some or all of the components traveling along one dominant path where echoing conditions are best. Helliwell [1965, pp. 99-100] and Morgan et al. [1959] show examples of mixed path whistlers.

Figure 4.5 shows two examples of this type of mixed path whistlers occurring at times of good echoing. In (a) a one hop whistler is seen from 1750:38 UT at Siple Station. It has three distinct groups of components. If these components continued to travel along their original paths the third hop would show these groups separated by three times the one hop separation. However the third hop has the same separation between these three groups as the first hop. The second, fourth and sixth hops seen at Roberval also have the same separation between these three groups. All the components traveled along the same path except during one hop. In this case the path corresponds to that of some component in the last group of the one hop whistler. The arrow marks the time of the causative atmospheric. In Fig. 4.5b the second and fourth hops of a whistler are shown. There are two distinct groups which again maintain the same separation in time, showing that they are traveling along the same path. In the data the first few hops of the whistlers penetrate

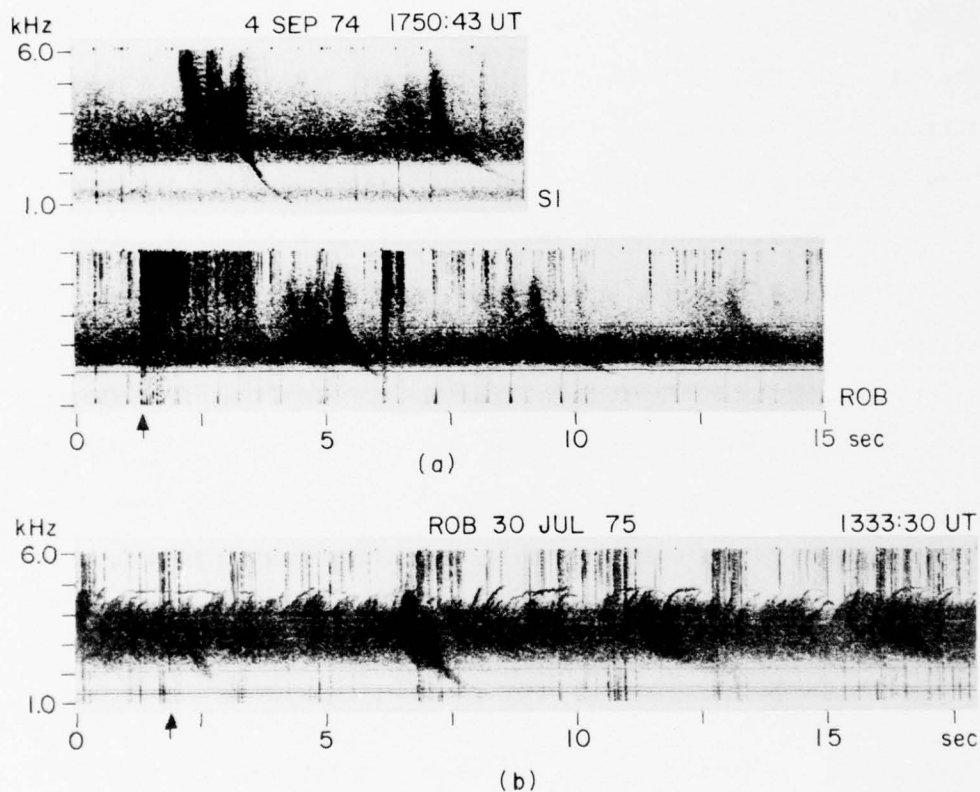


FIGURE 4.5 SPECTROGRAMS SHOWING MIXED PATH WHISTLERS. Conjugate records from Roberval and Siple Station are shown in (a). The one hop whistler seen between 2 and 4 s at Siple has three distinct groups. The two-hop and three-hop whistlers seen at Roberval have the same separation in time between these three groups suggesting they traveled on the same path after the one-hop. Again in (b) the two hop and the four hop of the whistler at 7 s and 12 s respectively show the same separation in time between the two groups. The arrows in both (a) and (b) indicate the location of the relevant atmospherics.

the quiet band, while the later hops do not. This confirms that only the later hops travel along one path, which is the same as that of the hiss.

F. QUIET BANDS PRODUCED BY OTHER SOURCES

Up to this point quiet bands related to the transmitter alone have been considered. Figure 4.6 shows that quiet bands can be produced by other sources. The spectrogram at the top shows a number of quiet bands other than the two produced by the transmitter. In fact, the spectrum of the hiss is almost completely broken up into enhancements and quiet bands. From A-scans similar to that in Fig. 4.1b, the width and the level of suppression of the various quiet bands were measured. The results are plotted in Fig. 4.6 against the amplitude of the source producing the quiet band. The source amplitudes were measured from the enhancements just above the quiet bands. The bandwidth plot is a least-squares fit to a straight line while the level of suppression plot is a least-squares fit to an exponential. Measurements corresponding to the quiet bands produced by the Siple transmitter are shown circled. Though the measurements are few, they suggest that the width of the quiet band increases more or less linearly with the amplitude of the source while the level of suppression tends to a limiting value. Figure 4.6 shows this limiting value to be roughly 5 dB. It is actually greater because part of the unsuppressed noise is not of magnetospheric origin. The direct correlation between the source amplitude and the width and level of suppression is further evidence that quiet bands are not random noise minima in spectra.

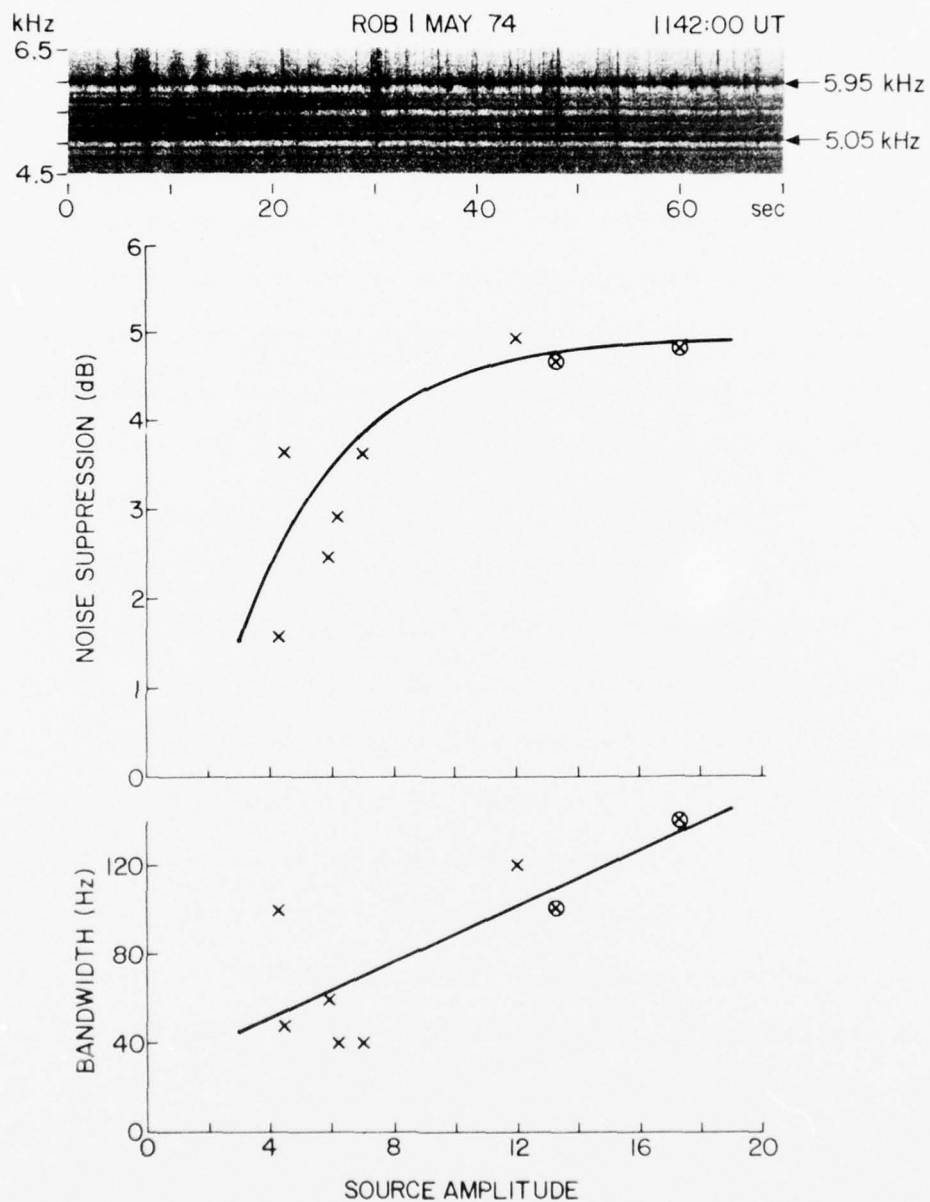


FIGURE 4.6 SPECTROGRAM SHOWING QUIET BANDS PRODUCED BY SOURCES OTHER THAN THE TRANSMITTER. The width of these quiet bands increases more or less linearly with the amplitude of the source. The level of suppression within the band tends to saturate when the amplitude is ≈ 10 units. The amplitude scale has arbitrary units.

Helliwell et al. [1975] show evidence that radiation from power lines at harmonics of 60 Hz is present in the magnetosphere. This radiation appears to be responsible for the production of the other quiet bands in Fig. 4.6. The radiation itself is seen at times as lines in the spectrograms and the lines are called magnetospheric lines [Helliwell et al. 1975]. The conditions under which quiet bands and magnetospheric lines are seen are similar, and the two sometimes even occur together. The reduction in noise amplitude between two magnetospheric lines is like a quiet band, while the lines themselves are like enhancements in noise seen on spectrograms below the quiet band.

Figure 4.7 also illustrates the link between magnetospheric lines and quiet bands. The upper spectrogram shows a quiet band produced by the transmissions at 5.9 kHz. Though discrete pulses were transmitted at this frequency, a continuous line is seen because of the good whistler mode echoing conditions. Transmissions were started at 0835:52 UT. The transmissions seen at the beginning of the spectrogram are whistler mode echoes of earlier transmissions which terminated at 0835 UT. The onset time and decay time for the quiet band are evident. So is the enhancement in noise below the quiet band. The lower spectrogram contains a number of magnetospheric lines starting from approximately 0858:40 UT. The lines are spaced roughly 240 Hz apart. The resemblance between the quiet band in the upper spectrogram and the gaps between these lines is striking. The lines also resemble the enhancement in noise below the quiet band in the upper spectrogram.

This link could conceivably explain the many puzzling features of the magnetospheric lines. If the lines are produced by power line radiation (PLR) they should be present at exact harmonics of 60 Hz. However,

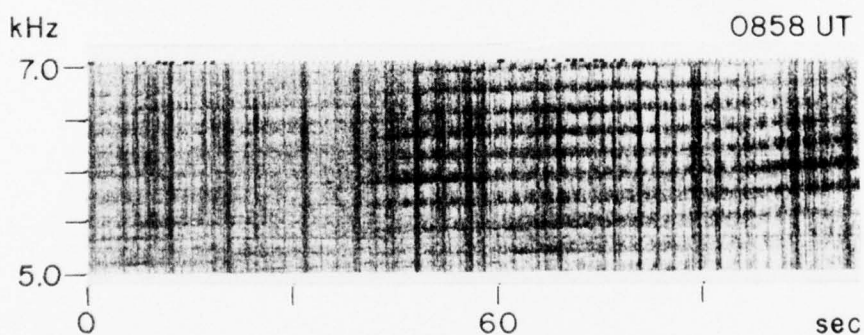
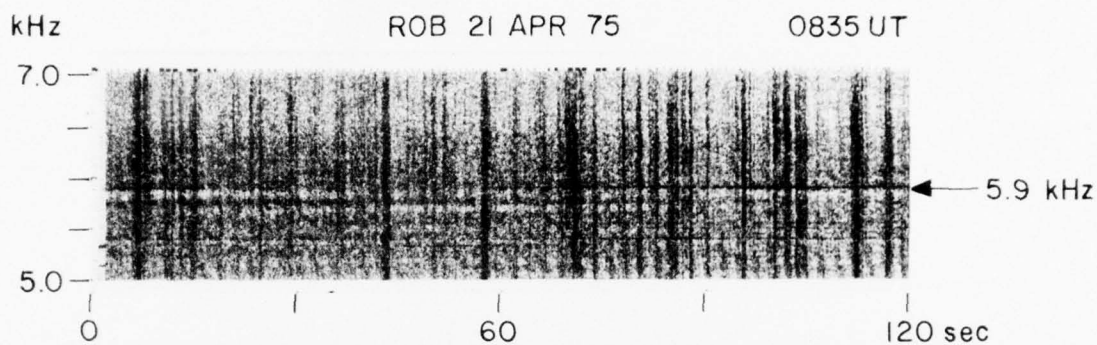


FIGURE 4.7 SPECTROGRAMS SHOWING THE SIMILARITY BETWEEN QUIET BANDS AND POWER SYSTEM RELATED MAGNETOSPHERIC LINES. The upper spectrogram shows a quiet band produced by transmitter signals at 5.9 kHz. The enhancement in noise below the quiet band appears similar to magnetospheric lines seen approximately 20 minutes later. Transmissions in the upper spectrogram were started at 52 s. The quiet band seen earlier is due to transmissions just prior to 0835 UT.

Fig. 4.7 shows the lines drifting up in frequency. The PLR, unlike the transmitter signal, is not strong enough to prevent the drift of the lines. Once a magnetospheric line is established it produces a quiet band below itself, thus becoming better defined. The weak PLR input at the next lower frequency then produces another magnetospheric line, since the conditions for enhancement are favorable just below a quiet band.

G. APPLICATIONS AND USES OF THE QUIET BAND

In a way phenomena like the quiet band belong to the second generation of wave particle interactions studied. Amplification of VLF waves can be considered as a more fundamental problem which might be explainable by assuming a homogeneous magnetosphere and waves propagating at zero wave normal angle. The explanation of the quiet band involves inhomogeneities in the magnetosphere and brings out the importance of including second order effects. More importantly the quiet band provides a means of improving VLF communication. Even a relatively low power transmitter (100 kw) like the one at Siple can produce a quiet band. By transmitting within such a quiet band using a conventional transmitter (power in megawatts) one can achieve a 6 dB improvement in signal to noise ratio.

V. SCATTERING CALCULATIONS AND THE PRODUCTION OF THE QUIET BAND

A. OUTLINE OF METHOD

Based on the observations on the quiet band presented in the last chapter an explanation is offered and then supported by pitch angle scattering calculations. An essential feature of the explanation is the occurrence of the quiet band in a frequency range just below the transmitter frequency.

Figure 5.1 indicates the region centered on the magnetic equator where wave growth occurs. The larger region where pitch angle scattering can occur is shown on just one side of the equator. It is assumed that waves do not grow sufficiently before they reach the equator to produce significant scattering. As in Chapter 3 doppler shifted cyclotron resonance is the mechanism considered here for both amplification and scattering. The hiss is assumed to be generated in the growth region.

For a given frequency, electrons resonant at the equator have the lowest parallel velocities and the parallel velocity required for resonance increases with distance from the equator. At a given place, the resonant parallel velocity increases as the frequency decreases. Consider electrons which resonate with the transmitter signal just outside the growth region. These electrons, if unscattered, resonate with the lower frequencies of the quiet band inside the growth region. The quiet band can then be accounted for by a suitable modification of the electron distribution function involving pitch angle scattering of these electrons. Scattering calculations using an inhomogeneous model and monochromatic waves, described in the rest of the chapter, show that such modifications do occur. The results are shown in the expanded

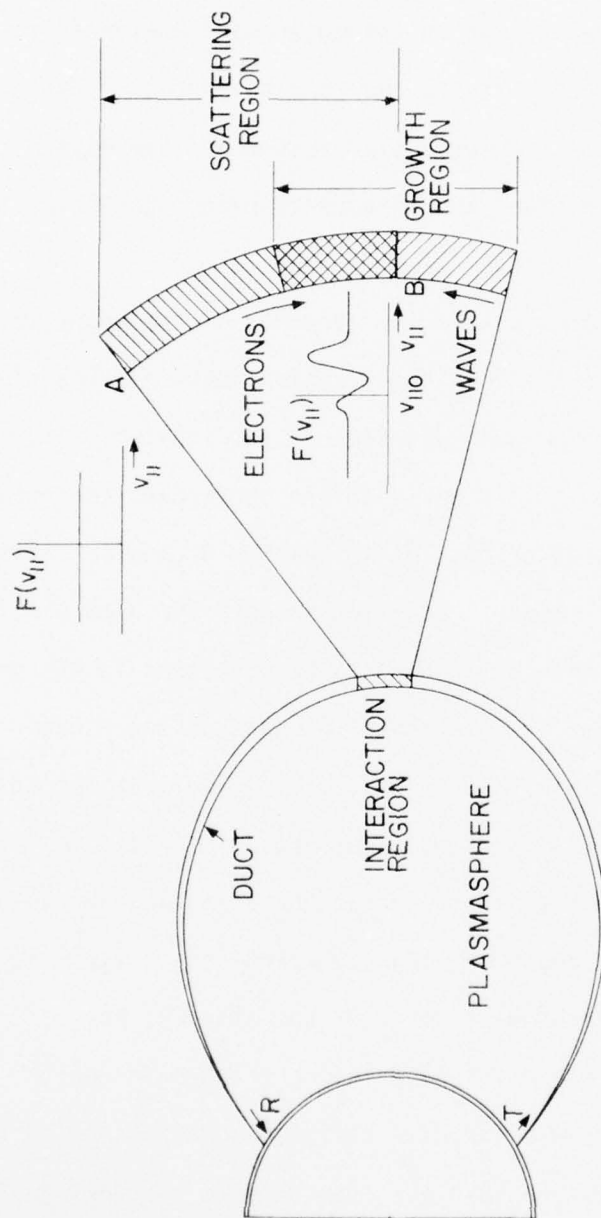


FIGURE 5.1 PROPAGATION OF TRANSMITTER SIGNALS ALONG FIELD-ALIGNED DUCTS. Amplification and pitch angle scattering occur near the equator. The electron distribution as a function of parallel velocity at points A and B is shown.

sketch of the interaction region in Fig. 5.1. A flat distribution as a function of parallel velocity at A just outside the scattering region becomes modified, as shown, at the equator denoted by B. In the figure $v_{||0}$ is the equatorial resonance parallel velocity at the transmitter frequency, f_0 .

The calculations done in this chapter amount to finding the distortion in the parallel velocity distribution function due to a monochromatic whistler mode wave propagating parallel to the earth's magnetic field. Similar analytical calculations were done by Brinca [1972b], but he assumed an homogeneous magnetosphere. Here the variations in electron density and magnetic field strength are taken into account. The calculation is done numerically and the inhomogeneity is the major factor causing perturbations in the parallel velocity distribution (see Inan et al[1977]). As Nunn [1974] points out, the inhomogeneity completely changes the problem, especially in the nonlinear case. While Nunn's objective was to calculate a resonant particle current as an explanation for VLF emissions the goal here is to study the perturbation in the parallel velocity distribution. The amplitude of the perturbing transmitter wave is assumed to be constant. In principle, a growth rate can be calculated from the change in energy of all the particles involved.

Given the perturbed distribution function the quiet band and associated effects could result in one of two ways. One possibility is that a reduction in flux at parallel velocities greater than $v_{||0}$ (corresponding to frequency less than f_0) produces the quiet band. The noise enhancement just below the quiet band is then explained by a similar peak in the distribution. The second explanation depends on the fact that the pitch angle distribution at a given energy will also be modified

when the parallel velocity distribution is modified. According to quasilinear theory [Kennel and Petschek, 1966; Liemohn, 1967] slopes in the pitch angle distribution function produce wave growth or damping depending on the sign of the slope. The different slopes of the perturbed distribution function could then account for the quiet bands and the enhancements. Calculations show that these slopes are comparable to slopes occurring in the loss cone as predicted by Kennel and Petschek [1966] (see also Theodoridis and Paolini [1967]). Moreover they occur at higher pitch angles where more particles are available for energy exchange. Thus wave growth or damping is more likely. It should be pointed out, however, that in the case of distribution functions inseparable in pitch angle and energy, the correspondence between slopes in pitch angle and wave growth is less direct [Bernard, 1973]. It has been assumed that the hiss is generated in a region contained within the scattering region, i.e., the particles must be scattered before they encounter the interaction region for the hiss. This assumption can be relaxed if the scattering is assumed to take place over several bounce periods of the electrons.

The equations describing the motions of an electron in a whistler mode wave for an inhomogeneous medium are developed in the Appendix. The computer model for calculating pitch angle scattering is described in the next section and is followed by the results of the computations. Later, the implications of the results are discussed.

B. NUMERICAL SOLUTION OF THE ELECTRON MOTION

The equations governing the motion of an electron in an inhomogeneous medium are described in many papers and re-derived in the

Appendix. The equations for a homogeneous medium were considered in Chapter 3. Dysthe [1971] derives the equations for the general case but uses them primarily for the homogeneous case. Nunn [1974] assumes parabolic variations in space for the plasma frequency and the gyrofrequency. Here a diffusive equilibrium model is used for the electron density and a dipole model for the earth's magnetic field.

The interaction here is between a monochromatic wave and electrons close to resonance. Theories applicable to broadband spectra [Kennel and Petschek, 1966; Gendrin, 1968; Roberts, 1968] are not relevant here. Most quasi-linear theories fall under this category and use a homogeneous medium, which is inadequate to explain the quiet band.

The equations of motion (A.6) and (A.7) are solved by dividing the distance along a magnetic field line into many equal segments. The computer program was developed by Inan et al. [1977]. A diffusive equilibrium model is used for the electron density and a dipole model for the magnetic field. The intervals in time vary with the parallel velocity as the intervals in space (or z) are fixed. Thus the magnetospheric parameters need to be calculated only once for each field line, making the computation much faster. Rather than let a particle interact with a wave all along the field line from one mirror point to the other, it is useful to define an interaction region. It was found that when an electron's parallel velocity is more than 2% off resonance its pitch angle is not significantly affected by the wave. When this limit is exceeded the particle trajectory is assumed to be totally unaffected by the wave. Twelve electrons initially equally distributed in cyclotron phase are considered at several different initial parallel velocities, for a constant equatorial pitch angle. Using the terminology in Helliwell and

Crystal [1973] each set of twelve electrons at the same initial parallel velocity is called a sheet. The range of parallel velocities considered is small enough ($\pm 2\%$ variation) so that the unperturbed distribution may be represented as a horizontal line at the magnetic equator as in Fig.

5.2. The parallel velocity at the equator for a sheet is defined by the quantity A . A is given by

$$\frac{|v_{||} - v_{||0}|}{|v_{||0}|} \times 100$$

where $v_{||0}$ corresponds to resonance at the equator. Sheets are taken at intervals in A of 0.05% . It amounts to dividing the distribution function into rectangles with $\Delta A = 0.05$. By considering electrons symmetrically distributed in cyclotron phase this rectangle is further divided into 12 in the vertical direction. Each electron is represented by a smaller rectangle which can be moved as it interacts with a wave.

The distribution at the equator would not be flat if the electrons had been scattered by a wave before reaching the equator. The objective here is, of course, to find the modified distribution function. Each electron represented by a small rectangle in Fig. 5.2 is followed as it interacts with the wave from a point down the field line. The chosen point is where the electron has a parallel velocity such that its magnitude is initially 2% less than that necessary for resonance. Thus, different sheets start interacting with the wave at different points in the model. The larger the value of A the greater the distance of the initial point from the equator. All twelve electrons of a sheet start at the same point in space. The points in space chosen are at discrete intervals as mentioned earlier. The electrons therefore are initially off resonance by a value close to but not exactly 2% . The electrons are

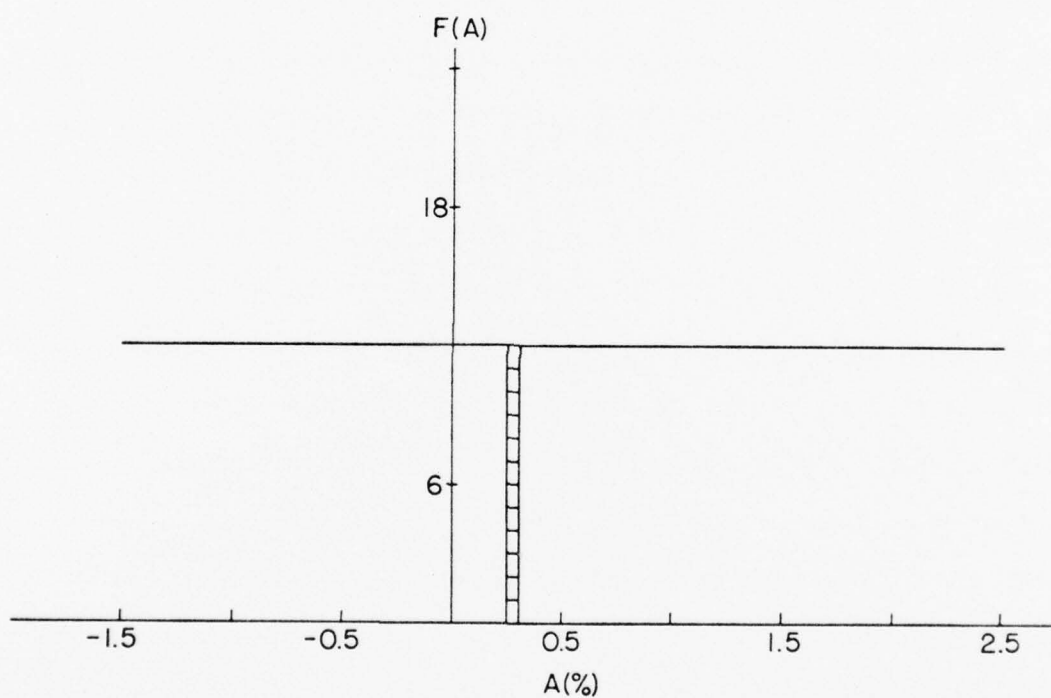


FIGURE 5.2 DIVISION OF THE DISTRIBUTION FUNCTION INTO STRIPS. A is the percentage deviation of the parallel velocity from that for resonance at the equator. Each strip with $\Delta A = 0.05$ is further divided into 12 representing 12 electrons equally distributed in cyclotron phase.

scattered in pitch angle so that the distribution at the equator is no longer flat. Each electron is put in a new ΔA slot depending on its perturbed parallel velocity at the equator. Some slots end with fewer than 12 electrons and some with more. The wave amplitude is assumed to be constant in the interaction region. The scattering beyond the equator is not considered, as the wave would be weaker before it reaches the equatorial region where most of the growth is assumed to occur.

While the results are presented in the next section for various cases, a qualitative picture of the scattering is presented here. The effects of the inhomogeneity and wave field are considered separately. Consider electrons with positive A . The electrons in a sheet are initially 2% off resonance. As they travel to the equator they move in an anticlockwise direction relative to B_w in Fig. 3.1. Neglecting the effect of the wave fields, for the moment, θ varies as shown in Fig. 5.3 (also see Helliwell [1970]). At the point of exact resonance θ is maximum after which it decreases. Figure 5.3 shows the unperturbed plots of θ for various values of A . These are easily calculated in the computer model by putting $B_w = 0$. Next consider the effect of the wave, ignoring the inhomogeneity. Helliwell and Crystal [1973] showed that the electrons are phase bunched with their perpendicular velocities opposite to B_w . Considering the two effects together it is seen that this direction of bunching will be rotated anticlockwise first and then clockwise as the electrons move through the interaction region. The sheet as a whole either gains or loses in parallel velocity (after changes due to the first adiabatic invariants have been taken out) depending on whether the phase bunched current has a net component opposite to E_w or along E_w during the interaction.

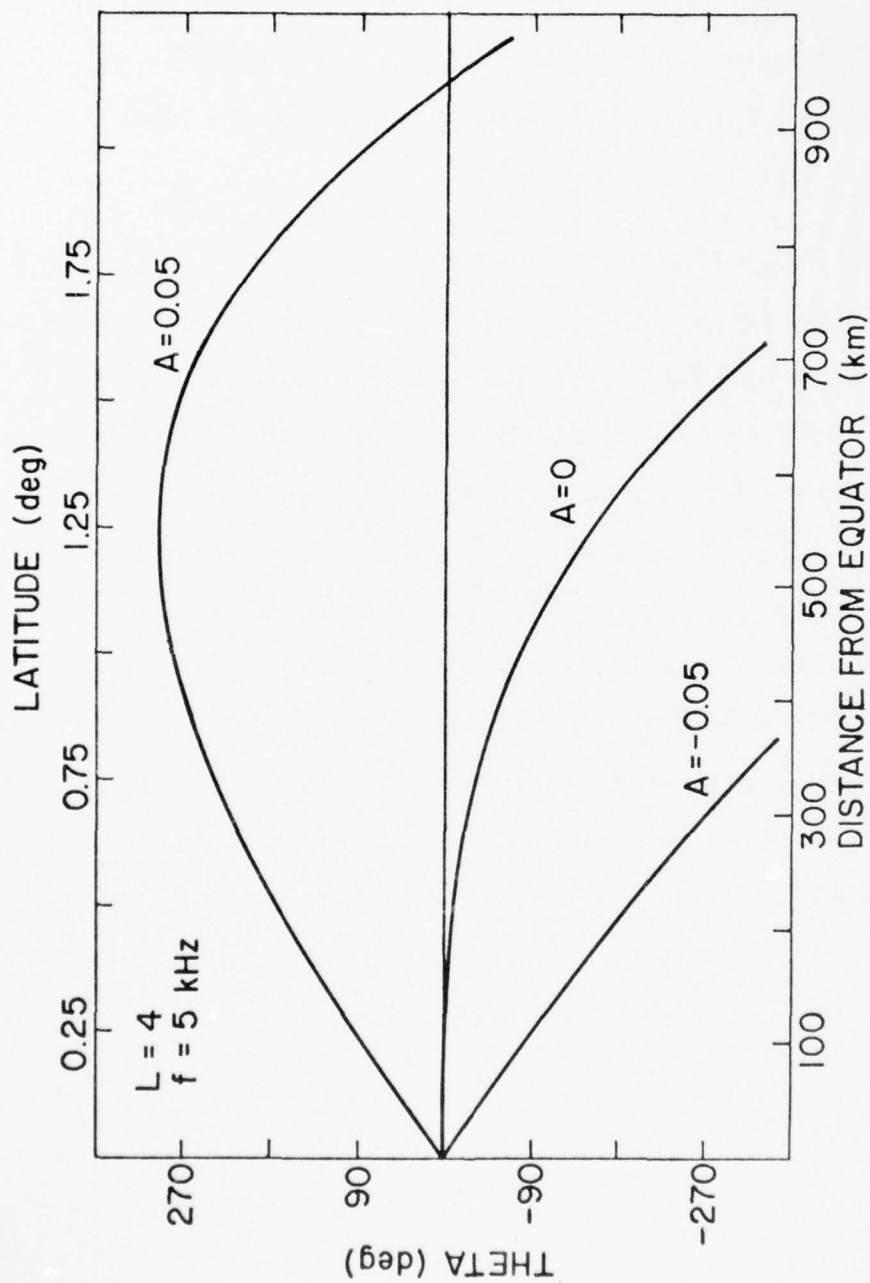


FIGURE 5.3 PHASE ANGLE BETWEEN THE PERPENDICULAR VELOCITY AND THE WAVE MAGNETIC FIELD AS AN ELECTRON MOVES TOWARD THE EQUATOR FROM RIGHT TO LEFT. Particles with positive A go through a region of exact resonance (Helliwell [1970] contains a similar figure) while particles with negative A do not.

AD-A042 245

STANFORD UNIV CALIF STANFORD ELECTRONICS LABS

F/G 20/12

SUPPRESSION EFFECTS ASSOCIATED WITH VLF TRANSMITTER SIGNALS INJ--ETC(U)

MAR 77 R RAGHURAM

N00014-76-C-0689

UNCLASSIFIED

SU-SEL-77-007

NL

2 of 2
ADA042245



END

DATE
FILMED

8 - 77

There is a limiting value of A , both in the positive and negative direction, beyond which scattering is negligible. Particles with negative A have a smaller interaction length as can be seen from Fig. 5.3. This is because the phase θ changes more rapidly and quite often the particles are not at exact resonance anywhere, especially for small amplitude waves (< 1 mV).

C. RESULTS OF THE SCATTERING CALCULATIONS

Figure 5.4 gives the perturbed distribution function at the equator. The calculations were done for $L = 4$, using a centered dipole model for 30° pitch angle particles. The diffusive equilibrium model for the electron density had an equatorial cold plasma electron density of 400 el/cc. The scale at top is in Hz corresponding to that in A at the bottom. The arrows along the horizontal axis indicate the range in A for which sheets were considered at intervals $\Delta A = 0.05\%$.

The frequency 5 kHz is 0.37 times the equatorial gyrofrequency. This frequency was chosen because the bandwidth in Hz is maximum for a given ΔA at this ratio of frequency to gyrofrequency, as shown below. In other words, the width of the quiet band would be maximum at this ratio, assuming all frequencies produce a depletion with the same ΔA . From the condition for doppler shifted cyclotron resonance

$$v_{\parallel} = \frac{c}{f_0} \frac{(f_H - f)^{3/2}}{f^{1/2}} \quad (5.1)$$

$$\frac{\Delta f}{\Delta v_{||}} = - \frac{f_0}{c} \frac{f^{1/2}}{(f_H - f)^{1/2}} \frac{1}{\frac{3}{2} + \frac{1}{2} \left(\frac{f_H - f}{f} \right)} \quad (5.2)$$

where $v_{||}$ is the magnitude of parallel velocity. The negative sign in Eq. (5.2) merely indicates that as $v_{||}$ increases f decreases. Using Eq. (5.1), Eq. (5.2) is written as

$$\Delta f = - \frac{f_H - f}{\frac{3}{2} + \frac{1}{2} \left(\frac{f_H - f}{f} \right)} \times \frac{A}{100} \dots \quad (5.3)$$

One is interested only in the depletion from $A = 0$ to some positive value of A as the quiet band exists immediately below the transmitter signal. By differentiating Δf with respect to f and equating it to zero the maximum Δf for a given A can be found. A quadratic expression is obtained

$$2f^2 + 2f \cdot f_H - f_H^2 = 0 \dots \quad (5.4)$$

On solving Eq. (5.4) one gets $f/f_H = 0.366$.

The maximum, though, is very shallow. While $\Delta f = 0.0027 f_H A$ at $f/f_H = 0.366$ it drops to only $0.0025 f_H A$ at $f/f_H = 0.5$ and $f/f_H = 0.25$ on either side.

There is a dip in the distribution function in Fig. 5.4 between $A = 0.5\%$ and $A = 1.25\%$ for the $10 m\gamma$ case. The curve is jagged because of the discrete sheets and the discrete cyclotron phases. A visual smoothing should be done when studying the figure and isolated peaks and valleys should be ignored. Though the rightmost sheet is at $A = 2.7\%$, particles are seen as far as $A = 3.5\%$ due to the scattering.

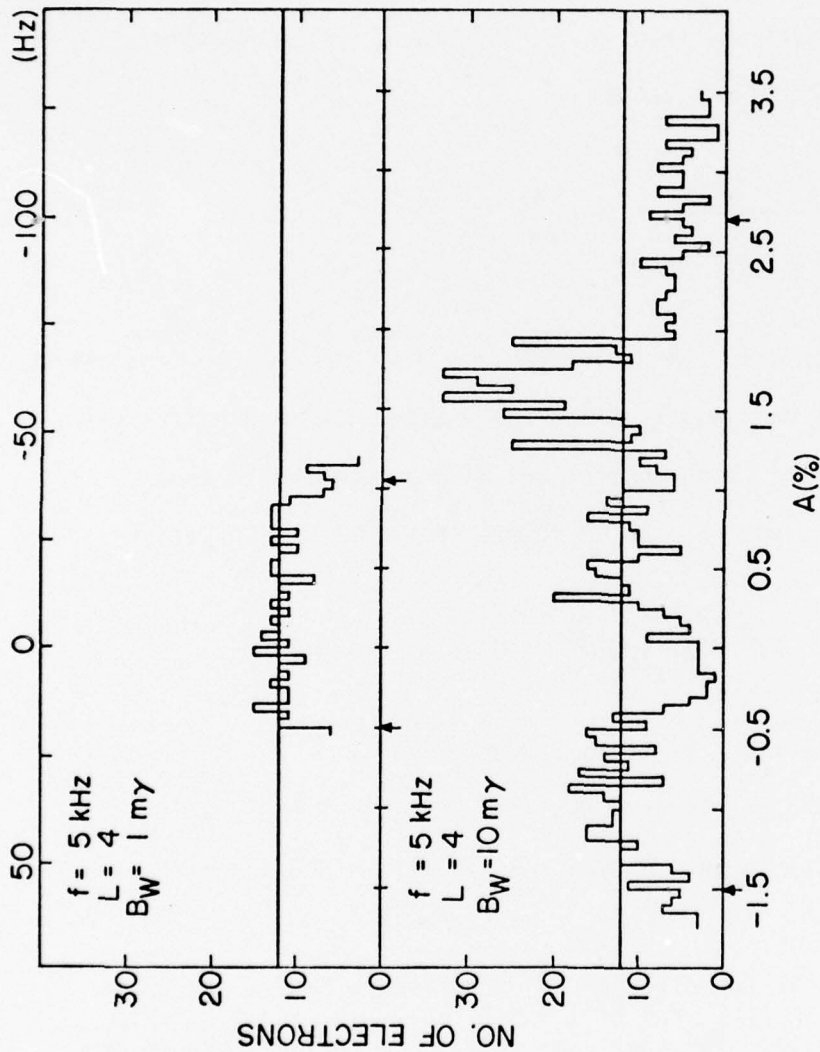


FIGURE 5.4 SCATTERING CALCULATIONS AT $L = 4$ FOR $1 \text{ m}\gamma$ AND $10 \text{ m}\gamma$ WAVES. The horizontal line at 12 represents the distribution at the equator in the absence of a wave. The arrows represent the extent to which calculations are done. While a $10 \text{ m}\gamma$ wave produces a depletion in the number of electrons between $A = -0.5\%$ and $A = 1.5\%$ and an enhancement between $A = 1.5\%$ and $A = 2.0\%$, a $1 \text{ m}\gamma$ produces negligible scattering. The calculations were done for 30° equatorial pitch angle particles. The scale at the top gives the deviation from the resonant frequency at the equator, corresponding to A .

The calculations to the right of $A = 2\%$ are not complete as particles from the sheets beyond $A = 2.7\%$ could fill up these regions. The same applies to the region to the left of $A = -1.25\%$.

The correlation between the calculations and the data is not good enough to determine whether the quiet band is due to the slopes in the distribution function or due to a reduction in the flux. While the depression above the transmitter frequency is puzzling (note frequency scale at top of figure), the one below, almost 50 Hz wide, could very well be responsible for the quiet band. The peak between -55 and -75 Hz could account for the enhancement in noise just below the quiet band in the data. Alternatively, the positive slope between $A = -0.2\%$ and 1.5% (ignoring isolated excursions) could be producing the quiet band and the negative slope between 1.5% and 2% could be producing the noise enhancement. To the left of $A = -0.5\%$ there is no definite depression with the average number of electrons equal to the unperturbed value.

Figure 5.4 also shows the effect of changing the wave amplitude. A $1 \text{ m}\mu$ wave scatters very little with no significant peaks or valleys. The sheet at $A = 1.05\%$ for example, scatters electrons only to $A = 1.2\%$. The minimum amplitude required to produce a quiet band is of the order of $10 \text{ m}\mu$. Even a $10 \text{ m}\mu$ wave produces a quiet band of only 50 Hz. This is small compared to the 200 Hz observed in Fig. 4.1. It is likely that even a weak wave could produce a significant depression in several passes if not in one pass. Thus the 200 Hz quiet band could have been produced over several successive passes. The onset time of 5 to 25 s mentioned in Section 4.3 is comparable to the time taken for several bounces of the electrons.

Figure 5.5 shows the same calculations at $L = 3$. The equatorial thermal electron density was 550 el/cc. The quiet band produced here is better defined and the figure as a whole is more representative of the observations. Though the depression has a smaller width in A it has the same width in frequency. The higher gyrofrequency is responsible for this. The frequency of the wave is 12 kHz, which is also equal to $0.37 f_H$. The peak between -60 and -100 Hz again could account for the enhancement seen below the quiet band. As in Fig. 5.4 it is not possible to say whether the quiet band and related effects are due to the slopes or actual magnitude of flux. This figure is complete to about $A = 2.0\%$. The difference between Figs. 5.4 and 5.5 is mainly due to the shorter interaction length at $L = 3$. The electrons are therefore scattered less. This is especially true for sheets with negative A and explains the absence of a depression for negative A at $L = 3$.

Figures 5.4 and 5.5 have been calculated for 30° pitch angle particles. To obtain the true perturbed distribution an integration over all pitch angles should be done. This would, for one thing, lead to a smoothing of the curves. It would also alter the depth and width of the valleys or depressions seen. In general, higher pitch angles are scattered more for the same $v_{||}$. The $\underline{v}_\perp \times \underline{B}$ force varies as $\tan \alpha$, where α is the pitch angle. There is a tradeoff between the larger forces and reduced fluxes at higher pitch angles. The effect of the wave is therefore maximum for pitch angles in the 20° - 60° range. Thus Figs. 5.4 and 5.5 are good representations of the distributions integrated over all pitch angles.

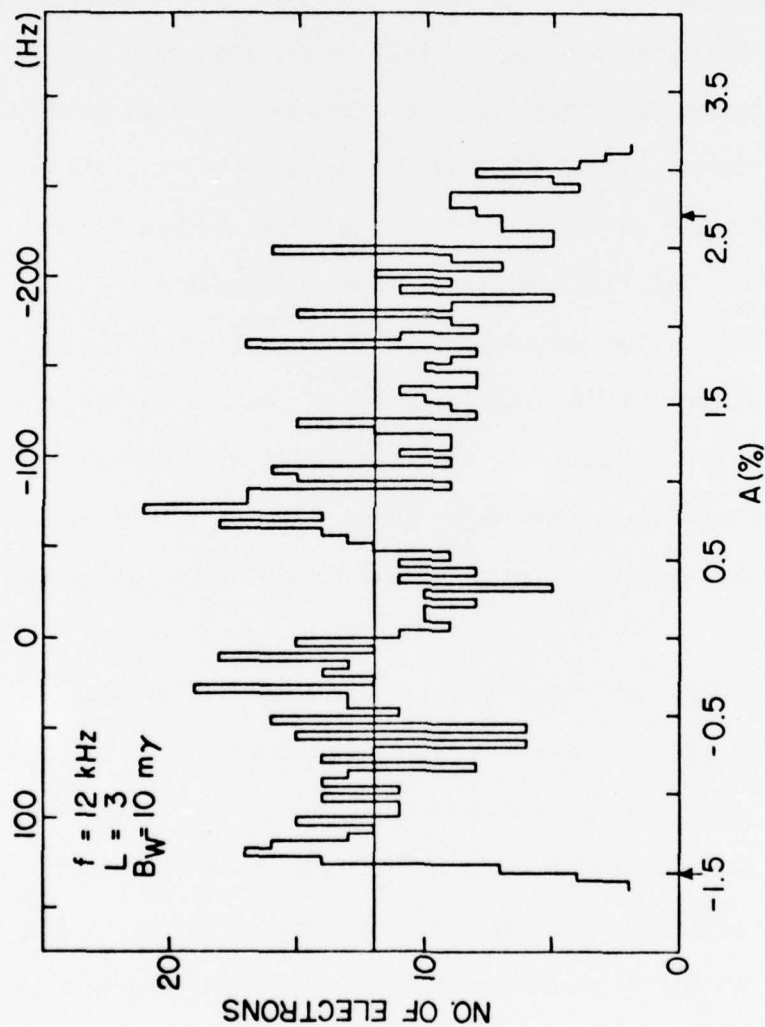


FIGURE 5.5 SCATTERING AT $L = 3$ FOR A 10 m γ WAVE. The figure is similar to Fig. 5.4 except that the depletion is confined to positive A. The depletion and enhancement are less pronounced. The width of the depletion region in Hz is still roughly the same as at $L = 4$. As in Fig. 5.4, electrons with an equatorial pitch angle of 30° alone are considered.

D. CONSISTENCY OF DATA OBSERVATIONS WITH THE SCATTERING THEORY

In the last section the quiet band and the enhancement in noise below it were attributed to perturbations in the parallel velocity distribution function. It is shown here that the other observations described in the last chapter are by and large consistent with this interpretation. The occurrence of the quiet band at $L = 3.5$, rather than near $L = 4$, is probably related to the fact that the quiet band has a larger bandwidth at lower L values for a given width, ΔA , of the depression. The scattering is more efficient at larger L values, but the bandwidths are lower. By comparing Figs. 5.4 and 5.5 it seems likely that $L = 3.5$ might be the optimum L value for production of quiet bands. The association between echoing and the quiet band is not obvious in the interpretation given in the last section. Neither is the association between the quiet band and quieting trends in K_p index. It appears likely that these two factors are necessary for the production of hiss rather than the quiet band.

In the calculations described above it has been implied that all the scattering takes place in one bounce period of the electrons. Actually, it might take several bounce periods for the depression in parallel velocity distribution to form. This time could be responsible for the onset time of the quiet band. As electrons of different energies and pitch angles have different bounce periods the quiet band develops gradually without sudden variations in intensity.

It was shown in Fig. 4.6 that the width of the quiet band was a linear function of the wave amplitude. Also, the amount of noise suppression at first increased with wave amplitude and then leveled off. The calculations shown in Fig. 5.4 are consistent with these observations.

The 10 mY wave produces a much wider quiet band than the 1 mY wave which has very little effect on the particle distribution. It is also clear that any further increase in wave amplitude cannot produce a much larger depression in the particle distribution. However, the width of the depression would increase with wave amplitude.

No special conditions need exist to produce the type of scattering described here. Quiet bands are rare only because the following conditions must be met for their existence:

- 1) Mid-latitude hiss must be present.
- 2) Frequency of transmission must be within the hiss band.
- 3) Transmitter signals must be amplified so that they are strong enough to suppress the hiss.
- 4) There must be extremely good whistler mode echoing.

One puzzling feature of the data is that the triggering of emissions above the transmitter frequency and growth at the transmitter frequency is apparently unaffected by the development and decay of the quiet band. The perturbations in the distribution function would be expected to modify the triggering and growth characteristics.

In any case, the interpretation offered here for the production of the quiet band seems plausible. While some features of the data are not completely explained, there are no major contradictions between theory and observations.

E. IMPLICATIONS AND USES OF THE QUIET BAND

(1) The recovery time for the hiss after a quiet band event could lead to the estimation of certain magnetospheric parameters. If the recovery time is due to the growth rate of the hiss, then the measurements

in Table 4.1.gives the growth rate as a function of frequency. On the other hand, if the growth time is far less than the recovery time, then the recovery time must be less than the time required for resonant electrons to drift across the duct. This therefore leads to a lower limit for the longitudinal duct width. At $L = 3.5$, for 45° equatorial pitch angle electrons resonant at 5.75 kHz, the drift rate is 2.6×10^{-3} degrees/sec (see Roederer [1970]). Thus a recovery time of a minute corresponds to a duct width of 0.156° in longitude. While this is considerably less than the value of 4° quoted in Angerami [1970] it is possible that the hiss is generated in an emission cell occupying only a small part of the duct.

(2) The width of the quiet band leads to an indirect estimate of the length of the scattering region. The lower cutoff frequency of the quiet band corresponds to electrons with the highest parallel velocity scattered by the transmitter signals. By calculating where these electrons are in resonance with the transmitter signals the scattering length can be found. For example, a quiet band 200 Hz wide at 5.95 kHz and $L = 3.5$ means that the transmitter signal effectively scattered scattered electrons from a point 3.25° (or 1265 km) off the equator.

(3) The perturbations in the electron distribution function discussed here could not be measured by any type of particle detectors used in past satellite experiments. Pitch angle resolutions of at least 0.1° and energy windows no greater than a few per cent wide are needed. Quiet bands give an indirect estimate of particle distributions perturbations of far greater resolution than present day satellite measurements.

(4) Besides providing insights into wave particle interactions, quiet bands could find use in VLF communication. Even a relatively low power transmitter like the Siple transmitter (output power \approx 500 W) can produce a quiet band. By transmitting within such a band a significant improvement in signal to noise ratio could be achieved.

VI. CONCLUSIONS AND SUGGESTIONS FOR FUTURE WORK

A. DIFFERENCES BETWEEN THE QUIET BAND AND THE ECHO-INDUCED SUPPRESSION

From the various examples shown in the last few chapters it is clear that the quiet band and echo-induced suppression are two distinct phenomena. However, it is sometimes not clear which one of these two effects is responsible for some suppression effects seen in natural data. Some of the differences are therefore listed below.

1) Echo-induced suppression occurs about 200 ms after the arrival of the echo. The amplitude starts to recover immediately upon termination of the echo. Quiet bands take 5 to 25 s to form and can last as much as a minute after the source is turned off.

2) Echo-induced suppression has been observed on a third of the days transmissions were detected at Roberval during a 6-month period. No special conditions are needed for its occurrence. Quiet bands are rare and also can be detected only if there is broadband background hiss. Hiss in the frequency range of interest here is seen only at times of extremely good whistler mode echoing.

3) The explanation for echo-induced suppression involves only waves, i.e., it is not directly dependent upon particle distributions. Quiet bands can be explained only by considering particles as well.

4) The echoes responsible for echo-induced suppression are usually in a frequency range which contains the direct signal. In the case of the quiet band the suppressed hiss is in a frequency range below the transmitter signal and its associated emissions.

5) Echo-induced suppression takes place before the waves are amplified. The particle scattering responsible for the quiet band takes place after the wave has been amplified.

B. SOME LONG RANGE IMPLICATIONS OF THE PHENOMENA

The two suppression phenomena described here provide some ways of controlling certain kinds of VLF emissions generated in the magnetosphere. It is also seen that great changes in the particle distribution can be made over limited spreads in parallel velocity. By transmitting more complicated formats, and perhaps using more than one transmitter at a time, one can envisage moulding the particle distributions according to one's desires. In other words, the magnetosphere can become a plasma physics laboratory where the waves and particle distributions are under at least limited control. The control can be increased by using satellites in addition to ground based transmitters.

A very practical application of plasma physics is in fusion. The plasma temperatures and densities in fusion reactors are orders of magnitude greater than those in the magnetosphere. Yet the study of instabilities in the magnetosphere cannot but help in the containment of instabilities in these reactors. A control over the instabilities leads to an easier confinement of the plasma. Thus, a study of magnetospheric plasma physics could conceivably find use in more down to earth applications.

C. SUGGESTIONS FOR FUTURE WORK

The VLF data described in this thesis are rather complex. While the broader details have been explained, many others have not. Attempts to explain complicated phenomena like echo suppression and quiet bands have necessarily to build upon theories that account for more elementary effects such as amplification of whistler mode signals. Unfortunately there is no general agreement on what the wave-particle interaction pro-

cess is. One of the reasons for this is the absence of particle and wave data at the same time for the same point in space. In principle it should be possible to continuously monitor the waves and the particle distributions using satellites. A high priority project should be to obtain suitable satellite data on waves and particles.

In connection with echo suppression it was mentioned that transmitter signals are broadband. In Chapter 3 it was suggested that this might be the result of propagation at non-zero wave normal angles. Brinca [1972a] and Kennel [1966] discuss the amplification of nonducted waves with non-zero wave normal angles. But they do not consider the generation of additional frequencies. Inclusion of non-zero wave normal angles in wave particle studies has the potential of explaining a number of VLF phenomena. Moreover, even ducted waves have wave normal angles as large as 30 or 40° . It seems logical that the assumption of parallel propagation should be relaxed if only to make the problem more realistic. Phenomena such as chorus, seen on satellites (see Burtis [1974]) have wave normal angles close to 90° as they undergo LHR reflection. The physics of wave-particle interaction is completely different under these conditions. Therefore the study of non-zero wave normal angle waves should be very rewarding in wave particle interaction studies in the magnetosphere.

In the data area, more examples of quiet bands are needed. As pointed out earlier, this is a rare phenomenon. By transmitting in frequency ranges within hiss bands, more cases could be obtained. Suitable formats can be transmitted to test for scattering in the absence of hiss. One possibility is to interrupt a relatively long pulse

(> 30 s) by shorter test pulses (≈ 1 s) 10 to 100 Hz lower in frequency. Any scattering produced by the long pulse would then affect the growth of the test pulses. These test pulses could also be transmitted 5 to 10 s after the long pulse so that their growth is not affected by echoes of the long pulse.

The complex interaction between the hiss band, the whistlers and the quiet band needs to be studied in greater detail. In this thesis it is suggested that whistlers echo only in one dominant path and that they produce part or all of the hiss. This should be confirmed by more data analysis. The puzzling relationships between magnetospheric lines and quiet bands should also be explored.

To prove the existence of PLR (power line radiation) more conclusively, data on the power systems in the vicinity of Roberval should be obtained. An accurate calculation of the power radiated can then be made. This, when compared to the radiated power from the Siple transmitter might explain why phenomena associated with PLR are not always similar to those associated with the Siple transmitter.

APPENDIX. EQUATIONS FOR THE MOTION OF AN ELECTRON IN
THE PRESENCE OF A WHISTLER MODE WAVE

Case 1. Monochromatic whistler mode waves traveling parallel to
the static magnetic field in a homogeneous magnetosphere.

Figure 3.1 defines the coordinate system. B_w and E_w denote the wave magnetic and electric fields respectively. B_0 is the static magnetic field and $v_{||}$ and v_{\perp} denote the velocity of an electron parallel and perpendicular to the static magnetic field. The cyclotron phase angle between B_w and v_{\perp} , θ , is measured as shown in Fig. 3.1.

Considering the various forces on the electron the equations of motion can be written as (see also Dysthe [1971]):

$$\dot{v}_{||} = \frac{e}{m} B_w v_{\perp} \sin\theta \quad (A.1a)$$

$$\dot{v}_{\perp} = \frac{e}{m} (E_w - v_{||} B_w) \sin\theta \quad (A.1b)$$

$$\dot{\phi} = \Omega + \frac{e}{m} (B_w \frac{v_{||}}{v_{\perp}} - \frac{E_w}{v_{\perp}}) \cos\theta \quad (A.1c)$$

where $\dot{\phi}$ = instantaneous angular velocity of the electrons. Therefore

$$\dot{\theta} = -\omega + k v_{||} + \dot{\phi} \quad (A.2)$$

The angle θ needs to be solved to get the phase bunched currents. Differentiating (A.2) with respect to time

$$\ddot{\theta} = k \dot{v}_{||} + \ddot{\phi}$$

For wave amplitudes relevant here (≈ 1 mV) $k \dot{v}_{||}$ is much larger than $\ddot{\phi}$ so that

$$\ddot{\theta} \approx k \dot{v}_{\parallel} = \frac{e}{m} B_w k v_{\perp} \sin \theta \quad (\text{A.3})$$

This is the equation solved in Helliwell and Crystal [1973] to calculate phase bunched currents.

Case 2. Non-monochromatic waves traveling parallel to the static magnetic field in a homogeneous magnetosphere.

Consider the special case where the spectrum consists of two frequencies in phase at $t = 0$ and spaced $\Delta\omega$ apart such that $\Delta\omega \ll \omega$. As shown in Fig. 3.3, let the quantities pertaining to the two waves be distinguished by the suffixes 1 or 2. B_{wr} and E_{wr} are the instantaneous resultant wave fields. θ is now measured between B_{w1} and v_{\perp} . The two new angles ψ and ψ' are also shown in Fig. 3.3. Equations (A.1) are now modified as follows:

$$\dot{v}_{\parallel} = \frac{e}{m} B_{wr} v_{\perp} \sin(\psi + \theta) \quad (\text{A.4a})$$

$$\dot{v}_{\perp} = -\frac{e}{m} B_{wr} v_{\parallel} \sin(\psi + \theta) + \frac{e}{m} E_{wr} \sin(\psi' + \theta) \quad (\text{A.4b})$$

$$\dot{\phi} = \Omega + \frac{e}{m} \frac{B_{wr} v_{\parallel}}{v_{\perp}} \cos(\psi + \theta) - \frac{e}{m} \frac{E_{wr}}{v_{\perp}} \cos(\psi' + \theta) \quad (\text{A.4c})$$

Since θ is measured with respect to the wave at frequency ω ,

$$\dot{\theta} = -\omega_1 + k_1 v_{\parallel} + \dot{\phi}$$

$$\ddot{\theta} = k_1 \dot{v}_{\parallel} + \ddot{\phi}$$

For $\Delta\omega \ll \omega_1$ (or ω_2) and $B_{wr} \ll B_0$, $k_1 \dot{v}_{\parallel} \gg \ddot{\phi}$. Therefore,

$$\ddot{\theta} = k_1 \dot{v}_{\parallel} = \frac{e}{m} B_{wr} v_{\perp} \sin(\psi + \theta) \quad (\text{A.5})$$

where

$$B_{wr}(t) = [B_{w1}^2 + B_{w2}^2 + 2B_{w1} B_{w2} \cos(\Delta\omega t - \Delta kv_{||} t)]^{1/2}$$

$$= [B_{w1}^2 + B_{w2}^2 + 2B_{w1} B_{w2} \cos(\Delta\omega t - \Delta kv_{||}(0)t)]^{1/2}$$

and
$$\psi(t) \approx \tan^{-1} \left[\frac{B_{w2} \sin(\Delta\omega t - \Delta kv_{||}(0)t)}{B_{w1} + B_{w2} \cos(\Delta\omega t - \Delta kv_{||}(0)t)} \right]$$

Variations in $v_{||}$ have been neglected in the expression for B_{wr} and ψ as these variations produce only second order variations in B_{wr} and ψ . Equation (A.5) is, in general, more difficult to solve than Eq. (A.3) because B_{wr} and ψ are functions of time.

Case 3. Monochromatic whistler mode waves traveling parallel to the static magnetic field in an inhomogeneous magnetosphere.

Both the gyrofrequency and the plasma frequency are functions of z in this case. The electron motion is affected not only by the wave fields but also by the inhomogeneity. The conservation of the first adiabatic invariant (see Roederer [1970]) is assumed to calculate variations in $v_{||}$ and v_{\perp} caused by the inhomogeneity. The equations corresponding to (A.1) can now be written as

$$\dot{v}_{||} = \frac{e B_w}{m} v_{\perp} \sin\theta + \frac{v_{\perp}^2}{2B_0} \frac{\partial B_0}{\partial z} \quad (A.6a)$$

$$\dot{v}_{\perp} = \frac{e}{m} (E_w - v_{||} B_w) \sin\theta - \frac{v_{||} v_{\perp}}{2B_0} \frac{\partial B_0}{\partial z} \quad (A.6b)$$

$$\dot{\phi} = \Omega + \frac{e}{m} \left(B_w \frac{v_{||}}{v_{\perp}} - \frac{E_w}{v_{\perp}} \right) \cos\theta \quad (A.6c)$$

Corresponding to Eq. (A.2)

$$\dot{\theta} = \Omega + \frac{e}{m} \left(B_w \frac{v_{||}}{v_{\perp}} - \frac{E_w}{v_{\perp}} \right) \cos \theta - \omega + kv \quad (A.7)$$

The inhomogeneity is used to explain quiet bands in Chapter 5 where changes in the electron's $v_{||}$ and v_{\perp} are needed rather than the phase θ . For this purpose the coupled equations (A.6a), (A.6b) and (A.7) should be solved using a suitable model for the electron density and static magnetic field. The relation $v_{||} \frac{d}{dt} = \frac{\partial}{\partial z}$ can be used to convert time derivatives to spatial derivatives.

Case 4. Monochromatic whistler mode waves traveling at an angle to the static magnetic field in a homogeneous magnetosphere.

Assume that the static magnetic field, B_0 , is still along the z axis. The \vec{k} vector of the wave is assumed to be wholly in the x - z plane making an angle α with the z axis. Wave fields for these conditions can be derived from those in Brice [1964] by a rotation of axis in the x - z plane. Let

$$Y_L = \frac{\Omega}{\omega} \cos \alpha, \quad Y_T = \frac{\Omega}{\omega} \sin \alpha, \quad \mu = \frac{ck}{\omega} \quad \text{and} \quad Z_0 = \frac{\mu_0}{\epsilon_0}.$$

Using the QL approximation and neglecting the spatial variation, the wave fields are written as follows

$$E_x = E_w \sin \omega t \cos \alpha + \frac{Y_T}{Y_L - 1} E_w \sin \omega t \sin \alpha \quad (A.8a)$$

$$E_y = E_w \cos \omega t \quad (A.8b)$$

$$E_z = -\frac{Y_T}{Y_L - 1} E_w \sin \omega t \cos \alpha + E_w \sin \omega t \sin \alpha \quad (A.8c)$$

$$H_x = -\frac{\mu}{z_0} E_w \cos \omega t \cos \alpha \quad (\text{A.9a})$$

$$H_y = \frac{\mu}{z_0} E_w \sin \omega t \quad (\text{A.9b})$$

$$H_z = -\frac{\mu}{z_0} E_w \cos \omega t \sin \alpha \quad (\text{A.9c})$$

The three cases considered so far had no wave fields along the z direction. The presence of a non-zero E_z and H_z introduces additional terms in the equations describing the electron motion. Also the propagation constant k has a component along the x direction so that term $kv_{||}$ has to be changed to $(k_z v_{||} + k_x v_x)$. The wave is elliptically polarized in the x - y plane and the instantaneous frequency of rotation of the wave field vector at a given place is a function of time. However it is still equal to ω when averaged over one rotation. Again in the x - y plane the wave magnetic field is perpendicular to the wave electric field on the average. As before,

$$\dot{v}_{||} = \frac{e}{m} (B_x^2 + B_y^2)^{1/2} v_{\perp} \sin \theta - \frac{e}{m} E_z \quad (\text{A.10a})$$

$$\dot{v}_{\perp} = \frac{e}{m} (E_x^2 + E_y^2)^{1/2} \sin \theta - \frac{e}{m} v_{||} (B_x^2 + B_y^2)^{1/2} \sin \theta \quad (\text{A.10b})$$

$$\dot{\phi} = \Omega + \frac{e}{m} B_z + \frac{e}{m} (B_x^2 + B_y^2)^{1/2} \frac{v_{||}}{v_{\perp}} \cos \theta - \frac{(E_x^2 + E_y^2)^{1/2}}{v_{\perp}} \cos \theta \quad (\text{A.10c})$$

$$\dot{\theta} = -\omega + k_z v_{||} + k_x v_x + \dot{\phi} \quad (\text{A.11})$$

Neglecting $\ddot{\phi}$, $\ddot{\theta}$ can be written as

$$\ddot{\theta} = k_z \dot{v}_{||} + k_x \dot{v}_x$$

Now,

$$\dot{v}_x = \frac{d}{dt} (v_{\perp} \cos \Omega t) = \dot{v}_{\perp} \cos \Omega t - \Omega v_{\perp} \sin \Omega t$$

Therefore

$$\ddot{\theta} = k_z \dot{v}_{||} + k_x \dot{v}_{\perp} \cos \Omega t - k_x \Omega v_{\perp} \sin \Omega t \quad (\text{A.12})$$

Substituting for $\dot{v}_{||}$ and \dot{v}_{\perp} from Eq. (A.10) and letting $(B_x^2 + B_y^2)^{1/2} = B_r$ and $(E_x^2 + E_y^2)^{1/2} = E_r$,

$$\begin{aligned} \ddot{\theta} &= \frac{e}{m} B_r k_z v_{\perp} \sin \theta - \frac{e}{m} E_z k_z \\ &+ \frac{e}{m} E_r k_x \sin \theta \cos \Omega t - \frac{e}{m} B_r k_x v_{||} \sin \theta \cos \Omega t \\ &- k_x \Omega v_{\perp} \sin \Omega t \end{aligned} \quad (\text{A.13})$$

REFERENCES

- Angerami, J. J., Whistler duct properties deduced from VLF observations made with the OGO 3 satellite near the magnetic equator, J. Geophys. Res., 75, 6115, 1970.
- Bernard, L. C., Amplitude variations of whistler-mode signals caused by their interaction with energetic electrons of the magnetosphere, Tech. Rept. No. 3465-2, Radioscience Laboratory, Stanford Electronics Laboratories, Stanford University, Stanford, Ca., 94305, 1973.
- Brice, N. M., Discrete VLF emissions from the upper atmosphere, Tech. Rept. No. SEL64-088, Radioscience Laboratory, Stanford Electronics Laboratories, Stanford University, Stanford, Ca., 94305, 1964.
- Brinca, A. L., On the stability of obliquely propagating whistlers, J. Geophys. Res., 77, 3495, 1972a.
- Brinca, A. L., A whistler side-band growth due to nonlinear wave particle interaction, J. Geophys. Res., 77, 3508, 1972b.
- Burtis, W. J., Magnetospheric chorus, Tech. Rept. No. 3469-3, Radioscience Laboratory, Stanford Electronics Labs., Stanford University, Stanford, Ca., 1974.
- Burtis, W. J. and R. A. Helliwell, Banded chorus-- a new type of VLF radiation observed in the magnetosphere by OGO 1 and OGO 3, J. Geophys. Res., 74, 3402, 1969.
- Carpenter, D. L., Whistler evidence of a "knee" in the magnetospheric ionization density profile, J. Geophys. Res., 68, 1675, 1963.
- Carpenter, D. L., Whistler studies of the plasmopause in the magnetosphere, 1. Temporal variations in the position of the knee and some evidence of plasma motions near the knee, J. Geophys. Res., 71, 693, 1966.
- Carpenter, D. L., Ducted whistler mode propagation in the magnetosphere: a half gyrofrequency upper intensity cutoff and some associated wave growth phenomena, J. Geophys. Res., 73, 2919, 1968.
- Carpenter, D. L. and T. R. Miller, Ducted magnetospheric propagation of signals from the Siple, Antarctica VLF transmitter, J. Geophys. Res., 81, 2692, 1976.
- Carpenter, D. L. and C. G. Park, On what ionospheric workers should know about the plasmopause-plasmasphere, Rev. Geophys. and Space Phys., 11, 133, 1973.
- Carpenter, D. L. and N. T. Seely, Cross-L drifts in the outer plasmasphere: quiet time patterns and some substorm effects, J. Geophys. Res., 81, 2728, 1976.

- Clemmow, P. C. and J. P. Dougherty, Electrodynamics of Particles and Plasmas, Addison-Wesley Publishing Co., Reading, Mass., 1969.
- Crystal, T. L., Nonlinear currents stimulated by monochromatic whistler mode (WM) waves in the magnetosphere, Tech. Rept. No. 3465-4, Radioscience Laboratory, Stanford Electronics Labs., Stanford University, Stanford, Ca., 1975.
- Dowden, R. L., Distinctions between midlatitude VLF hiss and discrete emissions, Planet. Space Sci., 19, 374, 1971.
- Dysthe, K. B., Some studies of triggered whistler emissions, J. Geophys. Res., 76, 6915, 1971.
- Gallet, R. M., The very low frequency emissions generated in the earth's exosphere, Proc. IRE, 47, 211, 1959.
- Gendrin, R., Pitch angle diffusion of low energy protons due to gyroresonant interactions with hydromagnetic waves, J. Atmos. Terr. Phys., 30, 1313, 1968.
- Gurnett, D. A., S. D. Shawhan, N. M. Brice and R. L. Smith, Ion cyclotron whistlers, J. Geophys. Res., 70, 1665, 1965.
- Helliwell, R. A., Whistlers and Related Ionospheric Phenomena, Stanford University Press, Stanford, Calif., 1965.
- Helliwell, R. A., A theory of discrete VLF emissions in the magnetosphere, J. Geophys. Res., 72, 4773, 1967.
- Helliwell, R. A., Low-frequency waves in the magnetosphere, Rev. Geophys. Space Phys., 7, 281, 1969.
- Helliwell, R. A., Intensity of discrete VLF emissions, Particles and Fields in the Magnetosphere, B. M. McCormac (ed.), p. 292-301, 1970.
- Helliwell, R. A. and T. L. Crystal, A feedback model of cyclotron interaction between whistler mode waves and energetic electrons in the magnetosphere, J. Geophys. Res., 78, 7357, 1973.
- Helliwell, R. A. and J. P. Katsufakis, VLF wave injection into the magnetosphere from Siple Station, Antarctica, J. Geophys. Res., 79, 2511, 1974.
- Helliwell, R. A., J. P. Katsufakis, T. F. Bell and R. Raghuram, VLF line radiation in the earth's magnetosphere and its association with power system radiation, J. Geophys. Res., 80, 4249, 1975.
- Helliwell, R. A., J. Katsufakis and G. Carpenter, Whistler-mode propagation studies using Navy VLF transmitters, Tech. Rept. No. SEL-62-035, Radioscience Lab., Stanford Electronics Labs., Stanford Univ., Stanford, Ca., 1962.

- Ho, D., Interaction between whistlers and quasi-periodic VLF emissions, J. Geophys. Res., 78, 7347, 1973.
- Ho, D., Quasi-periodic (QP) VLF emissions in the magnetosphere, Tech. Rept. No. 3464-2, Radioscience Lab., Stanford Electronics Labs., Stanford Univ., Stanford, Ca., 1974.
- Inan, U. S., T. F. Bell and R. A. Helliwell, Nonlinear gyroresonant interactions of energetic electrons with coherent VLF waves in the magnetosphere, submitted to J. Geophys. Res., 1977.
- Kennel, C. F., Low-frequency whistler mode, Phys. Fluids, 9, 2190, 1966.
- Kennel, C. F. and H. E. Petschek, Limit on stably trapped particle fluxes, J. Geophys. Res., 71, 1, 1966.
- Kimura, I., On observations and theories of the VLF emissions, Planet. Space Sci., 15, 1427, 1967.
- Liemohn, H. B., Cyclotron-resonance amplification of VLF and ULF whistlers, J. Geophys. Res., 72, 39, 1967.
- McNeil, F. A., Frequency shifts of whistler mode signals from a stabilized VLF transmitter, Radio Science, 2, 589, 1967.
- Morgan, M. G., H. W. Curtis and W. C. Johnson, Path combinations in whistler echoes, Proc. IRE, 47, 328, 1959.
- Muzzio, J. L. R., Ion cutoff whistlers, J. Geophys. Res., 73, 7526, 1968.
- Nunn, D., A self-consistent theory of triggered VLF emissions, Planet. Space Sci., 22, 349, 1974.
- Park, C. G., Methods of determining electron concentrations in the magnetosphere from nose whistlers, Tech. Rept. No. 3454-1, Radioscience Lab., Stanford Electronics Labs., Stanford Univ., Stanford, Ca., 1972.
- Parker, E. N., Dynamics of the interplanetary gas and magnetic fields, Astrophys. J., 128, 644, 1958.
- Raghuram, R., A new interpretation of subprotonospheric whistler characteristics, J. Geophys. Res., 80, 4729, 1975.
- Raghuram, R., R. L. Smith and T. F. Bell, VLF Antarctica antenna: Impedance and efficiency, IEEE Trans. Antennas. Propagat., AP-22, 334, 1974.
- Roberts, C. S., Cyclotron-resonance and bounce resonance scattering of electrons trapped in the earth's magnetic field, Earth's Particles and Fields, B. M. McCormac (ed.), p. 317, Reinhold, New York, 1968.

- Roederer, J., Dynamics of Geomagnetically Trapped Radiation, Springer-Verlag, New York, 1970.
- Smith, R. L., Guiding of whistlers in a homogeneous medium, J. Res. NBS-D, Radio Propagation 64D, 505, 1960.
- Smith, R. L., Propagation characteristics of whistlers trapped in field-aligned columns of enhanced ionization, J. Geophys. Res., 66, 3699, 1961.
- Stiles, G. S., Digital spectra of artificially stimulated VLF emissions, Tech. Rept. No. 3465-3, Radioscience Lab., Stanford Electronics Labs., Stanford, Ca., 1974.
- Stiles, G. S. and R. A. Helliwell, Frequency-time behavior of artificially stimulated VLF emissions, J. Geophys. Res., 80, 608, 1975.
- Stix, T. H., Theory of Waves in Plasmas, Mc-Graw-Hill, New York, 1962.
- Theodoridis, G. C. and R. F. Paolini, Pitch angle diffusion of relativistic outer belt electrons, Ann. de Geophys. 23, 375, 1967.